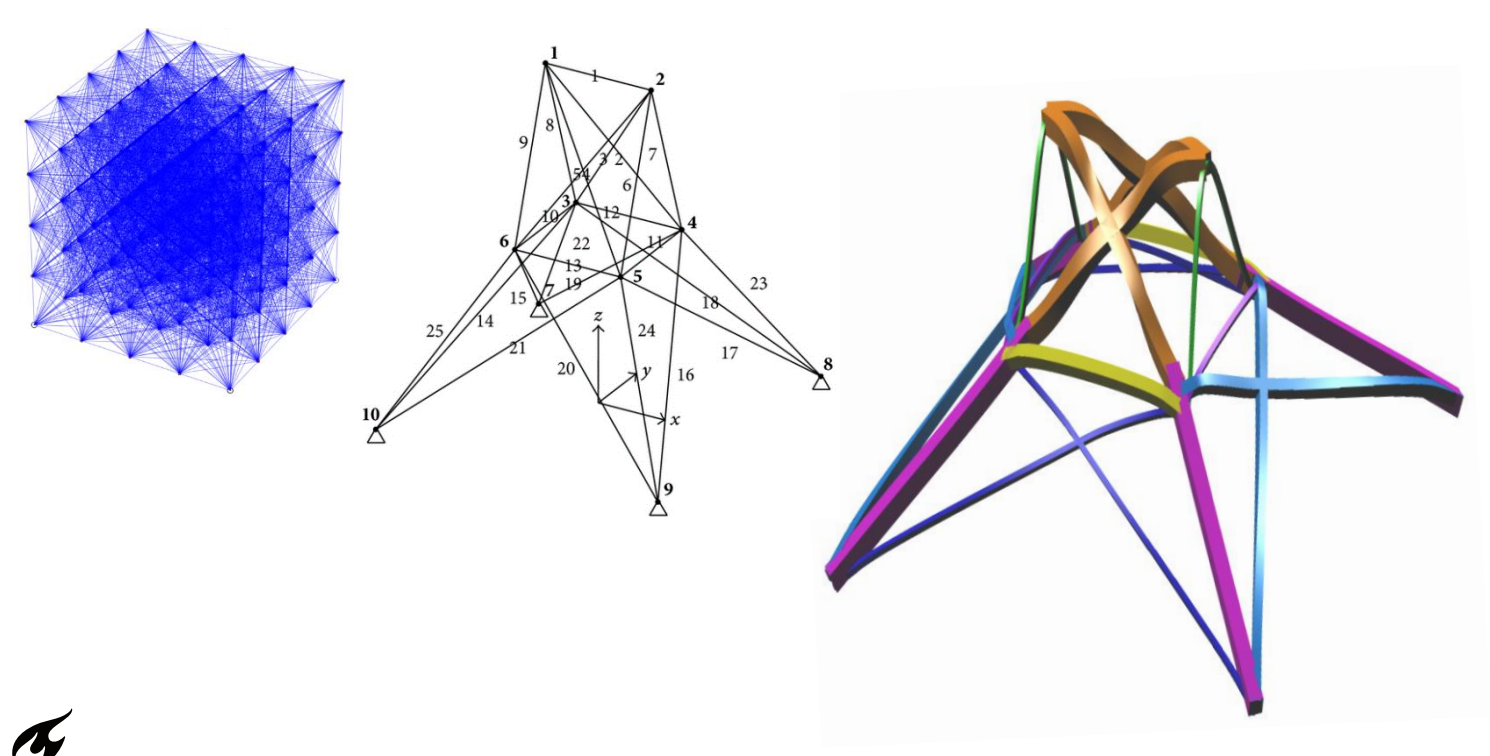
# Design and Optimization of 3D Skeletal Composite Structures

Master of Science Thesis





# Design and Optimization of 3D Skeletal Composite Structures

by

### W.M. Papenhuijzen

in partial fulfilment of the requirements for the degree of

#### Master of Science

in Aerospace Engineering

at Delft University of Technology, Faculty of Aerospace Engineering, Department of Aerospace Structures and Materials

to be defended publicly on April 26 2017.

This thesis is confidential and cannot be made public until April 26 2022.

An electronic version is available at <a href="http://repository.tudelft.nl">http://repository.tudelft.nl</a>.

The work in this thesis was completed with significant support from ATG Europe B.V. (<a href="http://www.atg-europe.com/">http://www.atg-europe.com/</a>). Their cooperation is gratefully acknowledged.





Copyright W.M. Papenhuijzen

All rights reserved.

Delft University of Technology Faculty of Aerospace Engineering Department of Aerospace Structures and Materials

### GRADUATION COMMITTEE

Committee Chair:	
	Dr. S.R. Turteltaub
	Delft University of Technology
Committee Members:	
	Dr. C. Kassapoglou
	Daily Supervisor
	Dr. ir. O.K. Bergsma
	Delft University of Technology
	ir. S.M. Simonian
	ATG Europe, B.V.
	Company Supervisor

### **Abstract**

A method has been developed for designing composite 3D skeletal structures. This method can be used to design weight optimized fiber reinforced structures that can carry complex loads in high performance applications such as satellites. These designs are realized through Size, Shape and Topology Optimization, using a ground structure approach as a starting point. This enables modeling of both the highly anisotropic properties of fiber reinforced materials, as well as arrangements in various stages of development that exploit those properties. Rather than applying these three optimization processes purely sequentially, a more robust approach is presented which increases the likelihood of arriving at design solutions that are global optima. A trade-off between theoretical optimality and manufacturability is made by implementing manufacturing constraints. This is done at various stages in the optimization process, rather than as a final translation step where a theoretically optimal solution is converted to a realistic design. Merely implementing manufacturing constraints as a final design step may lead to a design which moves away significantly from the optimal design that was arrived upon at an earlier stage. Manufacturing feasibility has been addressed by analyzing and building several samples showcasing a joint design that forms the building block for the type of structures that can be designed using the methodology presented in this thesis. The results indicate that, especially for stiffness-critical applications, this is a feasible approach for building structures that can be significantly lighter than state of art additive manufactured structures, while approaching similar levels of design freedom.

viii Abstract

# **Table of Contents**

Abstra	act		vii
List of	Figu	res	xiii
List of	Tabl	es	xvii
List of	Sym	bols and Abbreviations	xix
Ackno	wledg	gements	xxi
Chapt	er 1	Introduction	1
1.1	Back	ground Information	1
1.2	Resea	arch objective	2
1.3	Thesi	s Structure	3
Chapt	er 2	Literature Review	5
2.1	State	of Art of optimization methods for composite structures	7
	2.1.1	Sizing and Shape optimization of grid stiffened structures	7
	2.1.2	Layup optimization for planar or conical structures	8
	2.1.3	2D topology optimization of fiber reinforced structures	8
2.2	Appr	oaches to modeling 3D composite structures	10
2.3	Conc	lusions	12
Chapt	er 3	Project Objectives	13
3.1	Focus	s of Research	13
3.2	Resea	arch Objective	15
3.3	Expe	cted Outcome	18
3.4	Optin	mization Framework requirements	19
Chapt	er 4	Optimality	21
4.1	Sub p	process level Optimality	21
4.2	Struc	tural Optimizer level Optimality	22

4.3	Proje	ct Level Optimality	24
Chapt	er 5	Manufacturing	. 25
5.1	$\operatorname{Grid}$	Structure Manufacturing Methods	25
5.2	Proce	ess- and material selection	26
	5.2.1	Material type and draping method	27
	5.2.2	Molding and curing method:	28
5.3	Joint	design	29
	5.3.1	Methodology overview	30
	5.3.2	Thickness build-up and overlap requirements	31
5.4	Joint	Manufacturing Test Campaign	34
	5.4.1	Goals	34
	5.4.2	Design	35
	5.4.3	Results	37
Chapt	er 6	Optimization Framework	. 41
6.1	Choo	sing an optimization approach	42
6.2	Optin	nization process	45
	6.2.1	Overview of relevant built-in Nastran modules	45
	6.2.2	Assessment of applicability of Nastran modules	46
	6.2.3	Ordering of the optimization sequence	47
	6.2.4	Discussion	50
6.3	Analy	/sis	51
	6.3.1	Requirements	51
	6.3.2	Considerations and FEA model setup choice	52
	6.3.3	Buckling analysis	55
6.4	Grou	nd structure module	57
6.5	Topo	logy optimization module	61
	6.5.1	Topology optimization theory and implementation	61
	6.5.2	Difficulties of using 1D elements in topology optimization problems	63
	6.5.3	Mesh independency scheme	66
	6.5.4	Modal Analysis in 1D Element Nastran Topology Optimization	66
6.6	Sizing	g optimization	68
	6.6.1	Scope of optimizer module and inputs	69
	6.6.2	Choice of optimizer algorithm	70
	6.6.3	Result interpretation: Convergence and achieving robustness	70
6.7	Shape	e optimization	74
	6.7.1	Shortcomings of built-in Nastran functionality for shape optimization	74
	6.7.2	Choice of optimization algorithm	74

Table of Contents xi

	6.7.3	Notes on operation	75
	6.7.4	Relevant design constraints during shape optimization	76
Chapt	er 7	Finite Element Analysis of joints	77
7.1	Goals	and approach	77
7.2	FEA	Results	82
	7.2.1	Strength Analysis	82
	7.2.2	Stiffness Analysis	86
7.3	Mome	ent balance and joint redesign	88
7.4	Conc	lusions	91
Chapt	er 8	Conclusions and Recommendations	95
8.1	Conc	lusions	95
8.2	Recor	mmendations	97
Refere	ences.		99
Appen	ıdix A	Joint manufacturing campaign layup	103
Appen	ıdix B	FEA Element type considerations	107
Appen	ıdix C	Beam modeling property derivation	109
Appen	ıdix D	Topology optimization initial element size sweep	113
Appen	dix E	Fluttering in Sizing Optimization	117

xii Table of Contents

# List of Figures

Figure 2.1 Result of a topology optimization for a motorbike frame (left) and a 'translation'	
of this solution into a printable design (right). (Source: Airbus APWorks)	5
Figure 2.2 Topology optimized aluminum bracket for a satellite antenna (Source: Ruag,	
Altair, EOS)	6
Figure 2.3 Anisogrid Structure as presented by Vasiliev	
Figure 2.4 2D optimization of a cantilever beam as presented by Ye et al	
Figure 2.5 Optimization of a cantilever beam for different input settings as presented by	0
Nomura et al. These beams are clamped on the left side, while a vertical load is applied	
on the right side.	Q
Figure 2.6 Ground structure (a) and optimized structure (b). Source: (Rajan, 1995)	
Figure 3.1 Schematic of A freeform composite structure	
Figure 3.2 Depiction of topology, shape and sizing manipulation principles	
	11
Figure 4.1 Topology optimization results with penalty method applied (b) and both penalty	
method as well as filtering applied (c). Note the checkerboard pattern in (b). Adapted	00
from (Labanda, 2015)	
Figure 4.2 Hollow bird bone structure (source: www.sciencepartners.info)	23
Figure 5.1 Schematic of hybrid tooling consisting of base tool and expansion tool (source:	٥.
Huybrechts et al.)	25
Figure 5.2 Adaptations from 25 bar sizing problem to structures reinforced with continuous	
(a) and interrupted fibers (b). Highlighted joint is shown in close-up in Figure 6.5	
Figure 5.3 Schematic of a standard 25 bar truss structure (source: Xiao et al. (2014))	
Figure 5.4 Overview of main material and process choices	28
Figure 5.5 Close-up of joint detailed design, note: thickness build-up has not been modeled	
here	29
Figure 5.6 Simplified node with full overlap (a) and after redesign (b)	30
Figure 5.7 Schematic representation of staggered drop-off strategy with four regions	31
Figure 5.8 Maximum fiber curvature reduction due to joint symmetry and drop-off strategies	
between members	34
Figure 5.9 Schematic of the joint manufacturing prototype design. Regions A through D	
denote different overlap zones. Widths are fixed at 6.3mm, heights are indicated	35
Figure 5.10 Base tool (left), 3D printed expansion tool mold (middle) and expansion tool	36

xiv List of Figures

Figure 5.11 Different stacking approaches for joints	36
Figure 5.12 V1 sample before (a) and after curing cycle (b), showing significant, asymmetrical	
thickness build-up	37
Figure 5.13 Joint test sample V2, showing better compaction and more symmetrical thickness	
build-up	38
Figure 5.14 Schematic illustrating local reduced joint compaction in case of compaction	
underestimation during expansion tooling design. The rib cavity in the expansion tool	
in (a) is too deep.	38
Figure 6.1 Schematic of a single member in red within an FEA model discretized as uniform	
squares for analysis of an isotropic material	42
Figure 6.2 Flow chart of optimization process	48
Figure 6.3 A bending beam, fixed on one end, guided and free on the other end, with a shear	
load applied	54
Figure 6.4 K-factors for different columns	55
Figure 6.5 Ground structure for a cubic design space, isometric (a) and front view (b)	59
Figure 6.6 Ground structure for a more complex design space with keep out zones	
Figure 6.7 Relation of Young's Modulus to material density for different penalization	
parameter values (p=1: no penalization)	62
Figure 6.8 Element Density Distribution of a topology optimization on a ground structure	
with 3736 elements with close to perfectly discrete 0/1 division	62
Figure 6.9 Topology optimization result (geometry) corresponding to the EDD in Figure 6.8.	
	64
Figure 6.10 EDD of a topology optimization identical to Figure 6.8, except with larger	
member cross sections.	64
Figure 6.11 EDD of a topology optimization identical to Figure 6.8, except with a smaller	
member cross sections.	65
Figure 6.12 Geometry corresponding to the EDD of Figure 6.11	65
Figure 6.13 Typical EDD for a modal analysis-based topology optimization result in Nastran	
for a simple structure	67
Figure 6.14 EDD of a purely static analysis-based topology optimization (left) and	
corresponding geometry after sizing optimization (right). Beam cross sections are not	
plotted to scale. Colors denote strain energy density: red is high, blue is low	68
Figure 7.1 Simple beam model, as applied in Optimization Framework (a) and boundary	
conditions and applied load for load case 1 (b)	79
Figure 7.2 Beam model result: $\sigma 11$ is displayed with the same color scale used in Figure 8.5	
Figure 7.3 FEA mesh of the solid model. Different colors denote different layups/fiber	
directions.	80
Figure 7.4 Section view of the joint as depicted in Figure 7.3. Note the individually modelled	
outer ply of member 2.	81
Figure 7.5 Result for load case 1 (compression of the main member): $\sigma 11$ plotted in the same	
color scale as Figure 7.2	82
Figure 7.6 The highest load factor for load case 1 occurs for tensile $\sigma$ 22 in the transverse	
member	83

List of Figures xv

Figure 7.7 Load Factor plotted for $\sigma 22$ in the transverse member, for load case 2 (max axial
tensile load on member 1)84
Figure 7.8 Load Factor plotted for $\sigma 22$ in the transverse member, for load case 5 (bending
load on member 2)
Figure 7.9 $\epsilon 11$ in beam model with both main members under compressive load of 10kN86
Figure 7.10 $\epsilon 11$ in solid model with both main members under compressive load of 10kN.
Fixed plane indicated in red86
Figure 7.11 Local rotation of the joint due to moment imbalance, undeformed shape displayed
as outline. Direction and approximate magnitude of input loads and reaction loads at
member ends indicated87
Figure 7.12 Schematic of moment-balanced joint, members numbered 1 and 3 are subjected
to compression loads (red). Reaction loads on members 2 and 4 indicated in orange89
Figure 7.13 Resultant moment due to axial member loads for each point of the initial joint
(a) and redesigned joint (b). Member numbers are indicated90
Figure 7.14 FEA result for redesigned joint, compression load of member 1 (right), compare
to Figure 7.591
Figure A.1 Joint Prototype V2 ply intersection design
Figure A.2 Joint prototype V2 layup sheet
Figure E.1 Schematic displaying load case and member numbering of sizing test problem $\dots$ 117
Figure E.2 Non-convergence due to design variable fluttering

xvi List of Figures

# **List of Tables**

Table 5.1 Selected material properties for Hexcel 8552 IM7	32
Table 6.1 Descriptor strings for nodes	58
Table 7.1 Strength (A-basis) and Stiffness properties for Hexcel 8552 IM7	81
Table 7.2 Load factors for load case 1: main load path member loaded in compression	83
Table 7.3 Load factors for load case 2: main load path member loaded in tension	84
Table 7.4 Load factors for load case 3: transverse member loaded in compression	84
Table 7.5 Load factors for load case 4: transverse member loaded in tension	85
Table 7.6 Load factors for load case 5: transverse member loaded in bending	85
Table 7.7 Load factors for load case 1: member 1 loaded in compression	90
Table 7.8 Load factors for load case 6: combined loading of members 1 (compression) and 2	
(compression)	93
Table C.1 Stiffness properties for Hexcel 8552 IM7	110
Table D.1 Topology optimization results for a range of initial element sizes	113

xviii List of Tables

### List of Symbols and Abbreviations

#### **Abbreviations**

CAD Computer Aided Design
DOF Degree Of Freedom

EDD Element Density Distribution FEA Finite Element Analysis

FPF First Ply Failure

FVF Fiber Volume Fraction
GA Genetic Algorithm

IPOPT Interior Point Optimization

MMFD Modified Method of Feasible Directions

MSCADS MSC Automated Design Synthesis
SLP Sequential Linear Programming
SQP Sequential Quadratic Programming

SUMT Sequential Unconstrained Minimization Technique

UD Uni-directional

VARTM Vacuum Assisted Resin Transfer Molding

### **Greek Symbols**

 $\epsilon_{11}$  Strain along the fiber direction

κ Shear Correction Factor

ν Poisson's ratio

ho Density  $\sigma$  Stress

 $\sigma_{11}$  Stress along the fiber direction

 $\sigma_{22}$  Stress transverse to the fiber direction

 $au_{12}$  In-plane shear stress

### **Latin Symbols**

A	Cross Sectional Area
b	Base of a rectangular cross section
E	Young's Modulus
$E_{11}$	Young's Modulus along the fiber direction
$E_{22}$	Young's Modulus transverse to the fiber direction
G	Shear Modulus
h	Height of a rectangular cross section
I	Area Moment of Inertia
J	Torsion Constant
K	Column Effective Length Factor
l	Length
P	Load
$S_{12}$	Maximum allowable in-plane shear stress
$S_{IL}$	Maximum allowable inter-laminar shear stress
$t_{ply}$	Ply Thickness
$X^c$	Maximum allowable compressive stress along the fiber direction
$X^t$	Maximum allowable tensile stress along the fiber direction
$Y^c$	Maximum allowable compressive stress transverse to the fiber direction
$Y^t$	Maximum allowable tensile stress transverse to the fiber direction

# Acknowledgements

I would first and foremost like to thank Samo Simonian, Leonid Pavlov, Michiel Vullings and all of my colleagues at ATG Europe for providing me with the opportunity to undertake this project and supporting me in various smaller and larger ways.

Special thanks are in order as well to Christos Kassapoglou. Thank you for agreeing to take up this project with me. Even before I started this thesis, you were the teacher who most challenged me to push harder. Your insight, work ethic and enthusiasm are inspiring.

I would also like to thank Sergio Turteltaub and Otto Bergsma for agreeing to be on my graduation committee.

I would like to thank Ivar te Kloeze for making himself available almost daily for tales about my latest ideas while being trapped in a car with me. I'm also grateful to you and many other friends for on more than one occasion spurring me on in my quest to obtain a degree by uttering that timeless creed that sums up the spirit of an impatient people: Duurt lang!

Thank you to my room mates who supported me throughout this whole ordeal while (almost) never complaining about my significantly reduced culinary output.

Finally, thank you to my loving family for always supporting me.

Delft University of Technology April 11, 2017

Thijs Papenhuijzen

"Nodeloos ingewikkeld..."

—ТР

# Chapter 1

### Introduction

A key assumption in this thesis is that for various applications in space industry and otherwise, lighter structures can be built by combining key aspects from two separate engineering fields:

- 1. The design freedom provided by 3D printing of metal structures, designed by using commonly applied isotropic topology optimization techniques.
- 2. The superior specific strength and stiffness of composites, as used in the types of regular grid structures described by Vasiliev et al. (2006) and Chapter 2 of this document.

ATG Europe has built up relevant knowledge in the second field by developing techniques that can be used to build so-called anisogrid composite lattice structures. This technology can provide efficient solutions for large load bearing structures, such as an inter-stage section in a rocket, measuring several meters in diameter and height, as well as smaller applications. The company is looking to expand these capabilities towards a more generalized approach for designing structures for load cases that are more specific and potentially more complex.

### 1.1 Background Information

Grid Stiffened structures have been around for a long time, having been mostly developed within the context of the Russian space program, notably in various publications by Vasiliev et al. (V. V. Vasiliev, Barynin, & Rasin, 2001; V. V. Vasiliev et al., 2006; V. V. Vasiliev, Razin, Totaro, & Nicola, 2005). The majority of these can be described as anisotropic grid composite lattice structures and are either planar or cylindrical/conical in shape. Figure 2.3 shows a typical example of such a structure, about which much has

2 Introduction

been published. Structures like these are versatile and can be used for a range of different applications in space structures, such as connecting elements between different parts of a rocket, as the central tube for a satellite, or as fairings, when combined with a skin.

The fact that such structures are cylindrical/conical is a direct result of their manufacturing method, which limits the design freedom for such structures, as described by Bakhvalov et al. (2009) and Totaro et al. (2012) among others. These manufacturing methods also limit the range of applications for structures that can be described as free-standing composite lattice structures. They cannot be currently applied to problems where any collection of free points in space need to be connected. Such technology would be useful for various applications. Many mechanical connections in satellites and other equipment which needs to be as light as possible, are made by milling a bracket out of aluminum billet. It is hypothesized that such structures could be replaced by a lighter part if the possibility existed to use the superior specific strength and stiffness that fiber reinforced materials offer. Other applications may include moving parts in wafer steppers, or various other machines that require low weight and inertia.

The current state of art is such that technology that addresses free form composites is vastly underdeveloped. There are two major obstacles to expanding the techniques used for building 'simple' planar and cylindrical structures to a completely free form 3D structure. First, the current state of art of composite manufacturing technology does not allow for placing (bundles of) fibers freely in space. Secondly, design techniques are lagging as well. Most current methods that optimize fiber reinforced structures deal with regular structures<sup>1</sup> and manipulate several geometrical design variables as opposed to thousands.

### 1.2 Research objective

The goal of this thesis can be summarized as follows:

Develop a framework for 3D composite structure optimization, within which manufacturability constraints can be implemented.

This technology is being developed as an assignment for ATG Europe. As such, it needs to fit into the context of, and where possible build on, their current state of knowledge with respect to design and manufacturing of composite structures.

A more precise formulation of the research objective is presented in chapter 3, and considers conclusions from a literature review. The outcome of this research can be highly relevant as it presents a new class of fiber reinforced structures that provides more design freedom than composite structures that are widely implemented today.

 $<sup>^{1}</sup>$  Regular in the sense of possessing orderly, periodic geometrical characteristics

Thesis Structure 3

### 1.3 Thesis Structure

A literature review presented in Chapter 2 assesses the current state of art of design and manufacturing of fiber reinforced composite free form structures. The following two chapters expand on the research objectives and project plan, and define the concept of optimality as used in the context of this thesis. Chapter 5 proposes a method to manufacture free form composite structures. Based on this, a design methodology is presented in Chapter 6 for such structures. Chapter 7 presents detailed Finite Element Analysis of some of the structures that have been proposed in Chapter 5. Chapter 8 presents conclusions and recommendations. Some test results and other additional information has been included in appendices.

4 Introduction

# Chapter 2

### Literature Review<sup>2</sup>

Most state of art structural design optimization methods for high performance applications are aimed towards one of two general categories:

- 1. Metal additive manufactured topology optimized structures
- 2. Composite grid structures consisting of curvilinear ribs in flat or singly curved planar arrangements

Despite having significantly differing densities, most metals that are used in high performance applications (i.e. typical magnesium, aluminum, titanium and steel alloys) have similar specific moduli, close to  $26 \frac{MPa}{kg/m^3}$  (or rather  $26 \cdot 10^6 \ m^2 s^{-2}$ ). High modulus carbon fiber composites on the other hand can exhibit far higher specific stiffness along the fiber direction, with values greater than  $180 \cdot 10^6 \ m^2 s^{-2}$ . Specific strength is significantly higher for fiber reinforced composites too. At the same time, additive manufacturing

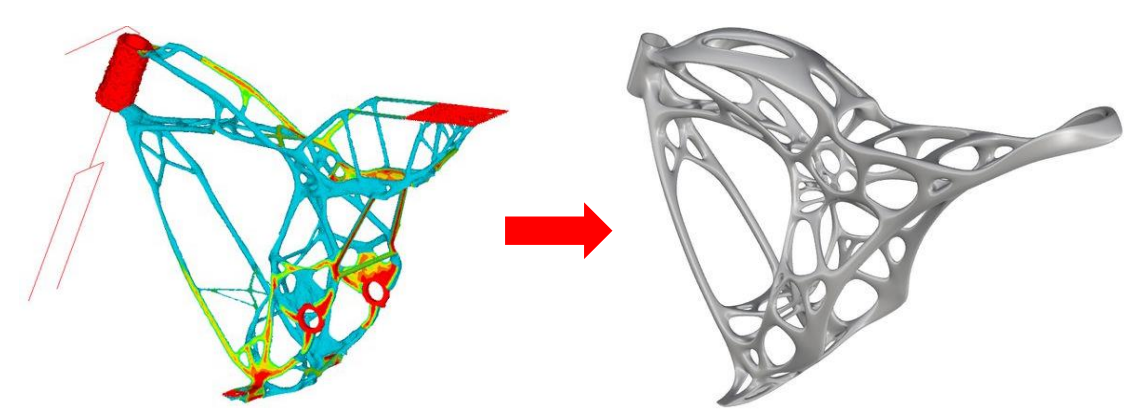


Figure 2.1 Result of a topology optimization for a motorbike frame (left) and a 'translation' of this solution into a printable design (right). (Source: Airbus APWorks)

<sup>&</sup>lt;sup>2</sup> This literature review has been written as a document that can stand on its own. For this reason, its introduction overlaps somewhat with the introduction of this thesis (i.e. Chapter 1).

6 Literature Review

provides increased design freedom compared to state of art methods for composite structures, granting the opportunity to connect free points in space in an efficient manner. Figure 2.1 shows an example of a structure that has been optimized for additive manufacturing. Especially the left figure, displaying the topology optimization result, shows that such a design problem leads to an open structure, many sections of which could be described as a collection of curvilinear ribs, albeit in far more complex arrangements than the one shown in Figure 2.3. Within this thesis, such open, rib-dominated layouts will be characterized as *skeletal structures*. Another example of such an open structure can be



Figure 2.2 Topology optimized aluminum bracket for a satellite antenna (Source: Ruag, Altair, EOS)

seen in Figure 2.2, which shows a bracket for a satellite antenna, for which the critical design constraint is a specified Eigen frequency lower bound.

The goal of this thesis is to present an optimization method for structures that can approach the design freedom offered by additive manufacturing methods while making use of the superior specific properties of fiber reinforced composites. The following observations are made.

- 1. Fiber reinforced materials are highly anisotropic, i.e. maximum strength and stiffness can only be taken advantage of along the fiber direction
- 2. Skeletal arrangements are suitable for a wide range of complex design problems in the context of highly optimal metal structures

In order to constrain the goals within a manageable frame in the context of a graduation thesis, the choice is made to develop a method for designing and optimizing composite skeletal structures, i.e. structures that can be described as a collection of curvilinear members. The two observations made above lead to the premise that such layouts can provide more efficient structures than the current state of art, by recognizing that skeletal arrangements are especially suited for taking advantage of the characteristics of fiber composite materials.

Most previous publications review a focused field, and few attempt to bring together the two separate aspects of composite structure optimization and design problems where free points in 3D space are connected. Many groups have published on the subject of topology optimization, but very few have done so with the use of highly anisotropic materials in mind. Rather, the vast majority of topology optimization research results in structures that are well suited for additive manufacturing. Therefore, this chapter will first review separately the state of art in composite structure optimization. The next section addresses modeling approaches within optimization methods that may exhibit greater freedom than the current state of art for composites optimization. Conclusions are presented in the final section.

### 2.1 State of Art of optimization methods for composite structures

Topology and shape optimization for structures built out of isotropic materials has seen great development in recent years, in conjunction with advances in rapid manufacturing that allow for unprecedented degrees of design freedom.

Much research in recent years on structural optimization of composites has been undertaken in these three categories:

- 1. Sizing/Shape optimization of grid stiffened structures
- 2. Layup optimization of fiber-placed variable stiffness planar or conical structures
- 3. 2D topology optimization of fiber reinforced structures

This section will provide a brief overview of those fields, with a focus on which aspects are transferrable to development of 3D skeletal structures.

#### 2.1.1 Sizing and Shape optimization of grid stiffened structures

As noted in the introduction of this thesis, much has been published on the topic of anisotropic grid composite lattice structures, notably by Vasiliev et al. (2001, 2006; 2005).



Figure 2.3 Anisogrid Structure as presented by Vasiliev

The height and width of lattice members in such structures may be varied according to

8 Literature Review

the load conditions of the structure (sizing optimization). The directions of lattice members are other design variables, and can be considered the shape parameters in this type of structure. Anisogrid structures are suitable for a range of functions, yet the leading principles largely limit these techniques to application in planar and conical sections. To a large extent, the topology of such a structure is fixed at an early stage in design. The leading surface is often not subject to design optimization (e.g. the surface of the cone describing the structure in Figure 2.3 is required to connect the top and bottom ring and is therefore fixed). Therefore the only topological design freedom that applies to this type of structure is the spacing between individual lattice members. For this reason, the leading design optimization principles give rise to regular, repeating structures, and are not directly transferable to a full 'free form' approach. However, much knowledge has been accumulated by the same group of researchers on the topic of manufacturing of grid stiffened structures, which will be referred to in Section 5.1.

#### 2.1.2 Layup optimization for planar or conical structures

A related field of research focusses on layup optimization of variable stiffness composite structures (Blom, 2010; Ijsselmuiden, 2011; Van Campen, 2011). Such structures are typically manufactured using advanced fiber placement. This provides some degrees of design freedom that anisogrid structures do not typically exploit, as they generally have straight members. The introduction of fiber placement makes variable stiffness structures possible with finely tunable in-plane behavior. However, with respect to transferability of techniques to application in 3D free form composite structures, many of the same observations can be made as for grid stiffened structures: To a large extent, the design freedom is limited in the sense that the shape and topology of the structure is fixed from the start, except for the possible introduction of holes. As for anisogrid structures, the main surface describing the shape of the structure is typically flat or (a section of) a cone or cylinder, and not subject to change. This limits applicability of current techniques to structures where it is clear a priori that they are appropriately described using a single surface.

#### 2.1.3 2D topology optimization of fiber reinforced structures

Some publications deal with actual topology optimization. For example (Ye, Chen, & Sui, 2010) present an approach in which base structures consisting of plies with different directions result in radically different topologies when optimized to exhibit a desired harmonic response (i.e. a certain natural frequency) as can be seen in Figure 2.4. Unfortunately, the results do not extend beyond very simple 2D planar structures subjected to a single load. The applicability of this technique is fairly limited, due to its narrow scope. Also, the resulting structures are not particularly efficient, as they are created by

making cut-outs from UD-plies that may or may not be locally aligned with the principle load direction of the structure.

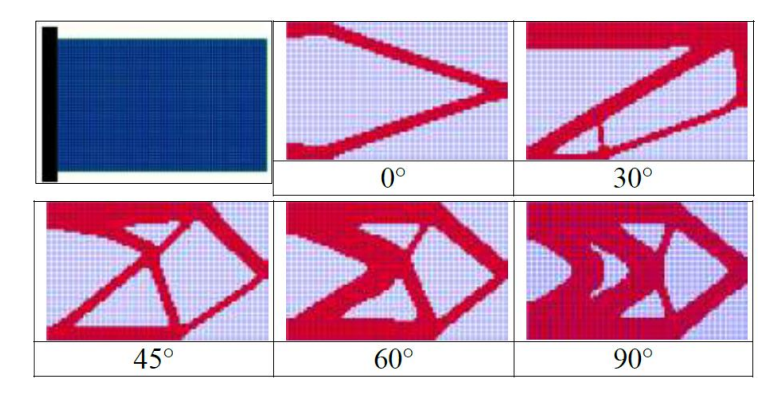


Figure 2.4 2D optimization of a cantilever beam as presented by Ye et al.

More relevant is recent work by Nomura et al. (2014) of the Toyota Central R&D Labs who have developed a method which simultaneously varies density and orientation of an anisotropic material. Results of this method can be seen in Figure 2.5.



Figure 2.5 Optimization of a cantilever beam for different input settings as presented by Nomura et al.

These beams are clamped on the left side, while a vertical load is applied on the right side.

These results were published in 2015, and the authors have indicated that they aim to eventually expand the method to be able to design 3D structures. This expansion effectively involves adding an additional design variable to describe the direction at each location. Also, the number of design nodes in the discretized design space increases drastically due to the addition of a third dimension, making this an ambitious project. Several intermediate steps have been proposed by the group to gradually get to this point. The first two being:

- 1. Layer-by-layer design for a multilayer 2D orientation design
- 2. Orientation design on 3D surfaces, which would expand the work to be implemented for e.g. conical structures, or more complicated surfaces.

Further steps beyond these two are necessary to actually achieve full 3D design freedom. As of early 2017, no further research has been published by this group.

Their work on 2D structures is innovative and presents a powerful optimization technique which results in efficient structures by implementing actual topology optimization while facilitating use of continuous fibers. However, the complexity of this technology and its current state of development prevent it from being readily adapted to more complex, 3D structures, as acknowledged by Nomura et al. as well.

10 Literature Review

### 2.2 Approaches to modeling 3D composite structures

A great difficulty in modeling composite structures is that many techniques that are used for isotropic topology optimization cannot be easily extended to optimization of a structure that is built up out of materials with highly anisotropic properties, such as fiber reinforced polymers which commonly exhibit stiffness and strength in the fiber direction several orders of magnitude larger than they do in transverse direction. Simply put, a topology optimization scheme for a design problem with an isotropic material will apply the prescribed load case to a discretized solid block that is shaped according to the full design space that is available. It will then assign different densities to different mesh elements according to how much they contribute to the overall stiffness of the object. Wherever element densities are sufficiently low, the algorithm may remove them completely, thus effectively removing material until only the areas are preserved which are most useful towards fulfilling the boundary conditions. Sigmund et al. (2013) provide a concise overview of different optimization approaches, and much other literature has been published on this subject (Bendsøe & Kikuchi, 1988; Bendsøe & Sigmund, 2003; Sokolowski & Zochowski, 1999; Wang, Wang, & Guo, 2003; Xie & Steven, 1993).

A fiber reinforced structure however, has crucial extra degrees of freedom in its design variables. Rather than just local density of elements (which may be either 1 or 0 for a usable final result, or any value in between for preliminary results), a fiber direction is also required for every location. In order for a 'simple' topology optimization scheme to be applicable to a fiber reinforced 3D structure, the base material must already contain

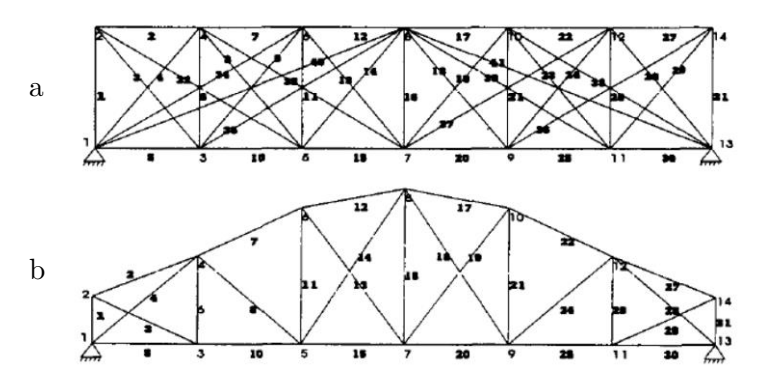


Figure 2.6 Ground structure (a) and optimized structure (b). Source: (Rajan, 1995)

the correct fiber directions at every point in the design space. This is of course not possible, as this direction is unknown beforehand, and is itself a design variable. A different approach is therefore needed.

Much has been published within the civil engineering community on optimization of truss structures, the building blocks of which are by definition highly anisotropic, as they can only be loaded axially. To the extent that a fiber reinforced structure can be described

as collection of trusses, the approaches described by various groups (Adeli & Balasubramanyam, 1987; Balling, Briggs, & Gillman, 2006; Rajan, 1995) may be very useful for reaching a high degree of optimality. They describe an optimization scheme that makes use of a ground structure, which is built up from a collection of trusses in multiple directions, between a set of nodes, see Figure 2.6. The algorithm is allowed to both shift the nodes and change the thickness of individual members, or delete them altogether. Oftentimes, in such problems, one of the crucial boundary conditions is that individual members may not buckle. Because of this, many local minima exist in the design space, where a member is assigned a certain minimum cross section, as a slightly lower thickness would cause buckling. A gradient based sizing method would likely not consider the complete deletion of the member, even though that is a crucial function of a design optimizer operating on a ground structure. This is one of the reasons that genetic algorithms have proven to be a powerful tool within this approach for this class of problems, where topology optimization is actually implemented within a sizing optimizer by accepting a zero-cross section as a member sizing solution. This approach and others have also been applied to 3D structures, as described by many research groups (Habibi, 2011; Kirsch & Topping, 1992; Soh & Yang, 1996).

The advantage of using ground structures as a starting point for optimization of a composite structure appears to be significant: It allows for topology and shape optimization of structures built out of highly anisotropic materials.

A disadvantage is that in its proposed form, this approach can only describe structures that are completely built up out of trusses. As such, other shapes such as webs cannot be considered as solutions. Further investigation will be needed if we are to determine whether this is a problem that needs to be addressed at this stage of development, i.e. can structures already be sufficiently close to 'optimal' as compared to current solutions while only describing them as collections of trusses? If this turns out to be a significant area of investigation, are there feasible ways of including more complex substructures than trusses, either in the initial optimization, or at a later stage?

In assessing the current state of art of design and manufacturing of composite free form skeletal structures, we can conclude that they are still underdeveloped, specifically in terms of design methods, in that no methodology has yet been developed which can robustly come up with a fiber reinforced composite-based solution for a design problem where the optimal solution has a more complex shape than a simple tube or cone. It was further found that in civil engineering there has in recent decades been much research into optimization of truss structures, which opens up a route to optimization of 3D structures with highly anisotropic elements. It is recommended that further research is done with respect to the feasibility of using a ground structure-based topology-, shape- and sizing optimization method for composite 3D skeletal structures.

12 Literature Review

### 2.3 Conclusions

Up to now, very little has been published on the subject of optimization and manufacturing of 'free form' composite skeletal structures. There is no generalized approach for creating designs for 3D structures that exploits the properties of fiber reinforced materials. Many studies in the aerospace industry have researched the design and production of regular anisotropic grid composite lattice structures, which serve as a starting point for this research. From a conceptual point of view however, inspiration can be drawn from work in the civil engineering industry, where much has been published on optimization of truss structures.

Within this thesis, a method will be developed that can help in designing structures that fall in a new class of composite structures, through topology- shape- and size optimization of structures with anisotropic elements, with the aim of minimizing weight. Figures 2.1 through 2.3 in this chapter indicate the current bounds of the state of the art. The aim is to develop structures that provide more design freedom than conventional grid stiffened structures, which are mostly restricted to cylindrical or conical forms, while providing better stiffness-to-mass and strength-to-mass ratios than what is available using advanced currently available design and manufacturing methods: 'conventional' isotropic topology optimization combined with additive manufacturing. Further developed, this technology could find applications in space- and other high-end industries.

# Chapter 3

# **Project Objectives**

This chapter presents a narrower focus of the thesis compared to its introduction by reformulating the research objective and laying out a set of research sub-questions.

### 3.1 Focus of Research

As noted in Chapter 1, one of the assumptions in this thesis is that lighter structures can be built if two aspects of current technologies are brought together:

- 1. The design freedom and optimization approaches provided by topology optimization methods
- 2. The building techniques as developed for fiber reinforced grid structures and the superior specific material properties that such structures exploit

Before discussing modeling and subsequent optimization approaches in the next chapters, it is important to define the type of structure for which a design framework will be developed. Analysis of common load carrying structures (whether they are built out of composites, metals or otherwise) allows us to identify several base features, or building blocks that can be used to describe them, such as:

- Solid, beam-like sections that accommodate the major load paths in a structure
- Joints that connect such beams
- Alternatively, load carrying 'solid sections' that accommodate the full load.
- Thin skin sections that provide some load carrying capability, but act primarily as shear plates or provide a method to create a closed space
- A variation on such skin sections is when several load-bearing skins combine to form a torsion box or bending beams

• Connections to other structures. These are the load introduction points and can take different forms, depending on the type and magnitude of the load, the shape of the structure and the shape of the structure that it connects to

It is beyond the scope of this work to incorporate all these base features into one overarching design method. Instead, a combination of building blocks needs to be chosen that will meet the following set of requirements:

- 1. The elements provide the means to develop a wide range of varying structures, for different types of load cases and shapes
- 2. The elements can be sufficiently described by a set of design variables that can feasibly be used in an optimization method
- 3. They need to provide the means to describe structures that can be lighter than current technologies allow
- 4. The whole project should reasonably produce relevant results within the scope of a master thesis
- 5. As noted in the introduction of this thesis, the results from this research need to slot into the greater context of technologies that have been developed by ATG.

  The main focus of their research has been on the following technologies:
  - a. Grid structures without skins, similar to those seen in Figure 2.3, both with pre-impregnated fibers as well as with resin transfer techniques
  - b. Grid structures with skins. Development specifically focused on node design and rib-to-skin adhesion
  - c. Load introduction into such structures. Load introduction points often take the form of a solid, monolithic section that is incorporated into the overall grid pattern. Research is primarily focused on how these local loads or edge loads transfer into the larger structure, and how to manufacture such sections

Besides itself being a requirement set by ATG, building on this knowledge works towards meeting requirement 4.

Taking into account the above, the choice is made to focus on truss structures that can be fully described by using solid beam-like members with constant rectangular sections, connected by joints.

This meets the above goals and requirements in the following ways:

- 1. Trusses can be used to build a wide variety of types of structures in an efficient manner
- 2. A truss structure can be fully described parametrically purely by defining joint locations and cross sections of the members connecting them. This works towards making manipulating the structure for the purpose of finding an optimum a feasible task.
- 3. Even more so than isotropic materials, fiber reinforced materials are more efficiently used in pure tension-compression as compared to bending. Beam sections provide a means to describe a structure in which all elements are loaded primarily in tension-compression, which is what an ideal composite structure would be expected to be. See also Section 4.2.
- 4. The significant reduction in modeling complexity that is achieved by not implementing the tools to describe and manipulate solid monolithic sections makes it more realistic to explore the full design space of the problems that are presented, and hence come to useful results within the time frame of a master thesis. Manufacturing is also simplified, meaning that achieving a proof of concept is more feasible.
- 5. A beam structure builds on the developments that have been made within ATG with respect to skinless grid structures. The fact that ATG also has experience with skinned grid structures means that there is a lower bar for future expansion of the research presented in this thesis by implementing shear plates which, like beams, are 'building blocks' that make efficient use of the specific properties of fiber-reinforced materials.

## 3.2 Research Objective

The objective as presented in the introduction of this thesis can now be formulated more precisely:

To develop a methodology for designing optimized free form (3D) composite skeletal structures.

Where a *skeletal structure* is understood to be a structure as seen in Figure 3.1, consisting of various constant section elements between joints.

A method will be developed that can help in designing such structures, which fall in a new class of composite structures. They will provide more design freedom, and result in solutions that provide better stiffness-to-mass and strength-to-mass ratios than what is available using current design and manufacturing methods.

The aim is to include manufacturing constraints, combined with robust and where needed new building methods to ensure manufacturability of the final designs that this framework will produce. This research objective can be split up in different sub questions. The most critical ones are mentioned in the overview presented below.

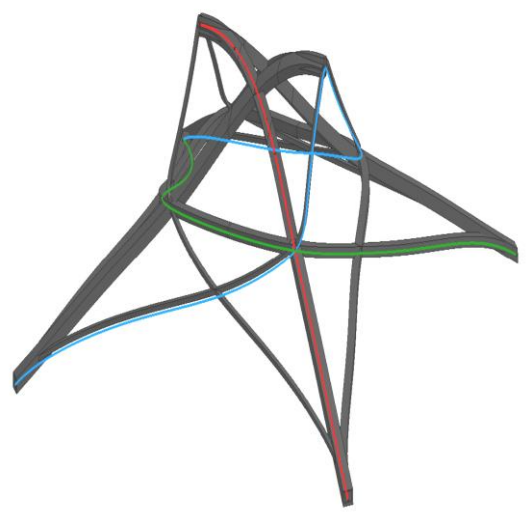


Figure 3.1 Schematic of A freeform composite structure

#### Research Sub-Questions

#### 1. How to analyze such a structure?

The goal is to use MSC Nastran simulations to analyze the skeletal structures. This is a requirement from ATG. Research will be needed to determine the proper way of describing them for the purpose of the sensitivity studies that will be used for the optimization process. Structures will primarily be optimized based on their performance with respect to weight and their performance in modal analyses, specifically the frequency of their first mode.

### 2. Is a ground structure approach an effective way to solve this problem?

From the Literature Research presented in chapter 2, the proposal has developed to focus this research on using ground structures as an optimization starting point, which contains many members in various directions, representing possible fiber directions that may be present in the final design. However, only after a higher level of maturity of the optimization method can we be certain that this is indeed the best way of approaching this complex problem.

### 3. Which variables should be changed?

The current goal is to come to an optimum by changing:

- topology (whether an element connects two joints)
- shape (the location of individual joints)
- sizing (the dimensions of the cross sections of individual connecting elements)

As depicted in Figure 3.2. Research must be done into determining an efficient method to perform these steps using Nastran and Python.

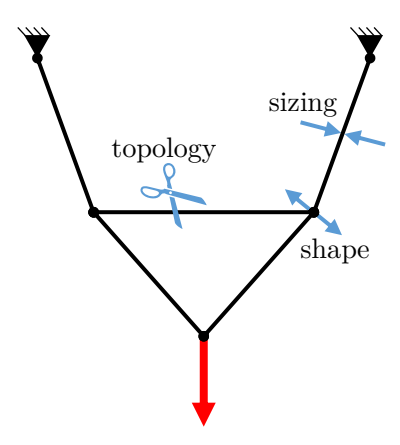


Figure 3.2 Depiction of topology, shape and sizing manipulation principles

#### 4. How to develop a method that reliably finds the global optimum?

A key challenge for any optimization scheme is not to 'get stuck' at a local minimum that delivers a significantly worse result than the global optimum. Different classes of optimizers are available which approach this in very different ways. Some schemes, such as Genetic Algorithms, incorporate a measure of randomness. In effect, this provides greater freedom to explore the entire design space and can be a powerful tool especially in the case significant non-convexity of the design space. For other problems however, it can be more efficient to incorporate a Mathematical Programming-based method and/or use a gradient based approach. Although it may be difficult to build an optimizer that can reliably find the global minimum in a complex design space, methods are available to determine how it performs in this respect. These focus primarily on feeding a design problem to which the solution is known. This could for example be a complicated initial ground structure for a relatively simple problem for which the optimum answer is trivial for a human designer.

#### 5. How to manufacture 3D composite skeletons, specifically the joints?

As noted in the literature review, most grid stiffened structures are highly regular in shape, being almost exclusively planar or cylindrical. This makes manufacturing them a controllable exercise, though still quite difficult. A structure that consists out of a monolithic collection of ribs in free space is much less trivial still. A manufacturing method for building such structures will be proposed in chapter 5. The focus here is on how to transfer the loads between individual elements, i.e. design and manufacturing of joints.

# 6. How to properly formulate and implement manufacturing constraints within an optimization framework?

Several methods are proposed to control the optimization framework in such a way that it works towards final designs that are feasible in terms of manufacturability.

## 3.3 Expected Outcome

This research aims to have two main results:

- 1. A design method which optimizes a ground structure using shape-, size- and topology optimization, towards a structure that can be manufactured out of a carbon fiber reinforced polymer.
- 2. A manufacturing method that can provide the type of structures that are being designed.

Simply put, the results of this research will be the answers to the research questions that were presented in Section 3.2. The aim is to provide an adequate demonstration of the effectiveness and reliability of the optimization scheme, as well as the manufacturability of the final proposed types of structures.

The outcomes can be assessed in a number of ways, to determine if the types of structure that the method produces fulfill the functions and requirements that have been set:

#### 1. Robustness analysis

How sensitive is the method to its initial condition? In other words: Can the method come up with the same solution, even if a less sensible initial condition is fed into the algorithm.

#### 2. Analysis of the efficiency of the optimization method

How long does it take to fully design a structure? How quickly does the method come within 5 percent in terms of weight of the fully converged solution? Efficiency is considered less critical than the first two requirements, especially for earlier iterations of the framework, as long as results can be delivered within a reasonable amount of time. For an industrial project, a computation time of two weeks may still be acceptable if that is a one-time analysis which produces useful results.

To prove the feasibility of the proposed manufacturing method, several proto samples will be produced to demonstrate various aspects of the overall methodology, primarily:

- 1. How to create a structure consisting of 'free beams' in 3D space.
- 2. How to ensure proper load transfer between independent carbon fiber members

It should be noted that the main focus of this research is on the design and analysis section, rather than the manufacturing part.

## 3.4 Optimization Framework requirements

This sections summarizes the main requirements that are set for the Optimization Framework which is presented in Chapter 6.

- 1. Any FEA functionality should make use of MSC Nastran, for reasons of availability at ATG, as well as acceptance within the space industry.
- 2. The Optimization Framework should provide the option of accepting as input the following parameters:
  - attachment/load introduction points
  - loads
  - connecting (point) masses/inertias
  - keep-out zones
  - available tape widths
  - strength requirements
  - stiffness requirements
  - modal requirements
- 3. The Optimization Framework will manipulate structures by carrying out optimizations with respect to topology, shape and size. For each of these operations, different tools will be required to carry out the associated manipulation.

# Chapter 4

# **Optimality**

It is important to define the term 'optimality' as it is used in this work. Within this thesis, there are three distinct levels at which this concept can be considered. At those separate levels, achieving optimality can be translated into the following goals:

#### 1. Sub process level

To design the processes that form the basis of the structural optimizer such that they robustly contribute to higher-level optimality

#### 2. Structural Optimizer level

To develop a design that is 'as good as possible' from a perspective of structural efficiency and manufacturability.

#### 3. Project level

To deliver an end result that is as valuable as possible within the scope of the project and the time available

This chapter discusses the use of the term at these separate levels in more depth.

## 4.1 Sub process level Optimality

This thesis presents a framework within which composite structures are designed. To accomplish this, several sub processes have been developed to perform separate operations, notably topology, shape and sizing optimizations. These processes work in sequential as well as nested configurations. Within the scope of each of these individual processes, the term 'optimal result' is narrowly defined as:

'The lightest possible solution which complies with all constraints'

22 Optimality

Each sub process provides a different toolset. When used in a complementary fashion within a larger framework, these can combine to provide higher level optimality, as described in Section 3.1. To this end, each of these processes need to be capable of performing optimizations on their own level in a provably reliable and robust fashion.

This can be done in theory, and it can be at least approached closely in practice. However, the extent to which such results actually contribute to a higher level optimal result greatly depends on how these processes are combined, and what their constraints and starting points are.

These processes are described in greater depth in Chapter 6.

## 4.2 Structural Optimizer level Optimality

The structural optimizer is the context that is generally referred to when discussing the term 'optimality' (e.g. in the title of this thesis), albeit often implicitly so. It is at the same time also the context within which the term is the hardest to define. As a starting point, it is safe to assume that, for a specific load case, a structure where each element is loaded close to its maximum allowed stress, as well as in an efficient manner (tensile/compression rather than bending), will be lighter than a structure where this is not the case.

It should be recognized that theoretically optimal structures can generally not be realized physically. Often, the lightest possible solution would call for a material with varying density, i.e. continuously varying microstructures, or countless hair-thin branches of ma-

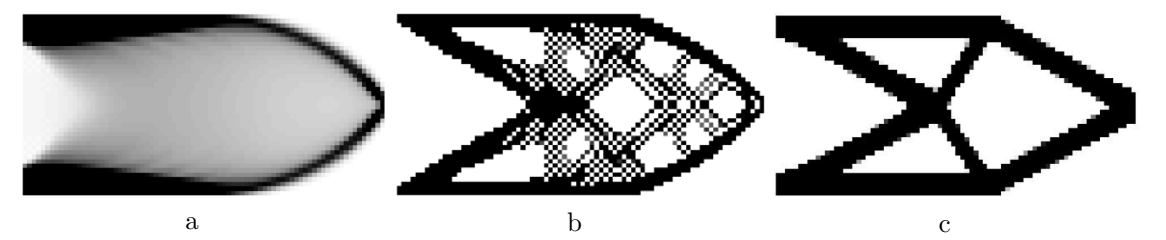


Figure 4.1 Topology optimization results with penalty method applied (b) and both penalty method as well as filtering applied (c). Note the checkerboard pattern in (b). Adapted from (Labanda, 2015)

terial. In many common topology optimization methods, this is actively counteracted by applying penalty methods, forcing elements to take a value of either 0 or 1. Further filtering methods may need to be implemented to prevent checkerboard patterns where locally areas within the structure are filled alternatingly with 1- and 0-elements in a way that effectively still results in a section that is closer to a 0.5 density on macro scale. This principle is shown in Figure 4.1.

In nature, this is no different. Figure 4.2 shows the hollow bone of a bird which on larger scale can be considered a 'low density' element. On a smaller scale however, it is clear that the structure is analogous to what in topology optimization is achieved through filtering schemes, as dis-



Figure 4.2 Hollow bird bone structure (source: www.sciencepart-

played in Figure 4.1 c: many smaller elements fill an otherwise empty void, but there is a lower boundary to how thin these elements become. 3D printing technologies are already close to providing similar levels of design freedom for polymers and metals, and future developments in this area will likely push further in terms of miniaturization of the smallest features that can be built, to the point where materials can be made that can for practical purposes be considered to have continuously variable density. However, stiffness and especially strength of a fiber reinforced structure rely to a large extent on a degree of continuity of the fibers. Therefore, even more so than current polymer and metal structures, fiber reinforced structures must be optimized using strategies that result in solid sections, as opposed to checkerboard patterns or densities between 0 and 1.

It is clear that a manufacturable design demands a degree of practicality that requires compromise with respect to optimality of a structure in the strictest sense. There are certain characteristics that can be expected of a structure that is close to optimal, such as:

- There should be efficient paths for the loads that are introduced. Those paths
  can be expected to be such that elements are primarily loaded in tension and
  compression, and bending loads are minimized.
- The observed strain energy density is close to uniform throughout the structure.

A manufacturable design on the other hand may exhibit the following characteristics:

- Individual members have a certain minimum width
- Sharp curves in individual fibers are avoided

The outcome of this trade-off is not fixed a priori, rather it follows from findings in this thesis, although it can be expected that the result will be closer to what is depicted in Figure 4.1 c as opposed to Figure 4.1 a.

24 Optimality

## 4.3 Project Level Optimality

There is currently no generalized approach to designing and optimizing a 3D, freeform composite structure. The goals set for this thesis must be realistic in taking this into account. It is understood by ATG that it is beyond the scope of this research to fully implement lower level optimality as defined in the previous two sections. Rather, as set forth in chapter 3, the goal is to build a method that can serve as a framework for different types of optimization, while taking into account manufacturability. Within this context, optimality of the final result is not primarily judged by the efficiency of an individual structure that may have been optimized, but rather by how comprehensive and applicable the underlying framework is, and whether its results are realistic and executable.

# Chapter 5

## Manufacturing

This chapter lays out how a non-regular (as opposed to the regular isogrid structures presented in earlier work), or freeform, truss structure can be manufactured and presents a proof of concept. The primary focus is on methods to design and manufacture the joints. Mold design is a significant subject in this context. Manufacturing test results are presented. Different types of structures that can be built are considered.

## 5.1 Grid Structure Manufacturing Methods

Much has been published on the topic of manufacturing grid structures. A widely-applied method involves hybrid tooling, as presented by Huybrechts et al. (2002) among others. A rigid base tool is combined with expansion tooling. The base tool is made from a thermally stable, hard material with grooves. Typically a metal is chosen, although epoxies have also been used. The expansion tooling is made from a material with a high coefficient of thermal expansion and

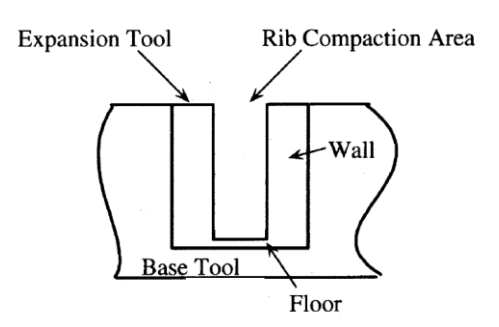


Figure 5.1 Schematic of hybrid tooling consisting of base tool and expansion tool (source: Huybrechts et al.)

is laid into the grooves of the base tool. Silicon rubber is often used. The crucial feature of this method is that the expansion tooling provides lateral compaction of the ribs during curing, while the base tool provides high positioning accuracy of individual sections.

ATG Europe has significant experience with this method and its most crucial aspects, like the theory behind the exact sizing of the expansion tooling. Most of their focus has been on using pre-impregnated carbon fibers to build autoclave-cured flat structures (i.e. featuring a 2D rib pattern), or sections of a cylindrical structure which can be built using

similar techniques (Maes, 2015; Smeets, 2016; te Kloeze, 2015). A caul plate was used to provide the amount of pressure deemed necessary locally to compact the nodes where ribs cross.

Previous efforts by ATG have been focused on maximizing the specific strength of the rib structures by achieving a fiber volume fraction that is as high as possible by combining various methods (autoclave pressure along with a caul plate) to achieve maximum pressure in relevant areas. Fiber volume fractions between 62% and 65% were achieved in different sections of those structures, compared to a datasheet value of 59.9%.

Conversely, in the context of this thesis, the aim is to adapt the core principles of the method described above and apply them to truss structures to provide a proof of concept to show that the types of structures that are proposed can indeed be manufactured. To that end, rather than immediately aiming for the highest possible fiber volume fractions, the prototypes presented in this work aim to show what is the *simplest and cheapest way* to build a skeletal composite structure that will still provide a result of sufficient quality. This approach recognizes that some of the aspects of the manufacturing method described above are not easily transferable to a fully 3D freeform shape. Importantly, the 3D equivalent of a simple flat caul plate for a 2D grid shape would be a complex shape (effectively a fully matched mold), for which expensive milling operations would be required to achieve the required tolerances.

### 5.2 Process- and material selection

Decisions have been made with respect to the following manufacturing aspects. As often when making such considerations for a composite structure, these choices are to an extent dependent on eachother. A key point to concider is how to drape the fibers in different scenarios.

As an example of the type of structure we want to be able to build, consider the 25 bar structure in Figure 5.3 that is often used as a standard sizing problem. In this problem, two loads in negative z-direction and negative y-direction are applied to nodes 1 and 2. Figure 5.2 shows two interpretations of what such a structure might look like when manufactured as a monolithic carbon fiber structure with square members. The cross sections have been adapted from a size optimized solution.

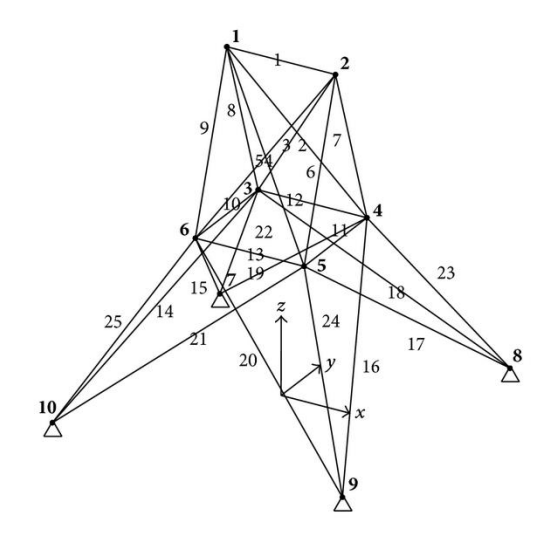


Figure 5.3 Schematic of a standard 25 bar truss structure (source: Xiao et al. (2014))

Figure 5.2 a shows a structure with continuous fibers. The red, green and blue line denote the bundles of continuous fibers. Figure 5.2 b shows a structure where every individual element is built out of a separate stack of fibers, as denoted by different colors. The structure on the left consists out of eight fiber bundles in total. The structure on the right constists out of 25 bundles. This section lays out how a decision was made between these two fundamentally different approaches, and how this follows from process- and material selection.

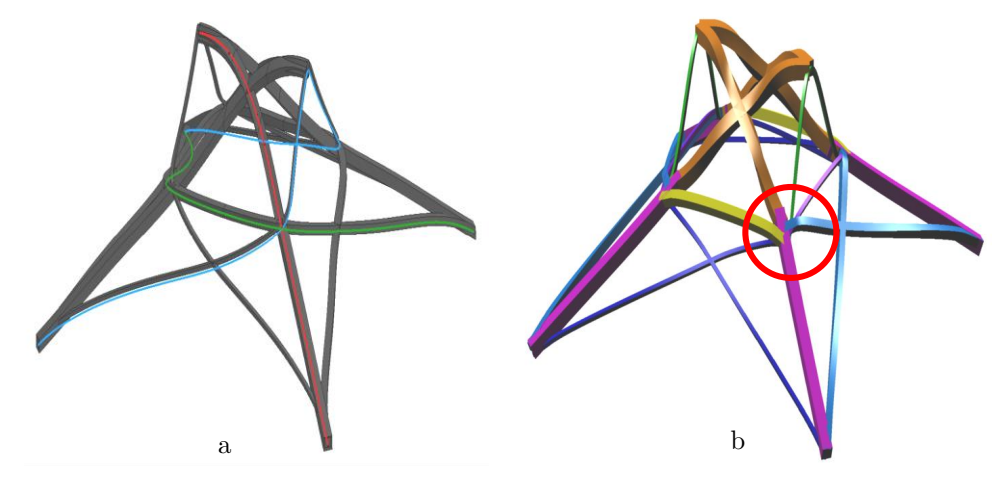


Figure 5.2 Adaptations from 25 bar sizing problem to structures reinforced with continuous (a) and interrupted fibers (b). Highlighted joint is shown in close-up in Figure 5.5.

### 5.2.1 Material type and draping method

It seems like an elegant method to have long continuous fiber bundles along the entire length of major load paths in the structure. However, these structures have many sharp bends in different directions. Pre-impregnated tapes are not suited for this kind of geometry, since only very slight radii can be realized when laying up a member that is bent

in-plane relative to the individual tapes. In the same frame of reference, out-of-plane bends can be made much tighter, but bends will occur in both directions. There are two ways to approach this problem:

- 1. Dry fibers can be used to build a structure as shown in Figure 5.2 a, with relatively sharp curvature in both directions (over the y- and z-axis when considering a regular local axis system for a members). However, previous tests at ATG have shown that grid structures with slender members built using a VARTM method achieve fiber volume fractions closer to 40% in ribs, and approaching 60% in nodes, as compared to close to, or even exceeding 60% which can be achieved with pre-impregnated fibers throughout the structure. The injection process is hard to monitor and control for monolithic sections. Even when accepting higher resin content throughout the structure, and creation of resin pockets, it is difficult to fully eliminate dry spots, specifically near joints, where compaction may be higher.
- 2. Pre-impregnated fibers provide significantly higher fiber volume fractions without the risk of dry sections. They can be applied to achieve a structure that is similar to that in Figure 5.2 b. In this concept, fiber bundles are terminated at joints where they meet other fiber bundles. Section 5.3 expands on the design of such joints.

The choice is made to design for pre-impregnated fibers with the goal of achieving structures with the highest possible specific properties.

### 5.2.2 Molding and curing method:

As noted in Section 5.1, previous manufacturing campaigns by ATG made use of caul plates and an autoclave to achieve maximum compaction in an effort to maximize fiber volume fractions. This compaction concept can likely be translated to a generalized 3D

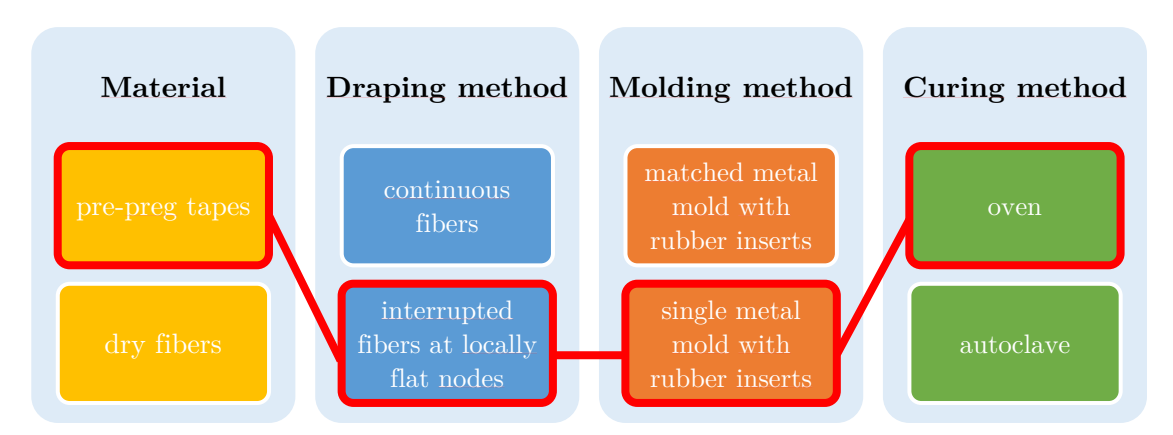


Figure 5.4 Overview of main material and process choices

Joint design 29

approach by using matched metal molds. Within this thesis however, the goal is to demonstrate feasibility of the overall design approach, rather than optimizing each individual aspect of production. The complexity and therefore cost involved in a matched mold approach is significant. Instead, the decision is made to apply a method that is close to the method shown schematically in Figure 5.1, with a vacuum bag directly on top of the product. Figure 5.10 shows this approach implemented for the joint prototype that is presented in Section 5.4. In line with this approach of experimenting with a simpler, cheaper method before determining that a more costly technique is warranted, an oven curing cycle is selected for production of the initial prototype. The use of rubber mold inserts presents great design freedom, as these can be manufactured using 3D printed molds. The flexibility of the rubber also means that the full mold assembly does not need proper release angles, accommodating for relatively complicated curved sections without increasing the manufacturing complexity of the molds. Section 5.4.3 presents the findings of the manufacturing campaign with respect to the suitability of the method presented here. Figure 5.4 summarizes the most important choices that have been made with respect to materials and manufacturing methods.

## 5.3 Joint design

Figure 5.5 shows a close-up of the joint that is highlighted in Figure 5.2b. This complex joint connects seven individual members of different thicknesses. These joints need to be 'locally flat', in the sense that tapes from different members that meet at that location need to be stacked in the same local z-direction. Between joints, individual ribs can twist, or bend in the out-of-plane direction relative to the pre-preg tapes, if a feasible mold can be manufactured to accommodate this.

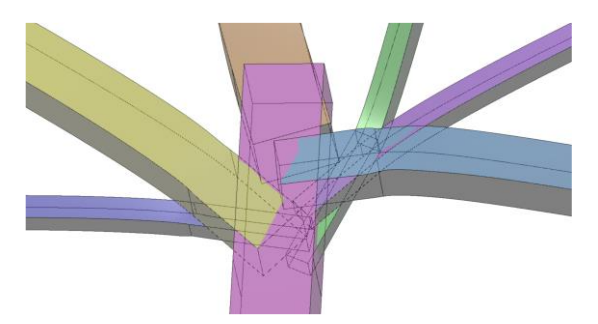


Figure 5.5 Close-up of joint detailed design, note: thickness build-up has not been modeled here

If all members would simply terminate in a single point, there would be significant buildup, resulting in a joint that would be more than four times thicker than the thickest members surrounding it for a joint as seen in Figure 5.5. Build-up reduction is desirable primarily because larger build-up means greater deviation of individual fibers from being aligned with the load path of the member in question, greatly reducing their effective

strength and stiffness in the relevant direction. Chapter 7 presents detailed FEA of joints. These analyses showed significant increases in both stress along the direction of the fibers, as well as inter-laminar shear stress.

Therefore, a method has been devised to design such joints in a manner that aims to reduce build-up to at most a factor 2, which is what is also seen in regular isogrid structures where ribs cross that are built up out of continuous fibers.

### 5.3.1 Methodology overview

The method prevents full local overlap of all members in a single patch while aiming to minimize the total weight of the joint by following an algorithm that can be summarized as follows:

- 1. The joint is built up by sequentially adding each member
- 2. Larger members are prioritized. The reasoning behind this is that distortion of established load paths should be minimized. Net distortion is minimized most effectively by prioritizing positioning of more highly loaded members.
- 3. Also prioritized are sets of members which are:
  - almost in line with each other (under a relative angle below 20 degrees)
  - similar in size
- 4. The other members are then built up around members placed earlier

Figure 5.6 introduces this approach in a simplified manner. Note that in an actual 3D structure, smaller ribs can pass under and over each other as can be seen in Figure 5.5. This allows for more compact solutions without violating the requirement of limiting build-up to at most 100%. Throughout this process, the ends of each member may be slightly moved to avoid excessive build-up. The impact of this should be limited in terms of axial load, since the change in location is generally small compared to the length of the member, but care needs to be taken that load paths are still properly accommodated after the joint redesign.

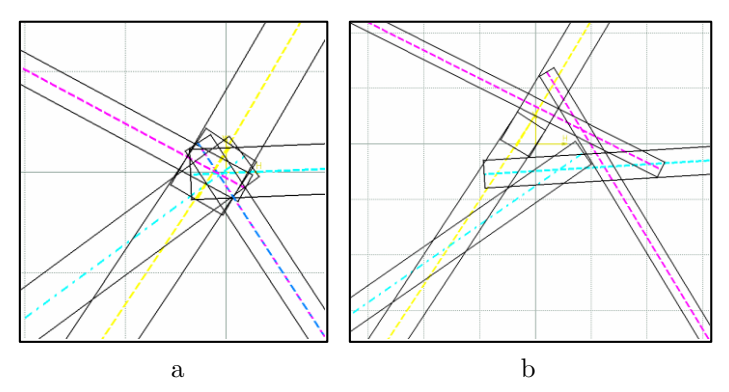


Figure 5.6 Simplified node with full overlap (a) and after redesign (b)

Joint design 31

However, contrary to the simplified joint that is seen in Figure 5.6 a, the final joint will normally not be balanced in terms of moments around the local z-axis, relative to the joint. If a joint is not specifically designed to be balanced in this sense, the result will be deformation that could be described as 'local rigid body motion', as well as a reacting bending load in all connecting members. Section 7.2.2 analyzes this behavior in further detail. When carrying out detailed joint design, i.e. the translation of the simple model which results from the Optimization Framework into a full 3D model of a joint that can actually be manufactured, a fixed procedure is proposed to accomplish a moment-balanced joint (effectively an extension to step 4 of the above list). The exact procedure depends on the number of members in a joint, and how many of those are 'highly loaded' (a typical joint will have one or two members that are loaded by at least twice the load of most other members and such more highly loaded members are positioned first during detailed joint design, as noted). Section 5.4 introduces a manufacturing prototype for which this procedure has not been taken into account (manufacturing considerations were given priority and the moment-balancing principle had not been fully developed at the time of production). Section 7.3 briefly shows the steps involved in redesigning this same joint to be moment-balanced.

### 5.3.2 Thickness build-up and overlap requirements

A method has been developed that can reduce build-up further when connecting sets of large members that are almost in line with each other and close in size, such as the yellow members in Figure 5.6. Such sets are likely to be encountered often in a structure along major load paths. By implementing a staggered drop-off pattern as shown in Figure 5.7, thickness build-up can be reduced to 40% compared to 100% for a simple overlap strategy.

Blue and red bars each represents individual plies from two members that join from opposing sides and need to transfer their load. Members that are perfectly in line can simply use continuous fibers, so this method is intended for members that meet under a small angle. This strategy has been successfully implemented in the manufacturing prototype which is presented in Section 5.4, where two members are connected that are

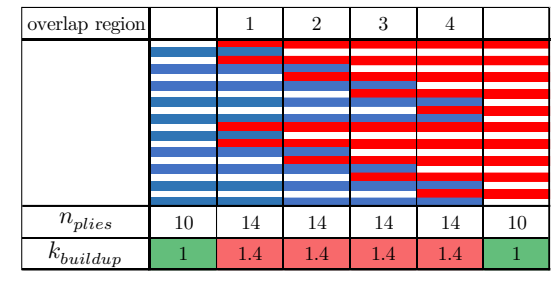


Figure 5.7 Schematic representation of staggered drop-off strategy with four regions

under an angle of 15 degrees. Figure 15 shows an example with 4 regions. More regions allow for greater build-up reduction at the cost of a longer joint. A connection with multiple overlap regions is heavier than a simple connection with a single overlap region. For example, a joint with 4 overlap regions has a volume that is 11% greater compared to a joint with a single overlap region if both use the same amount of overlap between adjoining plies. In exchange, fibers are on average loaded more efficiently by contributing more to overall strength, as they are better aligned with incoming loads. In strength-driven structures can result in a reduction in overall required thickness of members.

The thickness build-up factor is related to the number of overlap regions according to:

$$k_{buildup} = 2 - \left(\frac{n_{regions} - 1}{n_{regions} + 1}\right) \tag{5.1}$$

The amount of overlap between plies of joining members needs to be sufficient to fully transfer the maximum load that the members in question can carry based on maximum 0-degree compression/tension performance. The required overlap is a function of the thickness of the individual plies, the strength of individual fibers and the inter-laminar shear strength of the composite (i.e. matrix strength):

required overlap length = 
$$t_{ply} * \frac{X^c}{S_{IL} * 2}$$
 (5.2)

With  $X^c$  the compressive strength along the fiber direction and  $S_{IL}$  the inter-laminar shear strength.  $X^c$  is used here rather than  $X^t$ , as it is the lower value of the two.

The factor 2 in the denominator represents the fact that each ply interfaces with two other plies from the adjoining member.

Table 5.1 Selected material properties for Hexcel 8552 IM7

Variable	Value
$X^c$	1690 MPa
$\mathcal{S}_{IL}$	137 MPa
$t_{ply}$	$0.131 \ mm$

Joint design 33

Table 5.1 provides relevant properties for a typical high performance composite, Hexcel 8552 IM7.

overlap length = 
$$0.127 * \frac{1690}{137 * 2} = 0.78mm$$
 (5.3)

Theoretically an overlap of 0.78mm is enough to fully transfer the load from one stack of plies to another. Greater overlap would be required in harsher environments that affect resin performance more than fiber performance: In wet conditions at 71°C, overlap should theoretically be at least 1.17mm. One of the manufacturing requirements that has been set for structures designed in this thesis describes a minimum member width. In practice this provides a significant safety factor for all connections that are joined as shown in Figure 5.6, by full overlap across the width of the widest member involved in a connection.

However, careful consideration is important for the staggered drop-off strategy that has been proposed above, since this involves far smaller overlap regions than what is shown in Figure 5.5 and Figure 5.6. For these sections, the overlap that each ply has with neighboring plies is not symmetrical as can be seen in Figure 5.7, rather the total overlap is  $\frac{3n+1}{3n}*w_{overlap region}$ , or roughly  $3*w_{overlap region}$ . Equation (5.3) can be rewritten to reach a theoretical minimum required width for overlap regions in a staggered drop-off joint:

overlap region length = 
$$0.127 * \frac{1690}{137 * 3} = 0.52mm$$
 (5.4)

A 4-region staggered drop-off joint has been implemented in the manufacturing test sample that is presented in Section 5.4. An overlap region length of 1.5mm was used. It has been shown that a high placement accuracy of within 0.5mm can be obtained, resulting in an effective safety factor of greater than 2.

The effectiveness and usefulness of these build-up reduction strategies depends largely on the type of load case and the material that is being used. Specifically, a strength-driven design will be sensitive to the local loss of strength associated with fibers that are misaligned. However, in a stiffness-critical structure, a local loss of stiffness near joints is easier to compensate for in other ways. In practice, Finite Element Analysis (FEA) will need to be carried out on a case-by-case basis to determine the desired number of overlap regions.

## 5.4 Joint Manufacturing Test Campaign

To investigate the suitability of the methods proposed in the previous sections, a reduced version of the joint seen in Figure 5.5 has been manufactured as a proof of concept. It is flattened to simplify mold manufacturing. Two tests have been performed. This section focusses mainly on the second test. Lessons from the first manufacturing test prototype have been incorporated in this second design.

#### 5.4.1 Goals

The following goals were set for this prototype:

1. Test a manufacturing approach which can be easily translated to freeform 3D approach

All applied principles should be feasibly applicable to a more complex 3D shape.

2. Test joint compaction and ribs without caul plate and autoclave pressure

Previous manufacturing campaigns at ATG relied on a combination of increased pressure perpendicular to (i.e. 'on top of') the plies in the joints where individual ribs cross, and increasing lateral pressure elsewhere (i.e. on the ribs) to achieve ribs and joints of identical height, despite the fact that the joints have twice the number of plies through their thickness. In these joints, measured fiber volume

fractions (FVF) of 64% are seen in previous work on nodes of crossing fiber bundles at ATG<sup>3</sup>, which is high, yet only marginally higher than the nominal datasheet value of 59.9%. Hence this significant flattening of these nodes is partly achieved through displacement rather than actual compaction: the plies are significantly wider in the nodes than they are in the ribs (Maes, 2015; te Kloeze, 2015). The level of required compression will likely not be achievable with 1 bar of pressure. Instead, the aim is for joint thickness build-up to be symmetrical with respect to the centerline of the incoming member. This principle is demonstrated in Figure 5.8~a

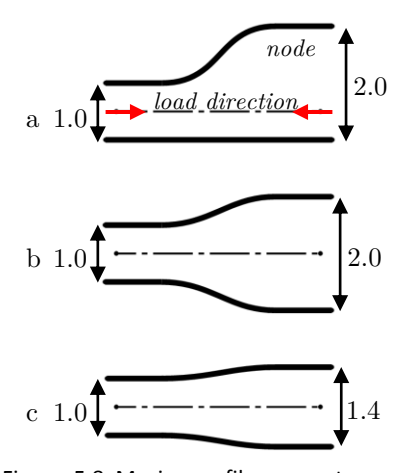


Figure 5.8 Maximum fiber curvature reduction due to joint symmetry and drop-off strategies between members

and b, and reduces the maximum curvature of fibers due to build-up.

CONFIDENTIAL PROPRIETARY INFORMATION. NOT FOR DISCLOSURE.

<sup>&</sup>lt;sup>3</sup> The same tests showed similar FVFs around in the ribs between these joints

### 3. Test feasibility of laying up a staggered drop-off joint.

The staggered drop-off overlap joints also work towards reducing fiber curvature, as is illustrated in Figure 5.8 c. As explained in Section 5.3, this principle is not applicable to all connections, but major load paths in the structures are expected to encounter joints where this can be used, as they would likely need the type of joint that is suitable for a drop-off strategy: highly loaded members that are relatively thick, and which are under a small mutual angle. An important aspect is to show that the required placement accuracy can be achieved.

### 5.4.2 Design

Four members with different rectangular cross sections are joined, as illustrated in Figure 5.9. All members have an identical designed width of 6.3mm to simplify preparatory work. Two thick members of 5.4mm under a mutual angle of 15 degrees are connected using the drop-off strategy illustrated in Figure 5.7. Two thinner members connect to the larger ones. In a real-life application, region D would perhaps not be necessary, as all load from member 2 can be absorbed in region B, although this extra connection does add stiffness. In the context of a manufacturability test however, it presents an extra opportunity to learn about how to weave together multiple members.

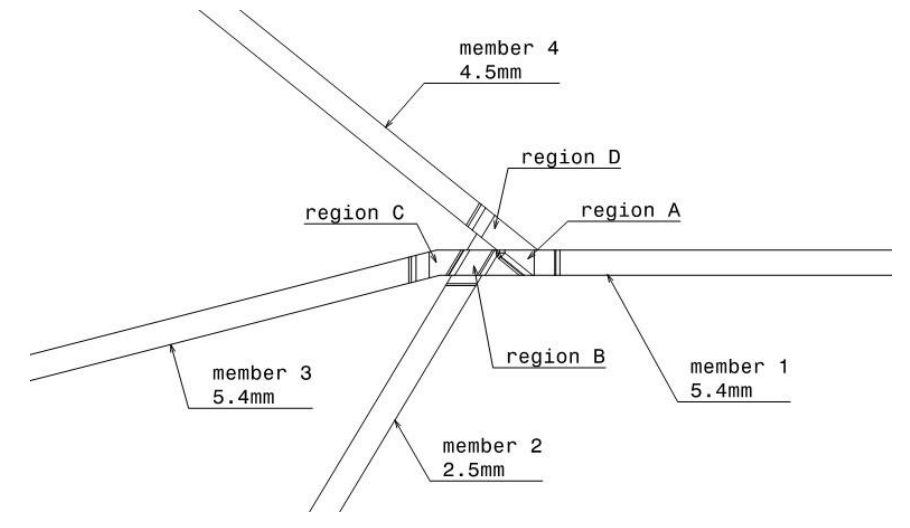


Figure 5.9 Schematic of the joint manufacturing prototype design. Regions A through D denote different overlap zones. Widths are fixed at 6.3mm, heights are indicated

An aluminum base tool was milled out of billet. The expansion tool was made by 3D printing a positive mold of the final shape of the members and joint. The expansion tool was made by casting a silicon rubber into the cavity formed when joining the base tool and the printed tool, see Figure 5.10. The tooling was dimensioned using the principles laid out by Huybrechts et al (2002) to determine the final shape of the expansion tooling at the curing temperature needed to exert sufficient lateral pressure to the ribs. Joint compaction for the second design was estimated using results from the V1 prototype.

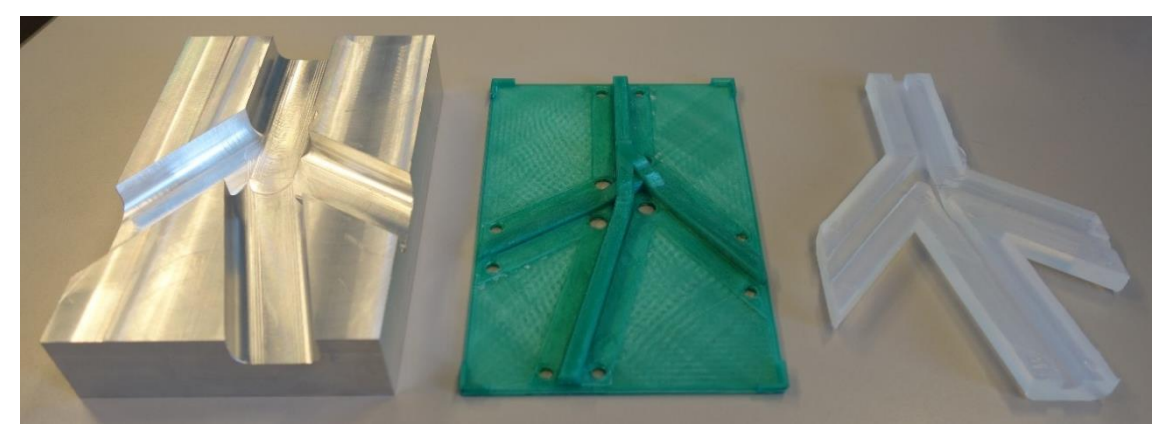


Figure 5.10 Base tool (left), 3D printed expansion tool mold (middle) and expansion tool

Appendix A provides graphs that give insight in the design of the interweaving patterns in the various overlap regions. The order of the plies follows from three basic principles:

1. Thickness build-up in each overlap region is symmetrical with respect to the middle plane of the joining members. In the first prototype, joint compaction was significantly higher than expected, resulting in an asymmetric joint (see Figure 5.12). The expansion tool was redesigned to take this into account.

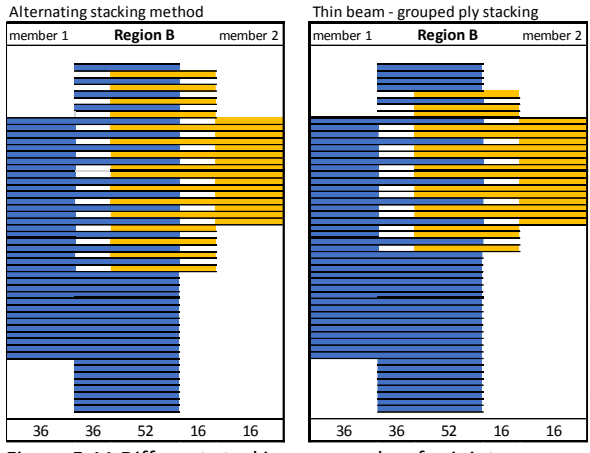


Figure 5.11 Different stacking approaches for joints

- 2. When a thin member weaves into a significantly thicker one in an alternating fashion, the thickness build-up of the thin member will be greater relative to its thickness compared to the thickness build-up of the thick member with respect to its thickness. Instead, the choice is made to design for similar percentagewise build-up for both members, by bundling multiple plies from the thinner member. Figure 5.11 demonstrates this principle.
- 3. The top surfaces of all four members are on the same plane to reduce complexity of the base tool.

The full layup sheet for prototype V2 is provided in Appendix A.

#### 5.4.3 Results

This section discusses the results from the manufacturing campaigns. The goals laid out in Section 5.4.1 are discussed and general observations are presented. Figure 5.12 shows the result of the first of two manufacturing campaigns.

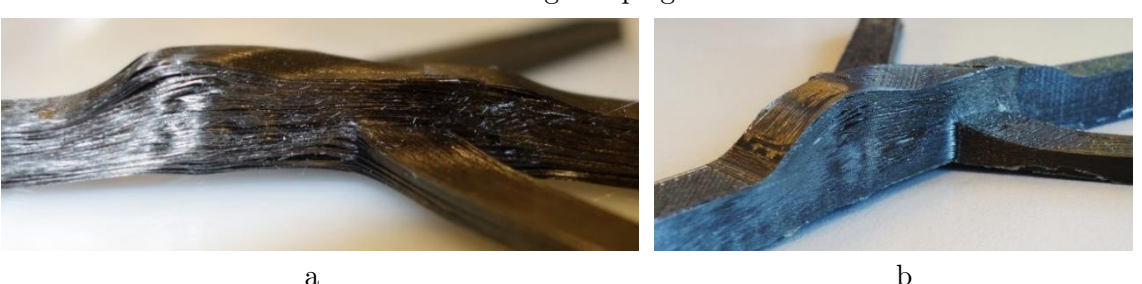


Figure 5.12 V1 sample before (a) and after curing cycle (b), showing significant, asymmetrical thickness build-up

The appropriate cure cycle for this material is as follows:

- 1. gradual ramp up to 120°C
- 2. retain this temperature for 60 minutes
- 3. gradual ramp up to 180°C
- 4. retain this temperature for 120 minutes
- 5. gradual ramp down to room temperature

During the V1 sample curing cycle, an error occurred in the oven control system, triggering a safety system which led to ramp down to room temperature soon after step 3. As a result, the resin was too viscous throughout the process to be squeezed out properly and allow full compaction of the material. Fiber Volume Fraction tests were performed on this prototype. The values that were found are still useful. However, they should be taken as an indication of a lower boundary of what FVFs can be achieved with this molding and curing approach.

As indicated in Figure 5.1, the bottom and the sides of each rib are in contact with cast silicon mold: the expansion tooling. The top side is covered by a vacuum bag. The pressure on the product is 1 bar. Thickness build-up was less than expected (i.e. compaction was better than expected), which led to a highly asymmetric joint. It was assumed that the lower pressure compared to previous ATG manufacturing campaigns would lead to significantly lower compaction throughout the product. This was not the case, except for the overlap regions where caul plate application in previous campaigns led to drastic local pressure increases, i.e. significantly higher than 8 bar autoclave pressure (Maes, 2015; te Kloeze, 2015). Using the mold layout shown in Figure 5.10 as a reference, the 'bottom side', or mold-defined side, is up in the above figure, showing that most of the build-up is in that direction. In the second prototype, the expansion tooling has been redesigned to account for this, with the goal of achieving a more symmetrical joint for reasons explained earlier.

Fiber volume fractions in prototype V1 are between 55 and 59% in the ribs. This compares to a datasheet value of 59.9%. Small voids near the surface of transition regions in the joint trap small air bubbles while submerged in liquid, making accurate density measurements for these overlap regions difficult.



Figure 5.13 Joint test sample V2, showing better compaction and more symmetrical thickness build-up

Figure 5.13 shows the result from the second manufacturing campaign. This sample was subjected to the appropriate curing cycle. A different layup order has been implemented, but the total *designed* thickness of each member is identical to the corresponding values in the first test sample. It can be seen that thickness build-up is at the same time lower and more symmetrical in the second test. Figure 5.14a shows the result of underestima-

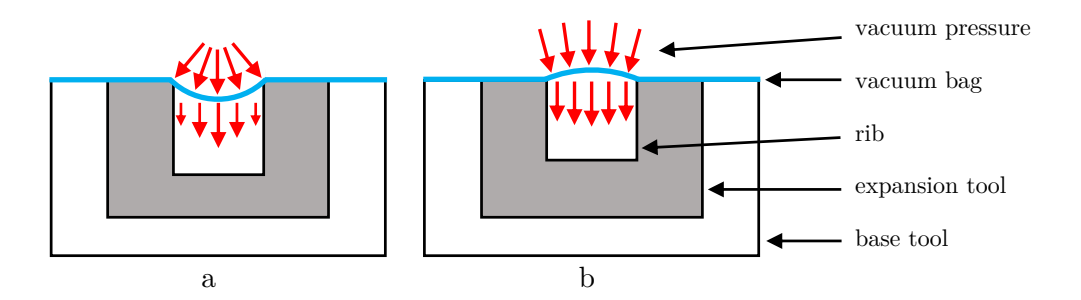


Figure 5.14 Schematic illustrating local reduced joint compaction in case of compaction underestimation during expansion tooling design. The rib cavity in the expansion tool in (a) is too deep.

tion of rib compaction during expansion tooling design: Effective compacting forces are diminished towards the sides of the ribs, the results of which can be seen in the final result of the first test. Figure 5.14b is a schematic representation of how the expansion tooling was redesigned for the second sample by slightly underestimating compaction (and thus overestimating final thickness) with the goal of achieving better compression throughout the cross section of the joint, especially at the overlap regions.

Layup of the staggered drop-off region was shown to be feasible: As expected, a significant thickness build-up reduction was achieved in overlap region C (see Figure 5.9). The thickness of this region is 7.5mm, compared to measured thickness of 5.45 mm of the ribs that overlap at that location, i.e. a thickness build-up of 38%. This compares well to the goal for this region of achieving 40% build-up, and even more so when compared to a regular full-overlap region which would approach 100% thickness build-up for two joining members of equal thickness. Accurate axial ply placement is necessary for this type of overlap, and was shown to be achievable to within 0.5mm.

Voids can be seen at the surface near the regions where the greatest change in thickness occurs, although they occur much less in the second test sample compared to V1. This is attributed to higher compacting forces due to the expansion tool redesign as well as better resin flow due to the higher curing temperature of the second sample. Section cuts of the first sample showed good compaction and few to no voids at locations where proper compacting pressure had been applied. Physical testing is required to assess the influence of any remaining voids like the ones seen in the second test sample, specifically with respect to failure strength.

It can be concluded that the method proposed in this chapter can be used to build composite skeletal structures. The fact that no caul plate or even fully matching molds are required, but rather a single-sided mold is used combined with a vacuum bag, significantly decreases mold complexity and required mold manufacturing tolerances. This means that more complex geometries can be achieved. Because the final product is only in contact with flexible expansion tooling and a vacuum bag, it does not need to have a releasable shape, further expanding design freedom. The required rigid base tool that positions the rubber expansion tooling may take a skeletal form and can be made modular to allow for complex shapes that can still be disassembled from around a finalized composite frame after curing.

# Chapter 6

## **Optimization Framework**

This chapter lays out an optimization framework that utilizes topology-, shape- and sizing optimization for designing 3D skeletal composite structures that can be manufactured using the principles laid out in the previous chapter. Several requirements have been listed in Section 3.4. One of those is that any FEA functionality should make use of Nastran for reasons of availability at ATG, as well as acceptance within the space industry. A single optimization task can in principle be formulated in MSC Nastran that combines topology, shape and size. However, the resulting design space has been found to be too complex for Nastran to converge to a global optimum using its built-in algorithms, and typically no convergence occurs at all. Instead, three individual modules are implemented within a Python framework, which never operate simultaneously. This chapter lays out the functioning of this optimization framework and explains the underlying decisions that have been. These decisions follow from specific strengths and shortcomings of the various Nastran modules that have been incorporated, as well as some inherent characteristics of different types of optimization which will be laid out.

In this chapter, the first section explains how a class of optimizer has been selected, building on conclusions from literature. Section 2 presents how the overall task of designing a lightweight, manufacturable structure is broken up between the topology- shape-and sizing modules, and how they interact. Section 3 presents the analysis approach of the designs. Section 4 introduces a method for generating ground structures that form the starting point for each problem. Sections 5, 6 and 7 explain how each of the three optimization modules have been implemented, using simple generic design problems for illustration purposes.

#### A note on terminology:

An *Element*, as used in the context of FEA is the smallest unit of model discretization. Elements can be seen in Figure 6.1 as the individual small black blocks that give rise to non-smooth edges in sections that are under an angle.

A *Member*, as used in a topological context is an individual segment between two nodes, where it connects to more than one other member. A single member is indicated in red in Figure 6.1.

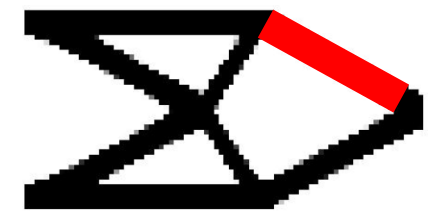


Figure 6.1 Schematic of a single member in red within an FEA model discretized as uniform squares for analysis of an isotropic material

In this thesis, members are often modelled as a single element across its cross section for reasons that are further explained in the following three sections, especially Section 6.3. However, the terms denote different concepts.

## 6.1 Choosing an optimization approach

In previous chapters, optimization problems for isotropic materials based on a solid mesh (as depicted in Figure 6.1) have been mentioned. In such a problem, in a conceptual sense, one can identify separate optimization of topology, shape and size. When introducing concepts like minimum member size, this is in fact necessary. However, on the lowest level, all necessary operations can be described in terms of topology changes, by virtue of the uniformity and small scale of the lowest level discretized elements. Size in this context is simplified to the number of elements across the cross section of a member, and can be changed by changing the density of individual elements near the current edge of a member. Note that size is only a meaningful term if members can be identified as such. Although this is the case for skeletal structures as presented in Figure 6.1, this is not necessarily so for more complex shapes. To an even greater extent, the term shape loses meaning when considering structures in a generalized way in the context of a topology optimizer operating on a finely discretized block of isotropic material, compared to the narrow definition as given in Section 3.2 (see also Figure 3.2).

These topology optimization problems are well defined in a mathematical sense, and various methods have been described that can find adequate solutions (Bendsøe & Sigmund, 2003; Sigmund & Maute, 2013). However, as has been shown, the associated modeling approach cannot be readily used to capture crucial properties of a material that has been reinforced with continuous fibers. For this reason, a ground structure approach has been proposed, which provides a method to describe directionality of material. Within the context of a ground structure, being a collection of nodes and connecting beams, the

concepts of topology, shape and size are separately and precisely defined, and design variables can be assigned that independently describe these aspects of a structure.

Various ground structure-based optimization schemes are available. Christensen and Klabring (2009) show how a combined topology/sizing optimization for truss structures using the Method of Moving Asymptotes can be applied to a problem that has been shown to be fully convex. They note that this could theoretically be expanded to include shape. However, like many others, they also note that most optimization problems are in fact not convex, and generally cannot be fully described using explicit functions.

There are two main ways that have been widely explored to deal with this problem:

- 1. Approach various aspects in a sequential manner (treating topology optimization and sizing optimization separately)(Adeli & Balasubramanyam, 1987; Kirsch & Topping, 1992), using mathematical programming methods. Many publications do not incorporate shape optimization, but rather focus on topology and sizing.
- 2. Implement a single procedure that optimizes topology, shape and size simultaneously using a Genetic Algorithm (GA) approach (Balling et al., 2006; Camp, Pezeshk, & Cao, 1998; Rajan, 1995; Shrestha & Ghaboussi, 1998; Soh & Yang, 1996). Other heuristic methods such as Ant Colony Optimization are presented by Kaveh & Shojaee (2006) among others.

A third category can be also considered that contains more novel approaches such as:

- The Stiffness Spreading Method (Wei, Ma, & Wang, 2014)
- Optimization with Orientation Design (Nomura et al., 2014)
- Principal Stress Line methods applied to beams (Li & Chen, 2010)

These are elegant methods that do not use a ground structure as a starting point but their results are truss-like structures with distinctive members. However, they have generally yet to be expanded in a practical way to 3D applications and will not be further considered here.

Genetic Algorithms can be powerful and can provide a method to avoid convergence to local minima. A GA's independence from sensitivity analyses can provide robustness in the sense that this allows freer exploration of the design space and may exhibit a lower level of sensitivity to the initial condition of the problem. However, a GA becomes relatively inefficient when these gradients *are* available for at least some of the design variables involved. The high number of design variables involved in the type of 3D ground structure needed to describe complex structural problems in a sufficiently generalized way, makes a GA approach unsuitable. For the initial ground structure, the number of independent design variables will generally be in the order of tens of thousands (For examples, see Section 6.4). Conversely, mathematical programming methods are well

suited for dealing with optimization problems with a great number of design variables (Labanda, 2015; Sigmund & Maute, 2013). This is an important reason that this is the method that is used in Nastran's Automated Design Synthesis suite SOL200 (MSC Software Corporation, 2011a), see also Section 6.2.1.

An important aspect of this thesis is the implementation of manufacturing constraints. Many of these are implemented in a sizing optimization procedure (minimum size, aspect ratio of beam cross sections, etc.). Others however, are more appropriately addressed at the shape level. For example, a structure where members within a major load path are more in line with one another can be favorable over another setup, if that enables use of more efficient connection joint designs (see Section 5.3). Similarly, a structure with fewer members may be favorable to reduce overall complexity and cost, which is addressed at the topology optimization level. It is critical to recognize that these separate constraints cannot be enforced within one procedure (e.g. sizing optimization) without influencing fitness of the overall structure when considered within the scope of the other two optimization sections. For example:

- If a minimum member width is implemented at the size optimization level, this affects the design freedom at the topology level: A structure that was in theory more efficient, but required elements that are considered too small for feasible production will now become heavier.
- A certain shape may be found to be more efficient, i.e. a node is moved in a certain direction and the total strain energy in the structure decreases. However, for a connecting member which has now become longer, its cross section may have to increase to still meet buckling requirements, even if the compressive loads have not increased. The resulting weight increase can nullify any gains that were to be found by adopting a shape that seemed more efficient theoretically when being considered purely in terms of shape optimization.

This is insufficiently recognized in many publications where optimizations are executed in a purely sequential manner, typically topology  $\rightarrow$  shape  $\rightarrow$  size. When considering purely sequential methods, this order does make sense (this point is clarified in Section 6.2.3), but a more sophisticated approach is required to ensure that each step taken at each of the three optimization levels actually leads to an overall weight reduction. This becomes more critical for structures where more manufacturing constraints are enforced on all three separate optimization operations.

The next section introduces a method in which Mathematical Programming-based optimization procedures are nested rather than executed purely sequentially to address this problem.

## 6.2 Optimization process

Two important choices must be made to decide on a process setup:

- 1. Which built-in Nastran modules can be used, when considering the three different optimization procedures? This decision is based on their applicability and performance in test scenarios.
- 2. How to order the optimization sequence?

At its core, Nastran provides a method to analyze a given structure for a variety of load types to provide either a pass/fail assessment, or preferably a set of safety factors for various loads and failure modes. By reanalyzing the same structure with small local changes with respect to topology, shape or member size, design sensitivities can be obtained which can be used in a gradient-driven design optimization process in Python. However, the process of feeding input data and extracting outputs from Nastran is inefficient, as data is exchanged by writing and reading text files. Instead, where possible, built-in Nastran modules are used, as they work far more efficiently, and Nastran provides several sophisticated optimization algorithms.

#### 6.2.1 Overview of relevant built-in Nastran modules

Much of Nastran's SOL200 Design Optimization solution sequence is built around DESVAR entries which define design variables that can be coupled to a wide array of properties (material-, element-, geometrical properties, etc.) and which can be precisely and individually controlled in terms of initial conditions, allowed values and allowed changes. Design response of the total structure is monitored using DRESP entries.

#### Topology

Nastran's TOPVAR functionality is a method for executing topology optimization on a structure. It uses the Density method, combined with power law penalization applied to the material density/stiffness to attempt to enforce a 0/1 density distribution (see Section 6.5.1). A TOPVAR entry is effectively shorthand for assigning individual design variables to the density/stiffness of each individual member in a structure. Nastran's built-in algorithms are powerful and efficient when dealing with static analyses on structures with large numbers of elements. However, the algorithms struggle to converge to a 0/1 density distribution when considering modal requirements.

#### • Shape

For shape optimizations, Nastran provides the DVGRID entry, which can couple the coordinates of a grid point in a single direction to a single design variable. This method can be used efficiently for example to optimize thickness of a section in a model that is built up out of solid elements, by scaling all nodes in a member perpendicular to its length-direction, relative to the center of the element. To fully manipulate skeletal structures, each individual node will require three independent DESVARs to fully describe its design space, one for each dimension. However, even for relatively simple shape optimization problems with trivial optimal solutions, Nastran has been shown not to consistently find the optimum. In some cases, solutions diverge away from lighter solutions. It seems that a DVGRID-DESVAR setup with the built-in Nastran optimization algorithms can only deal reliably with shape problems that are effectively 1D locally (either with just one actual independent DVGRID entry per grid point, or when structural fitness primarily exhibits sensitivity to movement along only one axis in the chosen coordinate system).

#### • Size

DESVARs can be coupled to the cross-sectional area (and if desired the aspect ratio) of individual beams. Nastran caries out efficient sizing optimizations with combined load cases with different types of analyses (static, modal) and proposes one set of values for the sizing design variables that fulfills all requirements in terms of stresses, displacements, individual member buckling, modal behavior and minimum member size. However, the sizing optimizer has been shown to not be reliably robust, in the sense that it will not always converge to an acceptable solution for more complicated structures, especially when modal requirements drive the design.

Further background information can be found in Nastran's Design Sensitivity and Optimization User's Guide and Quick Reference Guide (2011a, 2011b).

### 6.2.2 Assessment of applicability of Nastran modules

Based on the observations from the previous section, a choice can now be made concerning which built-in Nastran modules can be used, and for which functionality different solutions need to be developed:

#### Topology

The built-in TOPVAR method is well suited for the purpose of providing a structure that the shape- and sizing optimizers can operate on. As will be clarified in section 6.5, the shortcomings with respect to optimization of structures for which modal requirements are critical can be accounted for.

#### • Shape

The choice is made to develop a Python-based shape optimizer. Nastran is used

for analysis of individual designs, but all design variable changes are more directly controlled, so checks can be built in to prevent diverging solutions which were observed in test cases, as noted in Section 6.1. This comes at a cost of significantly reduced solve speed, due in part to relatively inefficient data transfer between Nastran and Python which cannot be circumvented. Section 6.2.3 describes how the shape optimizer has been implemented. Additional information is presented in Section 6.7.

#### $\bullet$ Size

As explained in the previous section, a Nastran based Sizing Optimizer is a versatile tool that can handle complicated combined design tasks. It will be used within the larger Python framework to determine member cross sections. Section 6.6 explains which robustness problems have been found, and how they have been accounted for.

### 6.2.3 Ordering of the optimization sequence

As discussed previously, for purely sequential structural optimization using a ground structure approach, the traditional sequence is:

- 1. Topology
- 2. Shape
- 3. Size

This order prioritizes operations that have greater influence on the overall design. Starting with topology optimization realizes a reduction in the number of members that is typically highly significant. This leads to drastically increased efficiency for any subsequent steps, i.e. shape and size optimization. Like topology optimization sequences, these are iterative processes that require many cycles (typically between 60 and 200) to converge to a solution and are generally computationally expensive. Next, a shape optimizer positions the individual nodes. Note that the influence of the shape optimizer depends greatly on the density of the ground structure (and thus to which extent the topology optimizer could already approximate optimality). Finally, the sizing optimizer provides the cross sections for all members, without influencing topology or shape of the structure.

The Python Framework adopts a similar strategy, but with a number of adaptations. Four steps are distinguished, with two main phases:

- 1. Problem data input
- 2. Phase 1: Nested topology/sizing optimization for range of initial conditions
- 3. Select best result, model cleanup
- 4. Phase 2: Nested shape/sizing optimization

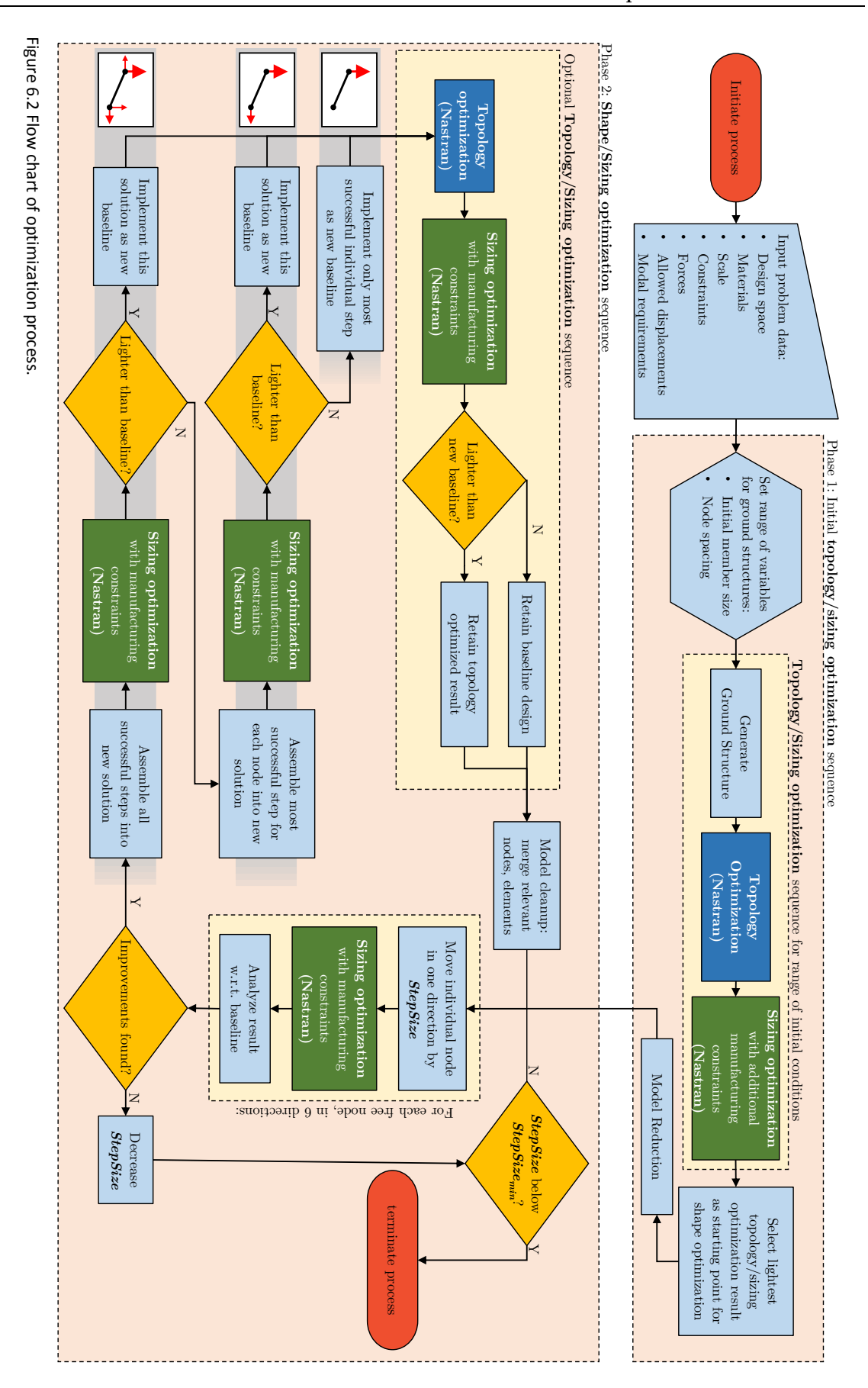


Figure 6.2 presents an overview of the full process within that Framework. Internal Nastran operations have been indicated. The Framework compiles input files for these simulations, extracts and interprets their results, and performs a variety of other functions that are described in this chapter.

Similar to the simple sequential order, an initial topology optimization is also used here. Even more so than when dealing with an isotropic solid element mesh, significant mesh dependency issues may arise when dealing with ground structures. To prevent this, a loop has been implemented that combines topology and sizing optimization and sweeps through a range of ground structure initial conditions to determine the best starting point for the shape/sizing optimization sequence. Section 6.5 explains this in more detail. Phase 1 is computationally relatively inexpensive compared to Phase 2. For this reason, it is feasible to examine a large number of different initial ground structures (in the order of hundreds if desired). Phase 1 produces a range of fully size-optimized structures that meet all design requirements. Next, the lightest structure is selected and cleaned up, drastically reducing the amount of data that needs to be handled in Phase 2 by the Python framework. The computation time needed for a single shape/sizing optimization cycle within Phase 2 is roughly proportional to the number of nodes in the model that results from Phase 1. As noted in the previous section, it has been developed as an alternative to Nastran's built-in DESVAR-DVGRID functionality. The optimization logic that it uses is simplistic, and several improvements could be offered in this regard when continuing the work presented in this thesis. However, Phase 2 implements two crucial aspects that Nastran itself does not integrally cover:

- 1. Phase 2 groups the shape design variables from each node.
- 2. It only accepts sub results and results if they in fact do provide an improvement in terms of the value of the objective function (in many cases lower weight will be desired, but other traits may be selected for).

The shape optimizer considers proposed improvements of coupled design variables together. Nastran's built-in algorithms typically aim to *simultaneously* implement all improvements that its sensitivity study flags as beneficial. However, these individual changes to the structure are never independent. Consider the following example: For a certain grid point, movement in the positive y-direction may be found to result in a lighter structure. However, a step in the positive x-direction for the same grid point also promises a lighter result. It is not given that the positive-y step is still beneficial if the x-direction step has already been carried out. Nastran has no mechanism to account for this and will always apply both moves.

The Python Framework presented here deals with this by only accepting steps that together result in a lighter solution, in the following way:

- 1. Pattern Search is employed by applying steps of a fixed magnitude in positive and negative x-, y- and z-directions for each grid point in the structure that is free to move, i.e. not involved in an external load introduction.
- 2. Initially, all the most successful steps per grid point (i.e. at most 3) are combined into a new design for the entire structure. If this gives a lighter result, it is accepted as the new baseline design for the next cycle.
- 3. If this results in a heavier structure, only the single most successful steps per grid point are combined in a new design. If this new design is lighter, it is accepted.
- 4. Finally, if this too does not present a lighter design, only the single most successful step across all grid points is immediately accepted.
- 5. If no successful steps had been found in the first place, the step size is reduced. This is repeated until a predefined lower threshold is reached, at which the optimization is terminated.
- 6. After each successful shape step, a cleanup procedure is carried out which checks if the new geometry allows for merging of nodes or members.

Tools have been implemented that provide the option of deleting members within Phase 2, by carrying out a topology/sizing optimization cycle that checks if lighter solutions become available as the structure changes shape.

#### 6.2.4 Discussion

The process layout discussed in the previous section accomplishes two main goals:

- 1. At every stage, intermediate results meet all crucial design requirements with respect to strength, stiffness and various manufacturing requirements, such as minimum member size. This offers an improvement over simplistic sequential approaches, where the dependency of operations in different optimization modules is not taken into account, as discussed in Section 6.1.
- 2. Heavier results than *current baseline* (i.e. the starting point of the active shape optimization iteration) are never accepted. This offers an improvement over built-in Nastran methods which are not equipped to consider previous intermediate results and implement improvements in an adaptive manner.

Progress can still be made, primarily by improving upon the rather simplistic pattern search method for determining which shape changes to implement. For this thesis however, the choice has been made to primarily focus on robustness rather than efficiency.

Analysis 51

It should be noted that full integration between all phases of optimization has not been pursued, rather, there is a 'hard cut' between Phase 1 and Phase 2. However, it is not feasible to carry out a full shape optimization sequence for each Phase 1 result in terms of computational cost. Nevertheless, results from Phase 1 are structures that fully meet all design requirements, and are therefore already much closer to a useful final design when compared to a typical ground structure topology optimization result.

## 6.3 Analysis

The previous two sections have explained the optimization approach that has been implemented to design composite skeletal structures. This section explains the choices that have been made with respect to the analysis of these structures in Nastran. First, a requirement overview is given. Next, the available modeling options are presented, followed by the final choices.

#### 6.3.1 Requirements

Several requirements need to be fulfilled to achieve an appropriate modeling method:

#### 1. Sufficient approximation of physical behavior

Appropriate choice of materials, element types and model build-up is needed to provide a sufficiently close approximation of real-life properties to accurately determine stiffness, assess which failure modes are critical, and to determine the loads associated with those failure modes.

#### 2. Manipulability within optimizer

The optimizer must be able to fully manipulate all relevant aspects of the geometry of the skeletal structures that are needed to design topology, shape and member size. In the case of sizing and topology optimization, this needs to be controllable through Nastran's SOL200 DESVAR functionality, as explained in the previous sections.

#### 3. Computational efficiency

The modeling approach must be capable of feasibly describing a ground structure containing tens of thousands of members, while also facilitating a full member sizing optimization sequence of a later-stage, reduced structure within minutes rather than hours in order to achieve an overall solve time that is acceptable (i.e. in the order of hours or several days at most, rather than months).

It can be broadly stated that requirement 1 calls for higher model complexity, whereas requirements 2 and 3 call for lower complexity. The following section presents an FEA modeling approach that provides a trade-off between these three aspects.

#### 6.3.2 Considerations and FEA model setup choice

Considering requirement 1 in more detail, a list can be made of relevant aspects that an FEA model may capture when analyzing a composite skeletal structure:

- 1. Global compliance
- 2. Global vibration modes/frequency response
- 3. Local vibration modes
- 4. Deformations of individual members, as well as strains and associated stresses:
  - a. due to tension/compression
  - b. due to bending
  - c. due to twisting
  - d. due to shear
- 5. Buckling strength of individual members as well as the global structure
- 6. Local strains and associated stresses in joints:
  - a. stress in fibers
  - b. inter-laminar stress
  - c. influence of stress raisers such as sharp bends and voids

Whether a certain FEA model can in fact analyze the performance of a structure in any of the terms listed above is largely dependent on the choice of element type and size. The joints, where multiple members meet, are the sections in the structure that are the most complex in terms of failure modes that can be expected. A complete structural analysis of a composite skeletal structure would include assessment of strength and stiffness of these joints. Compared to a simpler model that does not capture all failure modes, the added value of a model that can accurately describe the mechanics within a joint needs to be weighed against the cost associated with this expansion, in terms of development time, and especially with respect to computational efficiency. A trade-off needs to be made to come to a modeling approach that sufficiently satisfies all above requirements.

In Nastran, there are many different combinations of elements and materials that could be used to describe a composite skeleton. For example, there are at least seven different feasible ways of implementing a 1-D element to describe an anisotropic composite beam with varying degrees of complexity. These range from a 6 DOF (degrees of freedom) rod which cannot capture bending and twisting (Nastran designations: CROD + PROD + MAT1), but which may provide an acceptable approximation of global stiffness, to an 18 DOF beam which implements a stack of shells to model individual composite plies (Variational Asymptotic Beam method, using CBEAM3 + PBMSECT + PCOMP + MAT8). Instead of presenting the full range of underlying considerations by describing

Analysis 53

the benefits and disadvantages of each of the most feasible combinations, only the setup that is used in the framework is presented here. A brief overview of alternatives can be found in Appendix B. More in-depth information can be found in the relevant Nastran documentation (MSC Software Corporation, 2011, 2011).

A single model that can capture all aspects in the list in Section 6.3.2 would require at least a method using stacked 2D shell elements, and likely a full 3D solid element mesh. Either of these would result in ground structures with millions of elements, arranged in groups of thousands of coupled elements that together describe single parametrized members. Realistic modeling of joints would require building up every model in CAD.

However, a great reduction in modeling complexity can be achieved by choosing a 1D element-based approach, which approximates each member as a single element. Most aspects on the above list can be readily addressed using a modeling approach that purely uses beam elements to describe the beams of the skeleton: (CBAR + PBAR + MAT1). The Nastran CBAR element is a simplified beam element which nonetheless has the full 12 DOF's, and models twisting and bending behavior.

(Nastran CBEAM elements offer additional functionality: tapered beams and more realistic handling of non-symmetric sections, but require more inputs. Tapered beams and non-symmetric sections are beyond the scope of this research. Hence, the simpler element is preferred.)

In this setup, joints are simplified as single nodes, connecting multiple beam elements. A CBAR element can only be coupled to a MAT1 material, which is isotropic. However, for small displacements, the stiffness characteristics of a slender composite beam with only unidirectional fibers can be closely approximated in all directions. A Shear Correction Factor is implemented to acquire realistic bending stiffness. Appendix C clarifies how a proper Shear Correction Factor has been derived and how other beam properties have been coupled to design variables in the Python Framework. Buckling of individual members is assessed by performing Euler critical load analyses for each member, which is further explained in Section 6.3.3.

A shortcoming of this 1D element is that it does not provide proper shear stress analysis. However, it should be noted that for slender beams that are subjected to loads that are not fully in-line, the resulting stresses are primarily due to bending rather than due to shear. As an example: Consider a typical member, modelled as a beam, with one fixed end and the other end free and guided, with a cross section of 4x4mm and a length of 100mm (A member with similar length with a non-guided free end would experience bending stresses twice as high, but a guided end is in this case a more conservative representation of how skeleton members which are subjected to a lateral load are generally constrained). A lateral load of 1N is applied on the free end as seen in Figure 6.3.

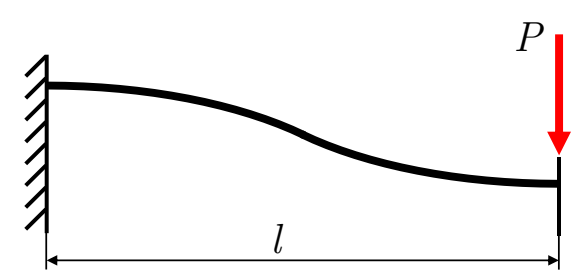


Figure 6.3 A bending beam, fixed on one end, guided and free on the other end, with a shear load applied

The peak stress due to a shear load in this rectangular section is given by:

$$\sigma_{shear,peak} = \frac{3P}{2bh} = \frac{3\cdot 1}{2\cdot 0.004^2} = 93.75 \text{ kPa}$$
 (6.1)

With P the load as indicated in Figure 6.3, b the base and b the height the beam.

The peak stress in the most outward plies in the beam due to a bending load is given by:

$$\sigma_{bending,peak} = \frac{P(l/2)}{bh^2/6} = \frac{1 \cdot (0.1/2)}{0.004^3/6} = 4.69 \ MPa \eqno(6.2)$$

With l the length of the beam.

As is thus demonstrated, for a square beam constrained as described above, the ratio  $\sigma_{bending,peak}/\sigma_{shear,peak}$  is equal to twice the slenderness ratio of that beam. The factor of 50 between the two stress levels indicates that shear stress can be disregarded in this example, since bending stress will be dominant. Moreover, one of the ways that the optimization framework achieves more efficient structures, is by using members that are primarily loaded axially, rather than laterally, thus further decreasing the likelihood that shear loads become critical.

An approach is provided which can model the critical mechanics related to points 1, 2, 4, 5 on the above list. Point 3 (local vibrations) can also be analyzed with reasonable accuracy if each individual member is modelled as five or more collinear elements.<sup>4</sup> The various modules that create input files for different operations in Nastran (i.e. topology and sizing optimization) therefore by default model each member as five elements. For structures where higher accuracy is desired, or where more complex mode shapes are expected locally as part of a critical load case, a higher number of interpolating elements

<sup>&</sup>lt;sup>4</sup> This same requirement of modeling individual members as at least 5 elements applies to global buckling analyses, which are further discussed in Section 6.3.3.

Analysis 55

can be chosen. Alternatively, for structures where static loads are critical, the number could be reduced to two elements for each member, allowing for increased computational efficiency, while still allowing modeling of the bending shape shown in Figure 6.3, which is more complex than what a single bending beam element can model.

Detailed analysis of joints is not carried out each step, as the required modeling work requires manual input and is prohibitively time-consuming. Instead, an analysis is carried out on the final design that is proposed by the Python Framework. It should be noted that for many space applications, global stiffness and global modal behavior are the critical design constraints. For structures that are strength limited, a stress analysis is however required for individual highly stressed joints. Chapter 7 presents a detailed FEA analysis of the joint prototype that is presented in Chapter 5.

#### 6.3.3 Buckling analysis

Many of the beams in a typical structure as designed by the Python Framework can be considered slender. Therefore, a method is needed to analyze local buckling failure.

There is a lot of literature specifically focused on analysis of buckling of composite beams. This mostly deals with beams that have already undergone local delamination failure, which is a non-trivial failure mode. For the purposes of designing beams in skeletal structures, simple Euler buckling will be used.

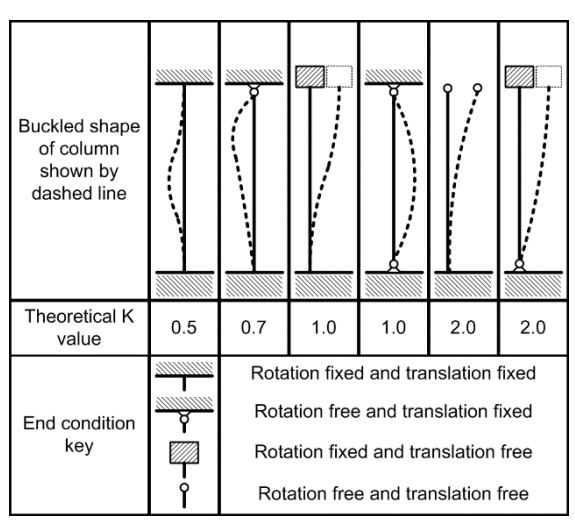


Figure 6.4 K-factors for different columns

The general equation for critical buckling load for the first mode (the lowest buckling load) is:

$$P_{cr} = \frac{\pi^2 EI}{(Kl)^2} \tag{6.3}$$

Where E is stiffness, I the area moment of inertia of the beam, K the column effective length factor, and l the unsupported length of the beam.

A buckling check is implemented by extracting the resulting average axial stress from the analysis for each element, and implementing the following rearranged equation as a boundary condition during the sizing optimization steps:

$$\frac{(Kl)^2 A \sigma_{axial}}{\pi^2 EI} < 1 \tag{6.4}$$

Where A is the cross section of the beam, and  $\sigma_{axial}$  is the axial stress. ( $\sigma_{axial}$  is kept in the numerator, to avoid computational errors in case  $\sigma_{axial} = 0$ )

In both equations, K is the column effective length factor, which depends on the boundary conditions and the type of load. For a freestanding column with two pinned ends and a purely axial load that is introduced at both ends of the column, K=1, as can be seen in Figure 6.4.

For the case of a beam between two points that are both fixed in translation and rotation, K=0.5. The latter case is considered to be a closer representation of the way individual beams in a skeletal structure are constrained, since each beam is manufactured monolithically together with the beams it is connected to. However, local deformation can lead to a node that rotates as a whole, in which case 0.5 is non-conservative. Although rotations are expected to be small, a safety factor is implemented by using a value of K=0.7, which equates to a column with one free-rotating end.

The above describes how local buckling (i.e. of individual members) can be considered within a Nastran optimization, using an efficient, analytical approach using length and axial stress as inputs. Additionally, global buckling checks are implemented by running a corresponding buckling subcase for each statics subcase in Nastran, by solving the eigenvalue problem.

#### 6.4 Ground structure module

As discussed previously, the first step in the structural optimization method is to establish a suitable ground structure. This entails creating a set of nodes and elements within the design space. Cartesian coordinates are used, although the underlying theory could easily be adapted for use in other types of coordinate systems, should those be judged more appropriate for a specific design problem. The following data is gathered in preparation:

#### 1. The design space is established

In short, this means that the 3D space that nodes and elements may occupy or intersect has to be described mathematically. It usually takes the form of a bounding box, together with smaller boxes and cylinders that describe keep-out zones.

#### 2. Design problem nodes are defined

Any externally defined nodes that need to be taken into account are entered into the model. This includes:

- a. Load introduction nodes
- b. Boundary condition nodes
- c. Nodes to which masses connect
- d. Nodes for which displacement needs to be monitored during simulation
- e. Nodes that for other reasons need to be included in the final design.

#### 3. The node density is set

This is described by three integers that denote the number of unit cells in x-, yand z-direction. These numbers are chosen such that density is similar in all three directions, resulting in unit cells that are as close as possible to being cubic.

#### 4. The Connectivity Level is set

Elements are created between each pair of nodes that are within a certain distance of one another. This distance is defined as a certain multiple of the characteristic length of the unit cells as defined in the previous step, following from the number of cells in the entire design space.

Unit cells are typically not cubic, so the greatest length of the unit cell will be used as characteristic length. The distance within which two nodes must lay in order to be connected by a member is thus defined as:

$$d_{connect} = CL \cdot \max(h, w, l)_{unit cell}$$
(6.5)

With CL the Connectivity Level and h, w and l the height, width and length of the unit cells. If for example a structure is desired in which elements are created that connect nodes to other nodes that are up to 3x3x3 unit cells removed within the ground structure, a Connectivity Level of  $\sqrt{3^2 + 3^2 + 3^2} = \sqrt{27}$  will be required.

Next, the following steps are taken:

1. All nodes are created in a single  $n_{nodes} \times 3$  array containing all coordinates. Within this array, various groups of nodes exist, which will be treated differently in various stages of optimization. To identify those groups, a corresponding  $n_{nodes} \times 1$  array is created, which designates a type identification to each individual node. The most important types are included in Table 6.1. Extra types can easily be added if the need arises. Of these categories, only the 'FREE' nodes are added by the program. All other nodes are part of the initial design problem, and must be entered manually or otherwise beforehand.

Table 6.1 Descriptor strings for nodes.

Name	Description
LOAD	Node is a load introduction point (and potentially subject to displacement constraints)
FIX	Node is subject to a fixed constraint. Pinned or rolling supports can also be included
MASS	A mass is assigned to this node. Rotational inertias optional
FREE	Node is free to be moved in shape optimization steps and free to be removed in topology optimization steps or model reduction steps

- 2. Nodes that are within a small threshold distance of each other (depending primarily on the scale of the overall structure), are merged. In case of close proximity, initially included design problem nodes are retained, and 'FREE' nodes are deleted.
- 3. All possible elements are created, with a maximum length as defined previously by the Connectivity Level. These elements are identified simply by the pairs of nodes that they connect, in an  $n_{elements} \times 2$  array.
- 4. All elements are checked for overlap. For example, if the Connectivity Level is such that body diagonals are created for 2x2x2 unit cell groups, they will overlap perfectly with some of the body diagonals that are also being created for individual unit cells. In this case, short elements are retained and longer elements are removed.
- 5. If any nodes are in a keep-out zone, they are deleted, along with any associated elements.
- 6. Even when connecting two nodes that are in the approved design space, individual elements can still cross a keep-out zone. A separate check using an interpolation approach is carried out to remove such elements from the element list.

Figure 6.5 shows a simple ground structure for a cubic design space with 4 unit cells in all directions and a connectivity level of 4.5, resulting in body diagonal elements in 3x3x1 cell unit cell groups as well as 4x1x1 cell groups, as well as all shorter available elements. Four nodes at the bottom corners with fixed constrained are visible as larger white dots, as are two load introduction nodes at the top row in the front view (b), as larger green dots that do not coincide with the regular grid.

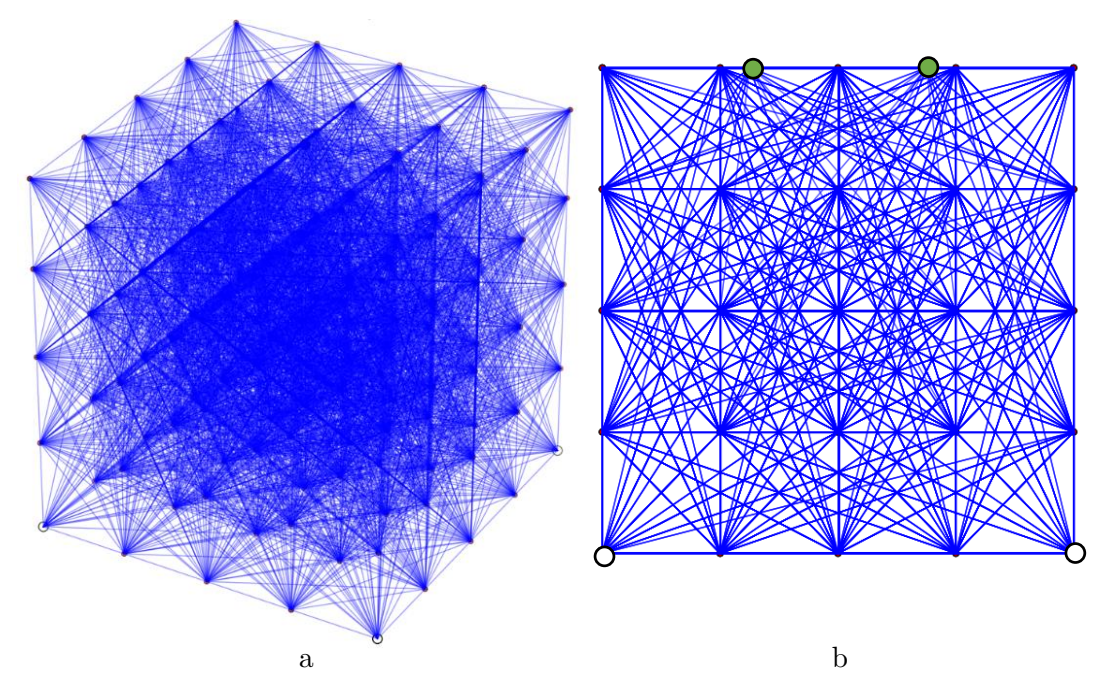


Figure 6.5 Ground structure for a cubic design space, isometric (a) and front view (b)

Figure 6.6 presents a more complex design space, filled with a 7x5x4 unit cell ground structure. The following features can be identified:

- Keep-out zones (red boxes)
- Load introduction nodes (large green points)
- Nodes with a fixed constraint (large white points)
- Nodes with associated inertias (large purple points)
- Free nodes (small red points), which may be manipulated in optimization steps

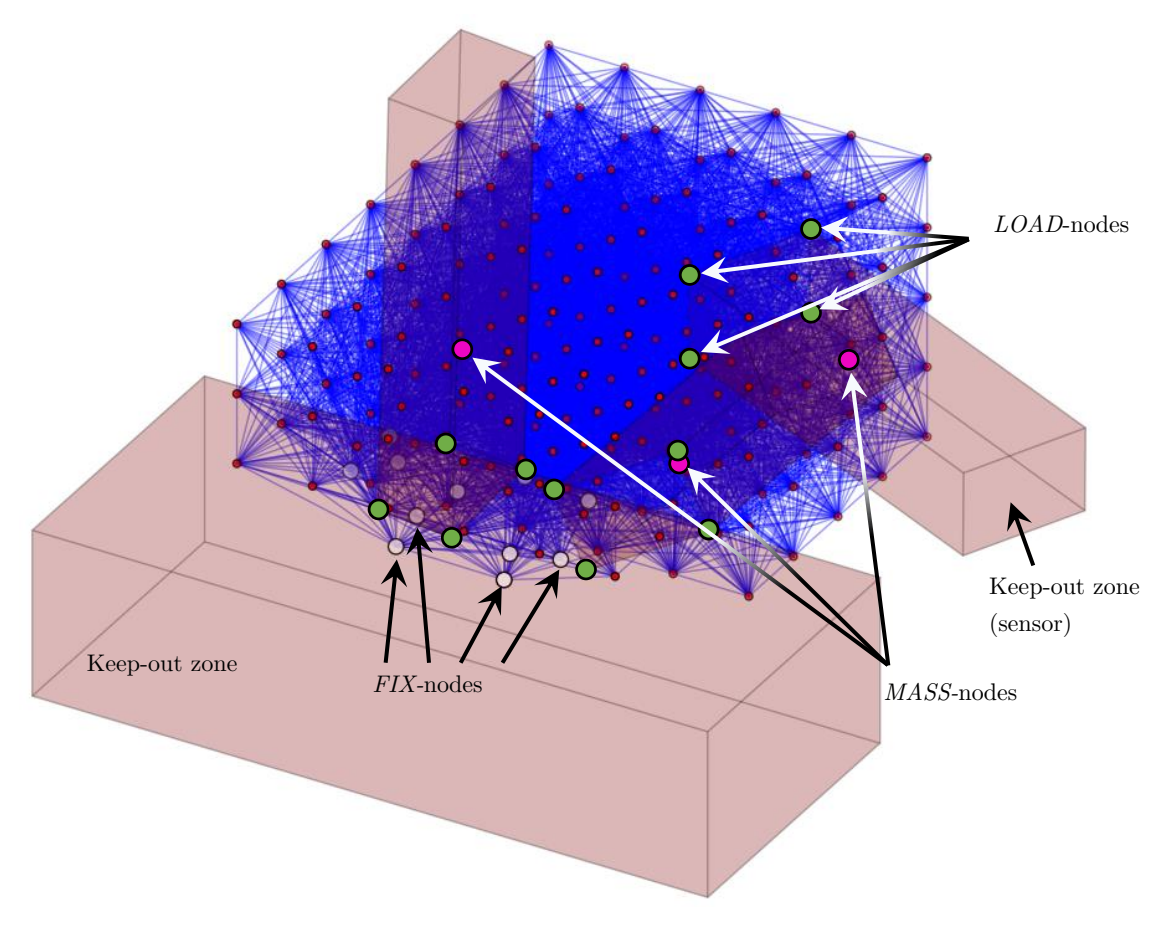


Figure 6.6 Ground structure for a more complex design space with keep out zones.

This is a design problem where three sensors (the smaller keep-out zones) are connected to a larger body (the fourth keep-out zone), with a predefined set of available interconnection points (the white nodes), not all of which need to be incorporated in the final design. Each of the sensors is modelled as a group of five nodes: four prescribed points to which the new structure can connect, together with a fifth point in the center of mass of the unit, to which all relevant inertias of that sensor are assigned. This node is connected to the first four through massless elements which are not part of the optimization process. Three sets of keep-out zone/mass node/load introduction nodes can be seen in the above figure. All three MASS-nodes have been indicated, along with all load introduction points of one sensor, as well as some of the FIX-nodes. In this design problem, maximum displacements are prescribed for the sensors, as well as a minimum frequency for the first Eigen mode.

The ground structures that are created in this way are fed into the topology optimization module where the next design step is executed.

# 6.5 Topology optimization module

Topology optimization is a method that is suited for determining load paths within a design space. This is generally achieved through analyzing a design space that is filled with elements, and selecting an element subset that is used for further optimization. As discussed in Section 6.1, the optimization module makes use of some of the MSC Nastran built-in design optimization capabilities. This section lays out how this functionality has been implemented in the context of the Python Framework. Performing a topology optimization on a ground structure with 1D beam elements requires a different approach compared to optimization of a design space filled with solid 3D elements, which will be illustrated in this section.

#### 6.5.1 Topology optimization theory and implementation

A brief overview of topology optimization theory is given here. Emphasis is put on the way it is applied within Nastran, and why this is a suitable approach within the framework that is presented in this thesis. The goal is not to provide a comprehensive overview of different topology optimization methods, for which many excellent sources are available, such as Bendsøe (1995).

Nastran makes use of the Density Method approach, also called the Artificial Material approach or Power Law approach. A penalization scheme is applied to the relevant material properties (i.e. stiffness for compliance driven problems) to force elements to assume densities close to either 1 or 0. The relation between Young's modulus and density is shown in Equation (6.6) and Figure 6.7.

$$\rho = \rho_0 x$$

$$E = E_0 x^p$$
(6.6)

With x the variable being manipulated within a topology optimization (taking on values between 0 and 1),  $\rho_0$  the density and  $E_0$  the Young's modulus for fully dense material, and p the penalty factor.

For topology optimization, Nastran provides two main classes of Mathematical Programming-based optimizers:

- 1. The Sequential Unconstrained Minimization Technique (SUMT) within the MSC Automated Design Synthesis (MSCADS)-suite. Vanderplaats (1985) laid the groundwork for this method.
- 2. IPOPT, which implements an Interior Point line search filter method. Wächter & Biegler (2006) provide an overview of this method.

Both of these are well suited for dealing with problems with a large number of design variables, which is a requirement for topology optimization problems with tens of thousands of elements. Nastran will attempt to apply the first method, as it is more efficient. Nastran may either not achieve convergence, or otherwise decide that SUMT is not a suitable method for a particular problem. In this case, IPOPT will be deployed, which is more robust. Nastran guides provides additional background information (MSC Software Corporation, 2011a).

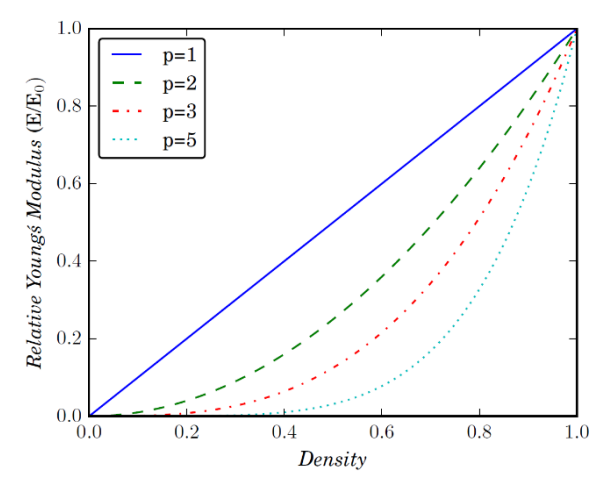


Figure 6.7 Relation of Young's Modulus to material density for different penalization parameter values (p=1: no penalization)

The Element Density Distribution (EDD) of a topology optimization result can be visualized. Ideally, applying a penalty method will result in an EDD as shown in Figure 6.8, with only elements with density either 0 or 1. The load case that is used for the common

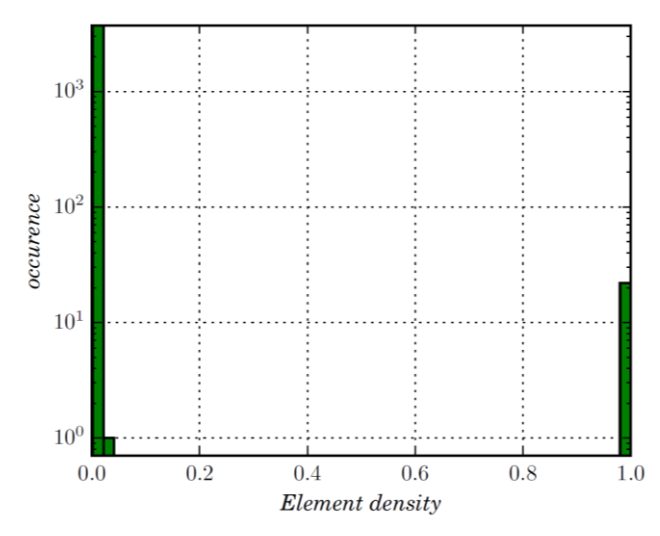


Figure 6.8 Element Density Distribution of a topology optimization on a ground structure with 3736 elements with close to perfectly discrete 0/1 division

sizing problem described in Section 5.1 has been applied to the ground structure shown in Figure 6.5. A topology optimization has been carried out, using a penalty factor of 4. 22 elements are assigned a density of 1 by the optimizer. All other 3714 elements have a density close to 0. In this case, filtering out useful elements is a trivial exercise: only the 22 fully dense elements are retained and passed on to the sizing optimizer to complete Phase 1 of the Optimization Framework.

#### 6.5.2 Difficulties of using 1D elements in topology optimization problems

Section 6.1 discusses the notion that optimization of ground structures with 1D beam elements involves separately controlling topology and member size. Conversely, a topology optimizer operating on a design space with finely discretized isotropic cube-like elements simultaneously controls topology and size of members: the cross section of an individual load carrying member can be increased by changing the density of elements at its boundary from 0 to 1.

As explained in Section 6.2, Nastran does not allow for simultaneous optimization of element size and topology. Therefore, for an optimizer purely operating on topology of a 1D beam ground structure, member size needs to be assigned explicitly beforehand, and needs to be the same for all members, due to limitations within Nastran (all elements subject to a single topology optimization operation must be described by a single element property entry). This can pose two different challenges, namely how to choose an initial member size, and how to determine a lower density threshold for filtering out the members that are to be retained. To illustrate this, let's consider three different situations:

- 1. The initial member size is about equal to the optimal size for the most heavily loaded members in the final result, and there is not a wide spread in member sizes in the final size-optimized result.
- 2. The initial member size is significantly greater than the optimal size for the most heavily loaded members.
- 3. The initial member size is significantly smaller than the optimal size for the most heavily loaded members.

The first situation will result in an EDD that is similar to that shown in Figure 6.8. Figure 6.9 shows the geometry that results when all 22 members that have a density of 1 are retained. In all figures in this section that illustrate geometry, cross sections are not plotted to scale, and colors denote strain energy density. Red is high, blue is low.

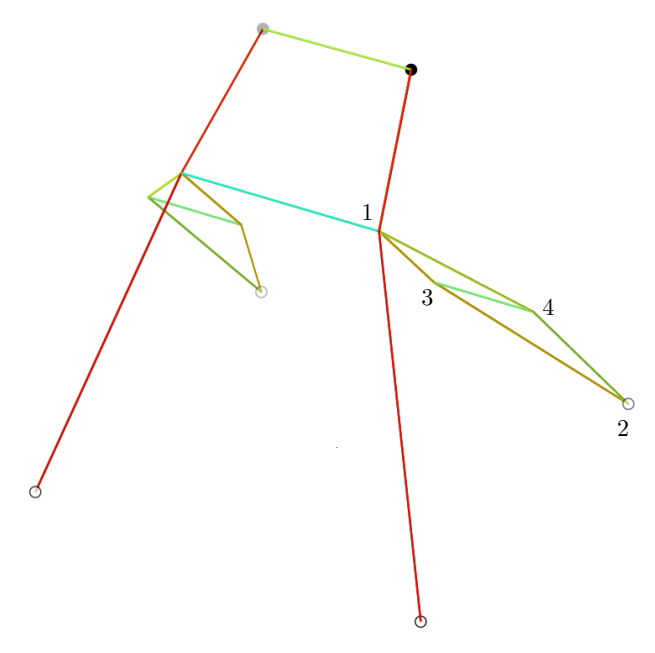


Figure 6.9 Topology optimization result (geometry) corresponding to the EDD in Figure 6.8.

Note the two sections on either side of the structure, consisting of five members each. These sections clearly do not provide the trivial solution for accommodating a load path between two points. This is a result of the choice of Connectivity Level as described in Section 6.4: No member was created initially that directly connects nodes 1 and 2. The later shape optimization phase provides robustness by not making the final result dependent on this initial 'shortcoming' in the ground structure: In the next phase, nodes 3 and 4 will be fused, after which each set of (now) four members is fused into a single member, since they are now all in line or fully overlapping. See also Section 6.7.

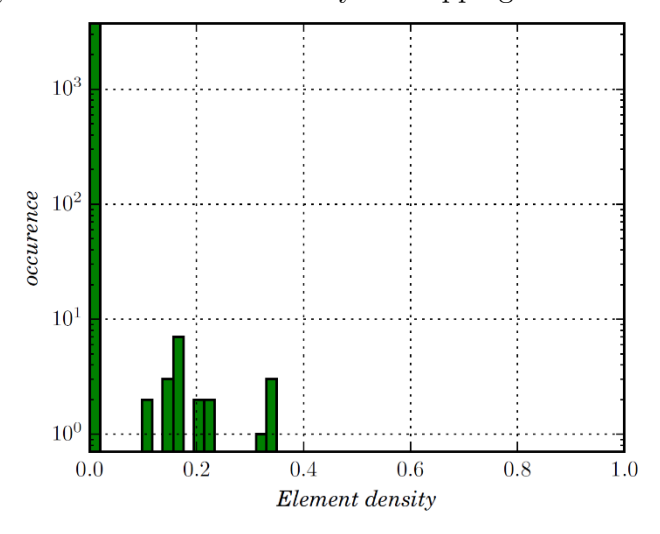


Figure 6.10 EDD of a topology optimization identical to Figure 6.8, except with larger member cross sections.

The Second situation will, for the same load case and ground structure, result in an EDD as seen in Figure 6.10: The most heavily loaded elements do not need to be fully dense in order to carry the loads. Already, translating the EDD into a usable set of elements is less straightforward than it was in the previous situation. A lower cut off density of around 0.05 must be chosen in order to select all elements that are to be retained and passed on to the sizing optimizer. For this simple structure and load case, this situation delivers the desired result (the same resulting element set as in the first case). However, for more complex cases, determining a proper cut off is not as trivial.

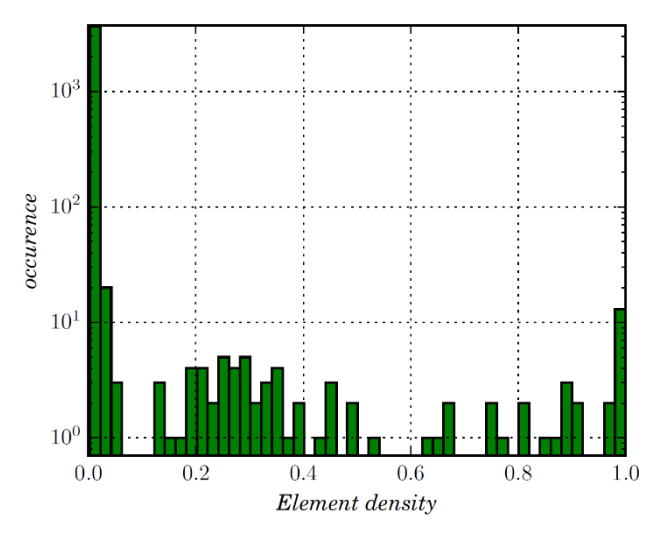


Figure 6.11 EDD of a topology optimization identical to Figure 6.8, except with a smaller member cross sections.

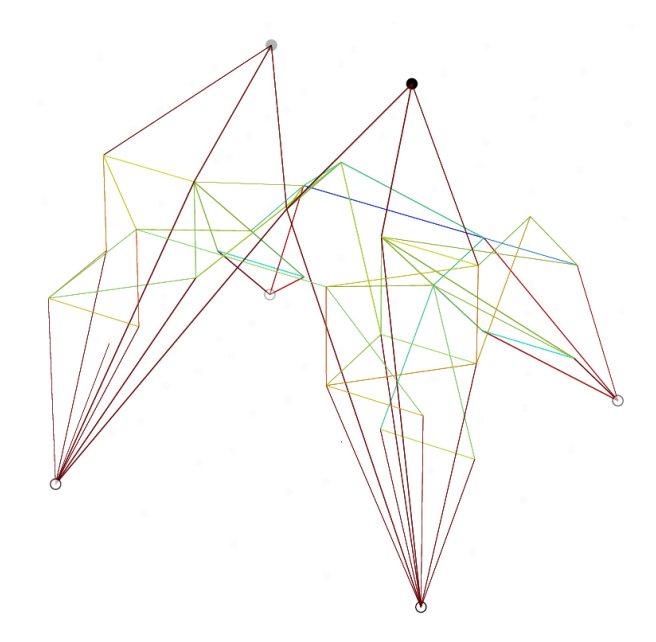


Figure 6.12 Geometry corresponding to the EDD of Figure 6.11.

In the third situation however, the EDD exhibits too much noise to properly select a subset for subsequent sizing optimization: The elements that are nearest to the most efficient load path are unable to carry the load by themselves when their density is 1. Therefore, elements nearby are forced to carry some of the load and are assigned a density of greater than 0. This results in the EDD and geometry seen in Figure 6.11 and Figure 6.12. Appendix D shows the geometry and EDD results for a sweep of topology optimization runs with the same ground structure geometry, but different initial member sizes.

#### 6.5.3 Mesh independency scheme

As has been shown, the result of a Nastran topology optimization is greatly dependent on the initial conditions. Member size (cross section) plays a large role, as well as the Connectivity Level and the number of cells that is chosen to discretize the design space. Especially for more complex design problems with multiple load cases and modal requirements, it is difficult to make a prediction of the optimal size of the most heavily loaded elements, which is a good starting point for element size in a topology optimization. In fact, it is undesirable to leave this decision to a human operator. For this reason, a mesh independency scheme has been implemented.

As is shown in the process overview in Figure 6.2, ranges of initial conditions with respect the number of design space subdivision cells and member size are selected. These lower and upper boundaries can be validated through running a topology optimization. They should clearly represent situations 2 and 3 as described in the previous section. Since the topology/sizing optimization process that constitutes Phase 1 is computationally relatively inexpensive, it is feasible to run a large number of simulations across a range of initial conditions. The simulation that results in the lightest overall size-optimized result is deemed the best candidate to be passed on to Phase 2 for the shape-size optimization sequence.

#### 6.5.4 Modal Analysis in 1D Element Nastran Topology Optimization

The sizing optimizer as implemented in Nastran has been shown to reliably produce usable results for complex load cases (combined static and modal), while respecting manufacturing constraints, see Section 6.6. The Topology optimizer however, produces much clearer results for static problems than it does for modal analyses and especially combined problems. For modal analyses, many semi-dense elements are created, as opposed to fewer, denser elements which result from a typical topology optimization for a structure of similar complexity. The latter is more desirable for two main reasons:

1. Due to the stiffness penalty that is applied, (nearly) fully dense elements more closely represent the actual properties of those elements. Penalized semi-dense

elements result in unnecessarily conservative weight estimates during topology optimization. (Note that this is solved by the subsequent Phase 1 sizing optimization.)

2. A 'cleaner' EDD, with fewer elements close to 0-density, can be more properly filtered to obtain a set of retained elements for the sizing optimizer. It has also been shown to typically result in a smaller set of elements, which is itself a trait that decreases overall complexity, thereby increasing manufacturability.

A test problem illustrates this issue, as well as the effectiveness of its solution: A point mass is attached to the top middle grid point in the ground structure that is seen in Figure 6.5. A downward vertical load is also applied to the same grid point. A topology optimization is executed, with the goal of minimizing mass while realizing a certain minimum Eigen frequency, and not exceeding a certain maximum stress in any of the members. Figure 6.13 shows the graph of the corresponding EDD. Note that no elements have been assigned a density of 0. Filtering out useful elements is non-trivial, if not impossible.

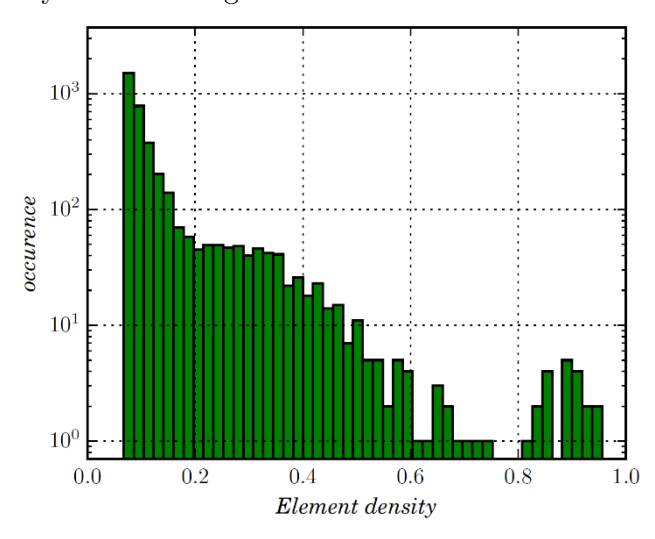


Figure 6.13 Typical EDD for a modal analysis-based topology optimization result in Nastran for a simple structure

To circumvent this issue, modal requirements in the topology optimizer are reduced to a statics requirement: relevant grid points (for example where a given mass is connected in the design domain) are independently subjected to loads in x-, y- and z-direction, and maximum displacements constraints are set. This establishes a starting point for the next phase where all proper load paths have been identified. In the next phase, the size optimizer will perform a full combined statics-modal analysis and determine a set of optimized element sizes. The determination of appropriate loads and allowed displacements is left to an operator and is based on the relative influence of requirements other than modal ones, i.e. to which extent the final result is driven by requirements that are ana-

lyzed purely statically. This is partly an iterative process, based on initial results. However, a full guide will not be given here. This process can be partly automated in the future. The validity of this simplified 'statically-executed modal analysis' depends on the criticality of the modal requirement of the topology-sizing optimized structure that results from Phase 1: If initial results indicate that requirements that are analyzed statically in the sizing optimizer are dominant as opposed to modal requirements, the modal analysis within the topology optimizer must also not be dominant, and should not be included. Figure 6.14 shows the EDD when the same problem as before (previously resulting in the Figure 6.13 EDD) is executed with a static approximation of the modal requirements during the topology optimization. The corresponding geometric representation of the result is also given.

Note: This EDD graph demonstrates that the topology optimization member size is much higher than necessary for the final structure, as explained in Section 6.5.2, but by virtue of the simplicity of the problem, a suitable subset of six elements can still be filtered out. Each of the three 'legs' of the stool in the right figure was described by two collinear ground structure elements. Because of buckling sensitivity for thinner beams, the optimal solution in this case turns out not to be a fully symmetrical stool with four identical legs, but a three legged stool with two thicker load carrying legs and a single stabilizing one.

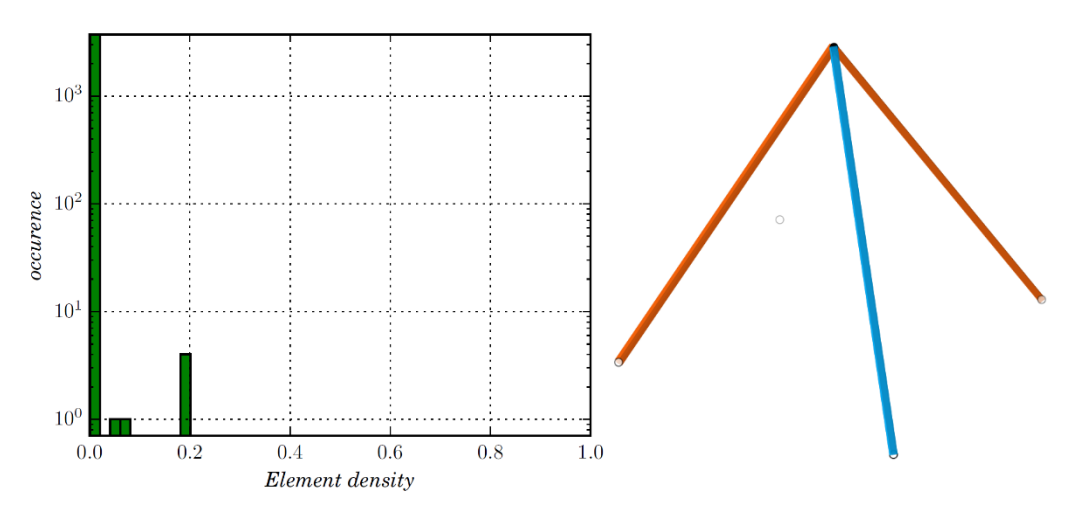


Figure 6.14 EDD of a purely static analysis-based topology optimization (left) and corresponding geometry after sizing optimization (right). Beam cross sections are not plotted to scale. Colors denote strain energy density: red is high, blue is low.

### 6.6 Sizing optimization

The Sizing Optimizer has been introduced in Section 6.2. It is founded on the built-in design sensitivity and optimization modules within Nastran. Design variables are coupled to the cross sections of individual members and an optimizer is used to minimize

the weight (or optimize another property) of the overall structure. The Sizing Module is at the core of the Optimization Framework in two ways:

- 1. It is implemented as the final step after topology optimization in Phase 1 as well as the basis of the shape optimizer in Phase 2, as described in Section 6.2.3.
- 2. For that reason, it is at this level that most (manufacturing) constraints are definitively enforced.

This section describes the implementation, scope and limitations of the sizing optimization module.

#### 6.6.1 Scope of optimizer module and inputs

Within the Sizing Optimizer, design problems can be solved which take into account the following design constraints:

- Modal requirements (specifically: a minimum value for the lowest Eigen mode of the overall structure)
- Maximum allowed stress in individual members
- Maximum displacement in different directions of individual grid points.
- Prevent buckling of individual members and the structure as a whole
- Minimum allowed member size

Many features that can be used to set up a model within Nastran can be incorporated in the models that are fed into the sizing optimizer. Importantly: multiple load cases can be combined into a single optimization. For example, a typical design problem may include the following loads:

- 1. An acceleration (simulating peak launch forces), during which certain displacements and stresses may not be exceeded and no buckling may occur.
- 2. A (quasi-)static load due to a separate connected structure whose acceleration load must be transferred during launch, during which max stresses and displacements are defined and no buckling may occur.
- 3. A separate load case which models operation with the goal of achieving adequate positioning accuracy of a measuring instrument.
- 4. A simulation can analyze the lowest Eigen mode of the structure, with the goal of preventing excessive vibrations during launch.

Regardless of whether Nastran has converged to a solution that it considers optimal, the outcome of the sizing optimizer is a set of values which describe the cross sections of each member, as well as additional performance indicators with respect to critical constraints in its last simulation cycle. These values are returned to the Python Framework, which evaluates them and interprets them as a set of safety factors for all constraints listed

above. This means that even an optimization run that has not converged according to Nastran's criteria, can be evaluated relative to other solutions. This is useful: especially for complex, combined load cases, optimizations do not always fully converge, in fact they often don't. However, in many of those cases, a suitable structure is nonetheless proposed (light, and within acceptable margins for all boundary conditions). This shows the need for an approach for deciding which results are valid that is more sophisticated than Nastran's pass/fail output, based purely on (non-)convergence. Section 6.6.3 discusses this further.

#### 6.6.2 Choice of optimizer algorithm

In the standard setup, Nastran will select the best suited optimization method within the MSCADS module which was discussed in Section 6.5.1, based on problem parameters such as the number of design variables and the number of active constraints. This automatic algorithm selection option chooses from the Modified Method of Feasible Directions (MMFD) as well as SUMT (see Section 6.5.1), Sequential Linear Programming (SLP) and Sequential Quadratic Programming (SQP). These four methods are complemented by the IJK Method, which allows the user to independently choose a strategy (I), optimizer (J) and one-dimensional search method (K). For a representative sizing optimization problem, all options have been compared in terms of convergence reliability, number of iterations required and final result. Other than for topology optimization problems, the most commonly applied module is MMFD. Nastran documentation (2011a) notes:

Experience has shown that the MMFD algorithm is the most reliable for MSCADS.

For the types of structures described in this thesis, these findings have been reproduced by running simulations. As a result, MMFD is the default optimization algorithm for the Sizing Optimizer described here.

#### 6.6.3 Result interpretation: Convergence and achieving robustness

The Sizing Module operates on two levels:

- 1. Nastran runs a DESVAR-based SOL200 optimization.
- 2. A higher level Python Framework compiles the input files for these runs, and interprets their results.

Specifically, the Python Framework assesses the validity and usefulness of Nastran's results. If non-validity is established, the framework has different options available which will be discussed later.

Whether a design optimization problem convergences can be taken as a first indication of the validity of its result. Nastran considers a problem converged when a set of design variable values is found that results in near-zero sensitivity, i.e. a small variation of their

value does not lead to an improvement of the objective function. This indicates that the solution is at least a local optimum. Among the aspects that can be assessed to evaluate robustness of an optimizer are:

- Whether the optimization converges to a solution which complies with all constraints.
- Repeatability of results.
- Insensitivity to initial conditions (such as design variable starting values).
- Whether the resulting optima are global optima.

A variety of sizing optimization tests has been performed on design problems of different types (static, modal, combined) and varying degrees of complexity in terms of load cases and design space. This has resulted in many observations, the most important ones being:

- Internally converged problems always comply with all design constraints. This is simply a result of hard criteria within Nastran.
- The reverse is not true. Rather, a non-converged problem may still comply with all design constraints, within desired margins, and may in fact be close to an optimum.
- Whether a problem converges can depend on the initial values of the design variables, although not in a predicable manner. The following extreme scenario was encountered:
  - 1. The initial design variable values for a certain simple design problem were set to their minimum allowed value, which was set at an arbitrary value, significantly lower than the ideal value. This resulted in a converged solution.
  - 2. This solution, i.e. a known optimum, was used as the initial value for a subsequent optimization run. This resulted in non-convergence: Nastran did not recognize the initial state as an optimum, diverged, and did not converge again.
- However, whenever convergence occurs, the value of the objective function is generally identical within a small margin, (dependent primarily on the convergence criteria), independent of initial conditions, even for complex problems. This is a critical observation, as it indicates one of two things:
  - 1. If it converges, the solver reliably converges to the global optimum
  - 2. The solver reliably converges to one of several local optima which are nearly equivalent to the global optimum

Within the context of a design problem for industrial purposes (as opposed to a purely academic one), these two scenarios can be regarded as equally valuable.

• More specifically, whenever a simple problem is considered for which a single trivial analytical solution is available, converged solutions closely approximate this solution.

- However, as should be expected, for non-converged problems which do comply with all design constraints, proposed solutions may be anywhere between close-to-optimal and highly non-optimal.
- The solver can become stuck by 'fluttering' between two close-to-optimal solutions, causing non-convergence. See also Appendix E.
- Whether a problem converges is often independent of strictness of convergence criteria. Specifically, problems that do not converge according to Nastran's criteria, yet do result in a close-to-optimal solution (objective function value close to global optimum and design criteria within acceptable margins), typically do not suddenly converge when relaxing the convergence criteria. 'Fluttering' can still occur in this case, just at a less optimal value of the objective function.
- As was also found in topology optimizations, Nastran's behavior is less stable (in terms of achieving convergence) for modal analyses than for purely static problems.

It can be concluded that by itself, Nastran's SOL200 suite does not provide a robust way of performing sizing optimizations. Especially for use in an automated context, with no human operator that can judge the validity of individual results, this needs to be addressed. Several measures have been implemented in the Python framework that drastically increase the number of usable Sizing Optimization results, in two main ways:

- 1. Increasing the likelihood of achieving optimization convergence
- 2. Applying a more sophisticated method to judge result validity than a pass/fail test based on (non-)convergence according to Nastran's internal criteria.

Assuming no outright errors occur (which would typically indicate human error or licensing issues), a Nastran optimization run normally terminates in one of three ways:

- 1. A 'hard convergence to an optimum' is achieved. All boundary conditions have been met, and the solution has converged.<sup>5</sup>
- 2. A 'best compromise design' is found. Such a solution generally violates one or more design variables by a relatively small amount
- 3. The run is terminated because the maximum allowed number of design cycles has been reached without converging.

The design constraints, maximum amount of runs and convergence criteria are all user inputs, and it was initially assumed that Nastran's would always be able to find a fully converged solution if these convergence criteria were progressively relaxed. As noted, this turns out not to be the case. Instead, the following strategy is employed:

<sup>&</sup>lt;sup>5</sup> Depending on settings, *soft convergence* may also be a valid termination criterion. This indicates convergence of design variables as opposed to the objective function for *hard convergence*.

- 1. Demand relatively strict coherence to design constraints from Nastran, and apply a relatively strict convergence criterion (i.e. constraint compliance and convergence criteria both within 0.1%)
- 2. When Nastran cannot fully converge to an optimized solution, the Python framework performs its own checks with slightly relaxed criteria for both optimization convergence and design criteria (i.e. within 1%). To that end, the framework has been expanded by implementing its own convergence analysis, by reading the relevant data from the Nastran output files to assess the objective function value, which design constraints were violated, and by how much.

An additional method to improve robustness follows from two observations:

- 1. A Sizing Optimization run will typically either not converge, or converge within a certain number of cycles, which is dependent on the complexity of the structure (a model with more elements will normally require more cycles) and the load case (a combined static/modal analysis requires significantly more cycles than a purely static one). However, sometimes problems do converge after a significantly higher number of cycles than would be expected.
- 2. As noted, problems that do not initially converge, may converge when different initial values are used for the design variables.

Especially for more complex design problems, a significant percentage of optimization runs do not converge, but terminate because the maximum number of cycles is reached. For this reason, it is computationally very expensive to set the maximum number of cycles high enough that every problem that can converge, will converge. Therefore, whenever a run does not immediately converge, and the non-converged result is not found to be satisfactory according to Python's convergence criteria, a second run is initiated using different parameter values: At the same time a different set of initial conditions (now all of them at their maximum allowed value instead of in the middle of their allowed range) is used, as well as a higher allowed number of cycles. If that solution does not converge, a third attempt is made with all design variables at their lowest allowed initial value, and a higher number of allowed cycles still.

Test cases have shown that attempting those two additional sets of initial values (lowest and highest allowed design variable values) increases the number of converged simulations, compared to only running one optimization with initial conditions inherited from a previous solution from a similar problem. The impact of these measures is greater for more complex problems. For a problem similar to that introduced in Figure 6.6, the number of useful results increases from about 30% of all simulations to >90%.

# 6.7 Shape optimization

The Shape Optimization module was introduced in Section 6.2. It manipulates the location of individual grid points, i.e. the connections between members, with the goal of achieving a structure that better meets the objective function (e.g. has a lower mass). Essentially, the Shape Optimization Module leverages the functionality of the Sizing Optimization module. Since its operation has a greater impact on the way the entire Optimization Framework is structured (primarily since it operates at a higher level than the Size Optimizer), the shape optimization process is more extensively explained in section 6.2.3, compared to the functioning of the other two modules (topology and sizing optimization). Therefore, this section provides only additional information with respect to its implementation.

#### 6.7.1 Shortcomings of built-in Nastran functionality for shape optimization

For reference purposes, this subsection provides a summary of conclusions presented in Section 6.2. Nastran's built-in DVGRID/DESVAR functionality for coupling grid point location to design variables is not suitable for 3D geometrical optimization. The main reason is that manipulation of the location of each grid point in each of the three different directions is regarded independently within Nastran. Even for simple design problems, it has been shown that this can result in diverging solutions. To achieve the desired optimizer behavior (i.e. convergence towards a global optimum) a more intelligent assessment is required for determining sensitivity of the objective function with respect to grid point location manipulation. As this is not possible using a built-in optimization algorithm, a controlling shell has been developed in Python which uses Nastran to analyze fitness of each solution.

#### 6.7.2 Choice of optimization algorithm

Since the method used for shape optimization is self-developed rather than a built-in Nastran process, its operation has been explained in more detail in Figure 6.2 and Section 6.2.3. Within the context of this thesis, a trade-off has been made between achieving higher computational efficiency and the time needed to develop the optimization algorithm. A pattern search method has been implemented. Reliability is the main goal for this method. Although the search algorithm is not particularly advanced, its operation and convergence criteria can be precisely controlled. Several problems that Nastran cannot deal with appropriately are addressed.

Not all details will be listed here, but the most important characteristics are:

- It is a stable algorithm with predictable behavior
- The Shape Optimizer takes the history of solutions into account, which leads to reliably converging solutions
- It is less computationally efficient than other, more sophisticated setups

This approach is likely not the most powerful method with regard to avoiding local optima in favor of the global one. However, the negative impact this has is largely dependent on the starting point of the shape optimizer. If Phase 1 operates properly (i.e. as described in Section 6.5.3, a sufficient number of initial conditions is considered to guarantee a certain degree of optimality), Phase 2 is not tasked with finding completely new layouts, which could involve overcoming 'hills' in the design landscape. Rather, the Shape Optimizer is tasked with further optimizing load paths that have already been established. Nonetheless, Section 8.2 proposes improvements that can be made to this relatively simplistic approach.

#### 6.7.3 Notes on operation

Section 6.6 explains how results in the Nastran-run Sizing Optimization are controlled and interpreted. As noted, not all optimization runs result in an accepted solution. With respect to this issue, there are some relevant observations to be made:

- Except for the very last iteration, exact quantitative determination of the optimal sizing solution is not required to compare two solutions within the sizing optimizer. Rather, convergence criteria can be relaxed to some extent as long as a reliable qualitative assessment can be made of the benefit of a certain proposed shape change step. Such a relaxation further increases the success rate of the Sizing Optimizer.
- Whenever, regardless of the measures described in Section 6.6.3, no acceptable solution is found, the proposed step is entirely disregarded as a feasible direction in the pattern search. As long as the number of discarded steps is low (i.e. significantly lower than 1/6, which equates to one step per grid point per cycle), the search algorithm can still find the same solution via a different route.
- As explained, the main reason DVGRID does not work for these 3D structures is the implied, and invalid, assumption that multiple moves in different directions of a single grid point are independent events. To a lesser extent, this also holds for moves of different grid points: moving one grid point influences how valuable a certain move is for other (primarily neighboring) grid points. This is counteracted in two ways:

- By gradually decreasing step size, the influence that a step has on moves
  of neighboring grid points is also gradually decreased as a solution nears
  convergence
- Even if two specific steps for two different grid points were flagged as beneficial, the combined result is always checked. If that result performs worse than the baseline, it is not accepted. Instead, the algorithm reverts to a proposed solution which implements fewer successful steps, as explained in 6.2.3.

#### 6.7.4 Relevant design constraints during shape optimization

As noted in Section 6.6, most design constraints are monitored within the Sizing Optimization level. Some design constraints however, are explicitly only monitored at the Shape Optimization level. A basic functionality of this module is assessing compliance with regard to keep-out zones. Only solutions where all grid points lie within the predefined design space are accepted. Additionally, no members may cross any keep-out zones. To this end, an interpolation scheme has been implemented which checks for interference between keep-out zones and interlaying points between each set of two grid points which is connected by a member, equivalent to what is used during ground structure generation.

The Sizing Optimizer can be expanded with design constraints that work towards increased manufacturability. Specifically, 'continuity' of members can be controlled at this level. For neighboring members that together are part of a major load path in a structure, a certain degree of collinearity can be expected. This opens up the possibility of using more efficient joining methods, as described in Section 5.3, and as applied in the prototype described in Section 5.4. The mutual angle of each set of major members can be included in the objective function in a way that angles below 15 degrees are given preference. However, this has not been developed further within this thesis.

# Chapter 7

# Finite Element Analysis of joints

As discussed in Section 6.3.2, in order to simplify parameterization and manipulability of the composite skeletons, as well as drastically increasing computational efficiency, a significant model reduction has been employed for the Nastran analyses in the Python Framework. These models are well suited for finding efficient skeleton layouts, assessing global stiffness and analyzing a range of potential failure modes. However, detailed analysis of the joints which connect individual members is not possible within these simulations. This is especially true when considering stresses and failure. This section lays out how this can be taken into account, focusing primarily on strength analysis. Results and considerations with respect to stiffness are also presented.

# 7.1 Goals and approach

Significantly higher stresses are expected at interfaces and other stress raisers in the joints. Their magnitude greatly depends on the combination of the directions and magnitudes of individual loads in each incoming member of a joint, which may either increase or partly cancel out each other's resulting stress peaks. The specific material also plays a large role. For example, it has been found that  $\sigma_{22,t}$ , i.e. tension transverse to the fibers, is often critical. Within the Optimization Framework, strength critical members are primarily optimized using Maximum Stress Failure Theory to establish First Ply Failure (FPF) by analyzing  $\sigma_{11}$  throughout its cross section. Therefore, a material with a higher  $X^c/Y^t$  or  $X^t/Y^t$ -ratio (depending on the critical load direction of the member) will likely require higher safety factors for certain load cases. Here,  $X^c$  and  $X^t$  are the symbols used to denote the failure strength of a material along the fibers in compression and tension respectively. Stresses in the corresponding directions are indicated as respectively negative and positive values of  $\sigma_{11}$ . In the same manner, stresses transverse to the

fibers are indicated using  $\sigma_{22}$ , and the peak allowable stresses in that direction are  $Y^c$  and  $Y^t$ . Different types of shear are indicated by the symbol  $\tau$ , followed by the accordant directions.

The aim of this investigation is not to derive a generally applicable set of safety factors which can account for stress peaks in different types of joints. Rather, a method is presented for accurately analyzing loads in a typical joint. The load factors found in such a simulation can be implemented as safety factors for that specific joint to account for the differences between stresses found using a simplified beam model (as used in the Optimization Framework) and those occurring in real manufactured joints. It is expected that each strength critical node will need individual analysis to derive its specific required safety factors. Failure modes that can occur in a real joint include:

- Failure along the fibers due to tension (i.e.  $\sigma_{11} > X^t$ )
- Failure along the fibers due to compression (i.e.  $\sigma_{11} < X^c)$
- Failure transverse to the fibers due to tension (i.e.  $\sigma_{22} > Y^t$
- Failure transverse to the fibers due to compression (i.e.  $\sigma_{22} < Y^c$ )
- Shear failure in a ply (i.e.  $|\tau_{12}| > S$ )
- Inter-laminar shear failure (i.e.  $|\tau_{13}| > S_{IL}$  or  $|\tau_{23}| > S_{IL}$ , see also Creemers (2009))
- Delamination due to e.g. crack propagation of voids or other flaws

As a demonstration case, the joint model that has been developed for the manufacturing tests described in Chapter 5 is considered. Results for strength analyses are presented in Section 7.2.1 for five different load cases:

- 1. Compressive loading of a member which is nearly in line with another member, representing a major load path (member 1 in Figure 7.1b)
- 2. Tensile loading of member 1
- 3. Compressive loading of a member with a smaller cross section, which is perpendicular to larger members in the same joint (member 2 in Figure 7.1b)
- 4. Tensile loading of member 2
- 5. Bending loading of member 2

Additionally, stiffness behavior of the two models is compared in a separate load cases. The corresponding results are presented in Section 7.2.2.

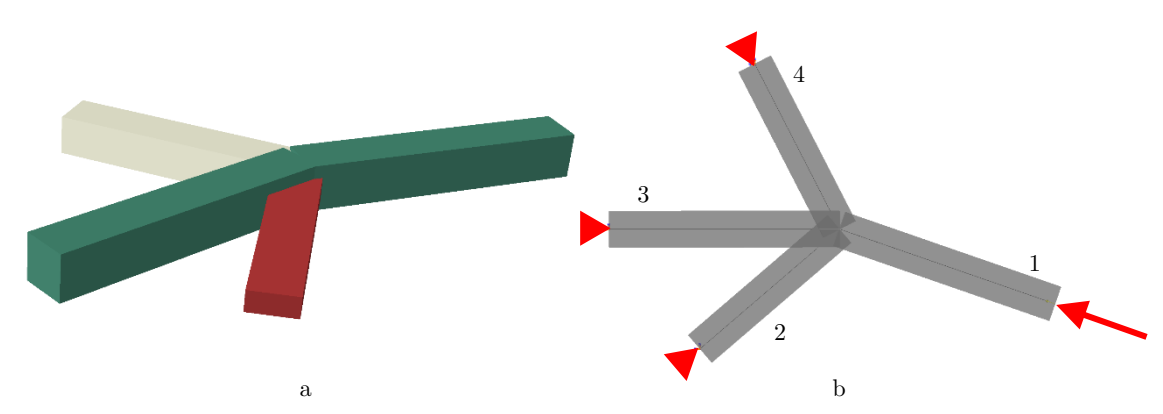


Figure 7.1 Simple beam model, as applied in Optimization Framework (a) and boundary conditions and applied load for load case 1 (b).

For strength analysis of the joints, a simple beam model is first considered, as depicted in Figure 7.1 a. This is representative of the method used in the Optimization Framework. The loads listed above are applied to the end of one member, with a magnitude resulting in a 1 Pa stress field in load cases 1 through 4, and resulting in a stress of 1 Pa in the most outward plies for the bending load case. The three other members are pinned at their end points. This results in normalized stresses in the structure, directly indicating the influence of any occurring stress raisers.

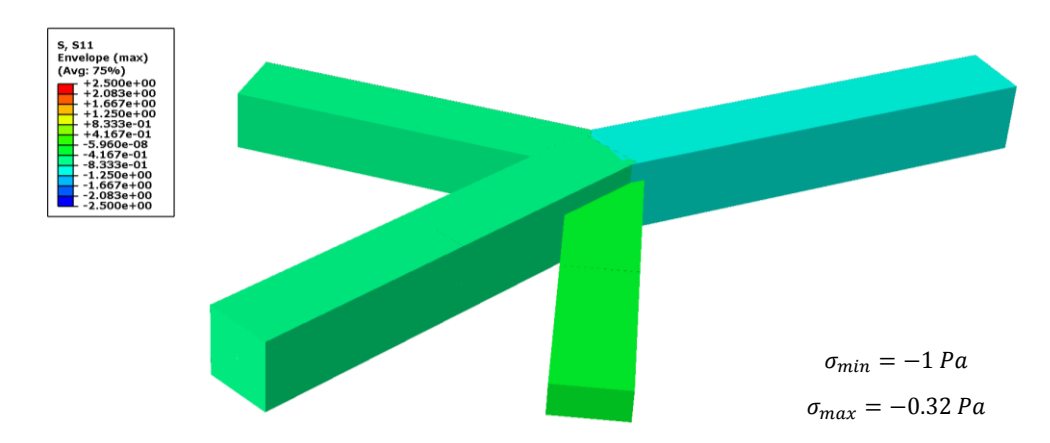


Figure 7.2 Beam model result:  $\sigma_{11}$  is displayed with the same color scale used in Figure 7.5

Predictably, this leads to the result seen in Figure 7.2: No compressive stresses beyond the applied 1 Pa are observed, since this model cannot model any stress concentrations and interactions between plies in different directions which occur due to the way members are interconnected in reality.

These results are compared to an analysis of a solid element model based on the CAD model for the manufacturing test presented in Section 5.4, which models fiber directions, layups and thickness build-up of stacked plies. Figure 7.3 depicts the mesh for this model.

This model provides the opportunity to investigate several crucial aspects:

- The influence of geometric stress raisers like the transition regions from the constant-section members to the thicker joint, and other edges that occur in the more comprehensively modelled joints.
- The stresses at interfaces between individual plies which do not lie in the same direction.

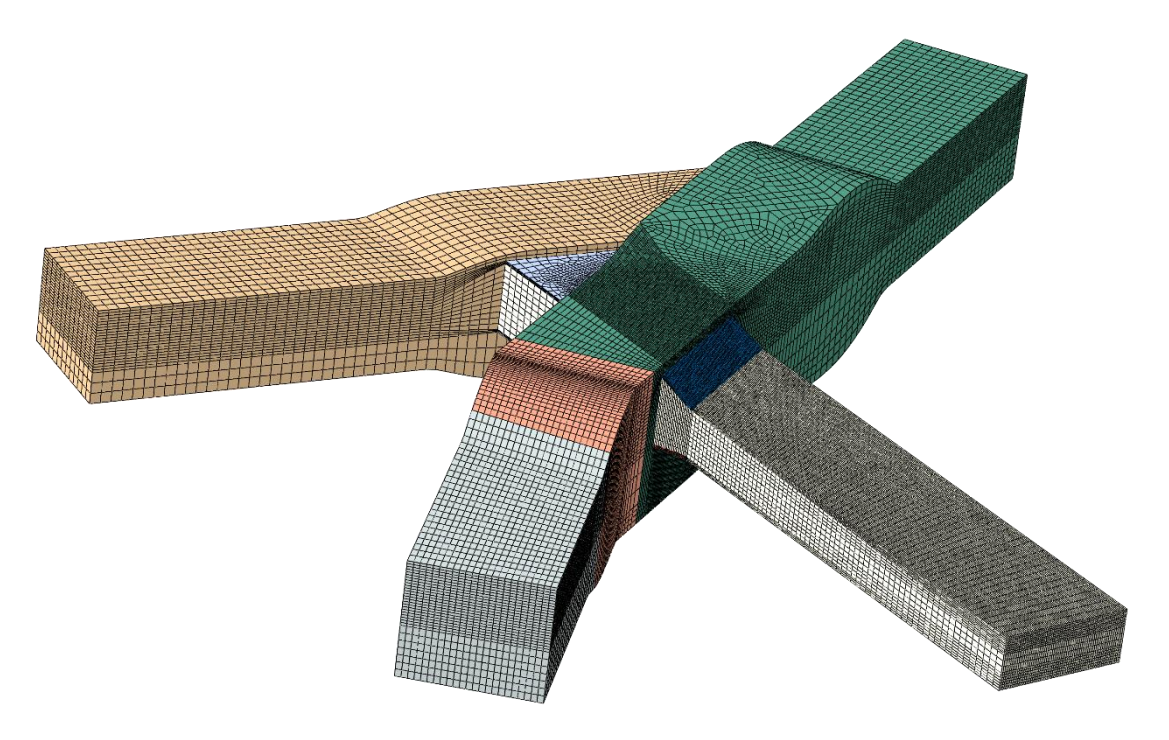


Figure 7.3 FEA mesh of the solid model. Different colors denote different layups/fiber directions.

The interface between two members with the greatest direction mismatch has been modelled explicitly, as seen in the section cut in Figure 7.4. Here, the assumption has been made that one of the following two statements is always true for stresses due to interaction loads between the outer plies of member 2, and the neighboring plies of member 1:

- 1. They are representative of the stresses found throughout the thickness of member 2 in the overlap region (in the case of pure compression or tension of the members involved)
- 2. The highest occurring stresses can be found in these most outward plies (in cases with bending load components, perpendicular to the ply stacking direction)

Except for these explicitly modeled interface plies, all sections are modeled using the built-in composites lay-up functionality in Abaqus. Rather than modeling individual plies using dedicated elements, this method assigns each section with appropriate laminate stiffness properties derived from the fiber directions that are present in that section.

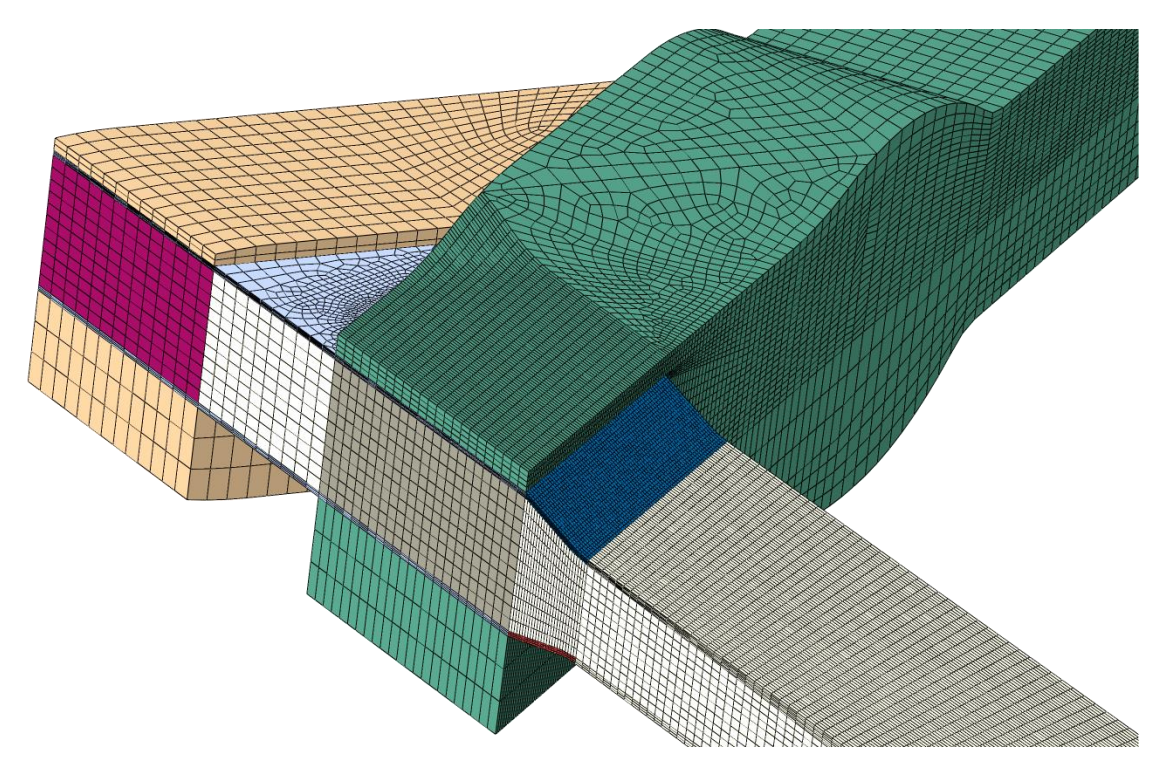


Figure 7.4 Section view of the joint as depicted in Figure 7.3. Note the individually modelled outer ply of member 2.

The material properties for the material that was also used to manufacture the test node are presented in Table 7.1. The same material is applied in the FEA model.

Table 7.1 Strength (A-basis) and Stiffness properties for Hexcel 8552 IM7

Stre	ength	Stiffness			
Variable	Value	Variable	Value		
$X^t$	2006 MPa	$E_{11,tension}$	161 <i>GPa</i>		
$Y^t$	81.36 <i>MPa</i>	$E_{22,tension}$	11.4 <i>GPa</i>		
$X^c$	1275 <i>MPa</i>	$E_{11,compression}$	143 <i>GPa</i>		
$Y^c$	222.7 MPa	$E_{22,compression}$	12.8 <i>GPa</i>		
$\mathcal{S}_{12}$	97.22 MPa	$G_{12}$	5.2 <i>GPa</i>		
$\mathcal{S}_{IL}$	120.7 <i>MPa</i>	$ u_{12}$	0.32		

#### 7.2 FEA Results

This section presents the results of the analyses introduced in the previous section. First, the results from the strength analysis are presented, followed by stiffness analysis in a separate subsection.

#### 7.2.1 Strength Analysis

Figure 7.5 shows a result plot that is equivalent to the 1D beam model plot shown in Figure 7.2. The peak stresses can be interpreted as an effective load factor, after taking into account that  $X^t/X^c = 1.57$  for this material: i.e. load factors of 3.58 and 4.48/1.57 = 2.85 are found for compressive and tensile fiber stresses respectively.

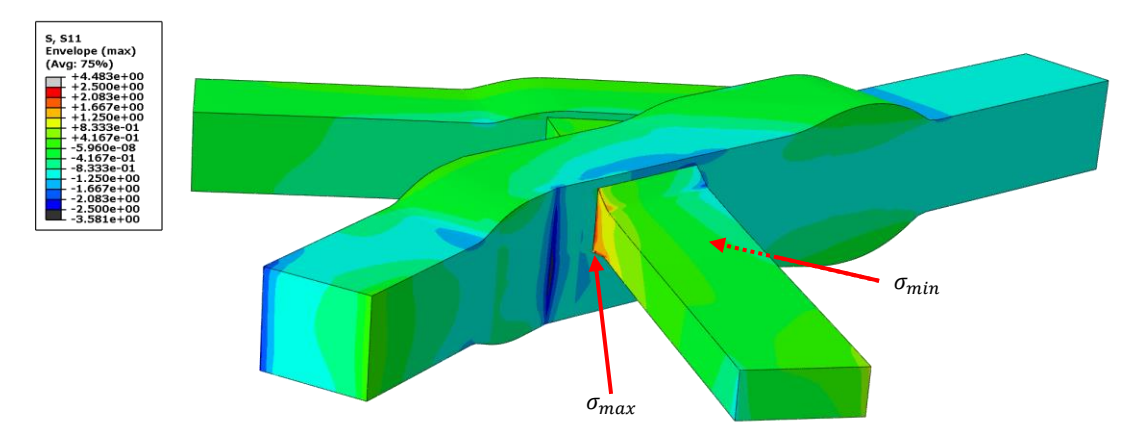


Figure 7.5 Result for load case 1 (compression of the main member):  $\sigma_{11}$  plotted in the same color scale as Figure 7.2

For each load case, peak stresses are assessed separately for the transverse member and the rest of the joint, so a good understanding is acquired with respect to the stresses at the interface between these two sections, where peak stresses are likely to occur. For load case 1, the most critical stress type is tensile  $\sigma_{22}$  in the transverse member, at the interface plane with the rest of the joint, as seen in Figure 7.6.

FEA Results 83

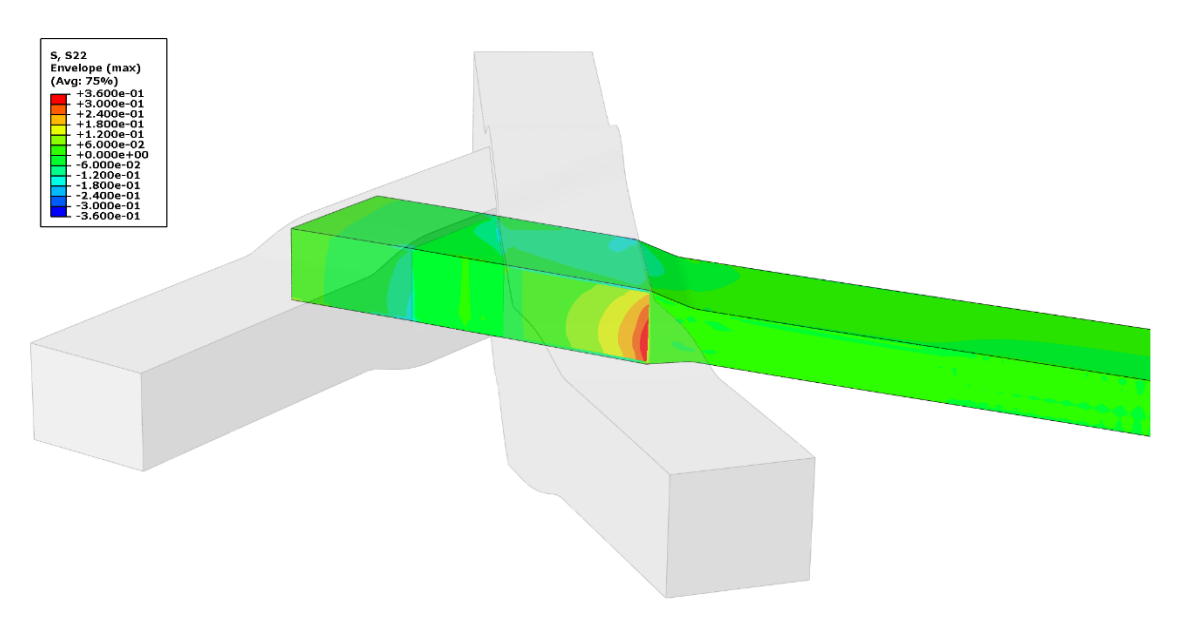


Figure 7.6 The highest load factor for load case 1 occurs for tensile  $\sigma_{22}$  in the transverse member.

Load case 1 results for other stress types are listed in Table 7.2. The highest load factors are indicated in orange.

Table 7.2 Load factors for load case 1: main load path member loaded in compression

			1		-:		•
		member		joint			
stress type	stress type		$\sigma_{max}$ , $\tau_{max}$	$\sigma_{min}$	$\sigma_{max}$ , $ au_{max}$	failure stre	esses (norm)
$\sigma_{11}$	results	-3.58	4.48	-2.916	0.466	$-1 (X_N^c)$	$1.57 \; (X_N^t)$
	load factors	3.580	2.854	2.916	0.297		
$\sigma_{22}$	results	-0.354	0.350	-0.120	0.303	$-0.175 \ (Y_N^c)$	$0.064~(Y_N^t)$
	load factors	2.023	5.469	0.686	4.734		
$ au_{12}$	results		0.296		0.213		$0.076 (S_{12,N})$
	load factors		3.895		2.803		
$ au_{13},  au_{23}$	results		0.280		0.222		$0.095 (S_{IL,N})$
	load factors		2.947		2.333		

The results for the other four load cases described previously are listed in Tables 5 through 8. As for the simplified beam model, for each load case, the magnitude of the load is chosen such that a  $\sigma_{11}$  stress of  $1\,Pa$  results in the critical fibers in the member, which corresponds to the FPF criterion that is applied in the Optimization framework. All failure stresses are then normalized to whichever is the critical stress according to this failure criterion, and follow from the material properties found in Table 7.1. For a tension load case, all failure stresses are normalized with respect to  $X^t$ , indicated as  $X_N^t$ . For compression load cases,  $X^c$  is used. Since  $|X^c| < |X^t|$ ,  $X^c$  is also used for the fifth load cases which assesses bending. In each load case result table, this relevant Framework failure criterion has been highlighted in blue.

Table 7.3 Load factors for load case 2: main load path member loaded in tension							
		member		joint			
stress type		$\sigma_{min}$	$\sigma_{max}, \tau_{max}$	$\sigma_{min}$	$\sigma_{max}, \tau_{max}$	failure stre	esses (norm)
$\sigma_{11}$	results	-4.48	3.59	-0.466	2.87	$-0.64~(X_N^c)$	$1 (X_N^t)$
	load factors	7.000	2.780	0.844	3.320		
$\sigma_{22}$	results	-0.350	0.354	-0.322	0.083	$-0.111 \ (Y_N^c)$	$0.041 \; (Y_N^t)$
	load factors	3.153	8.634	2.901	2.024		
$ au_{12}$	results		0.214		0.191		$0.0485~(S_{12,N})$
	load factors		4.412		3.938		
$ au_{13},  au_{23}$	results		0.285		0.226		$0.06 \; (S_{IL,N})$
	load factors		4.750		3.767		

Table 7.3 Load factors for load case 2: main load path member loaded in tension

Figure 7.7 shows the most critical stress type for load case 2,  $\sigma_{22}$ . The peak stresses occur very locally in the explicitly modeled outer plies, directly next to a sharp transition in the model.

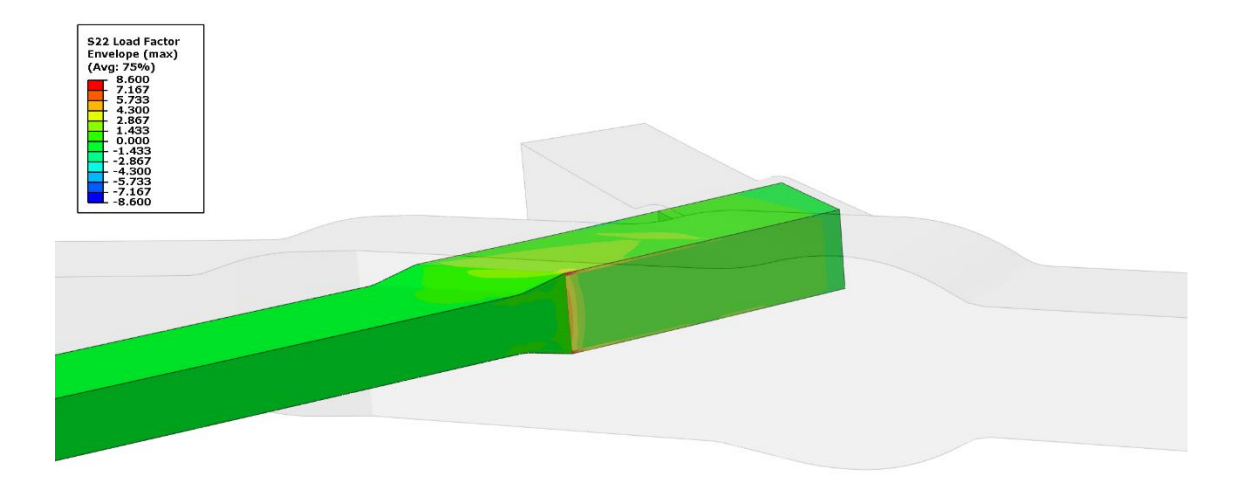


Figure 7.7 Load Factor plotted for  $\sigma_{22}$  in the transverse member, for load case 2 (max axial tensile load on member 1)

Table 7.4 Load factors for load case 3: transverse member loaded in compressio							in compression
		member		joint			
stress type		$\sigma_{min}$	$\sigma_{max}$ , $\tau_{max}$	$\sigma_{min}$	$\sigma_{max}, \tau_{max}$	failure stre	sses (norm)
$\sigma_{11}$	results	-1.93	2.75	-1.93	2.75	$-1 (X_N^c)$	$1.57 \; (X_N^t)$
	load factors	1.930	1.752	1.930	1.752		
$\sigma_{22}$	results	-0.290	0.344	-0.405	0.091	$-0.175 \ (Y_N^c)$	$0.064~(Y_N^t)$
	load factors	1.657	5.375	2.314	1.422		
$ au_{12}$	results		0.240		0.250		$0.076~(S_{12,N})$
	load factors		3.158		3.289		
$ au_{13}$ , $ au_{23}$	results		0.310		0.242		$0.095~(S_{IL,N})$
	load factors		3.263		2.552		

FEA Results 85

Table 7 Fland fastans fan	1	
Table 7.5 Load factors for	ioau case 4. transverse	member loaded in tension

		member		joint			
stress type	е	$\sigma_{min}$	$\sigma_{max}, \tau_{max}$	$\sigma_{min}$	$\sigma_{max}, \tau_{max}$	failure stre	sses (norm)
$\sigma_{11}$	results	-2.38	2.712	-2.27	1.934	$-0.64~(X_N^c)$	$1 (X_N^t)$
	load factors	3.719	2.712	3.547	1.934		
$\sigma_{22}$	results	-0.34	0.29	-0.09	0.36	$-0.111 \ (Y_N^c)$	$0.041~(Y_N^t)$
	load factors	3.063	7.073	0.811	8.780		
$ au_{12}$	results		0.24		0.212		$0.0485~(S_{12,N})$
	load factors		4.948		4.371		
$ au_{13},  au_{23}$	results		0.274		0.242		$0.06~(S_{IL,N})$
	load factors		4.567		4.040		

Table 7.6 Load factors for load case 5: transverse member loaded in bending

		member		joint			
stress type	e	$\sigma_{min}$	$\sigma_{max}$ , $\tau_{max}$	$\sigma_{min}$	$\sigma_{max}, \tau_{max}$	failure stre	sses (norm)
$\sigma_{11}$	results	-1.520	1.850	-0.120	0.160	$-1 (X_N^c)$	$1.57 \; (X_N^t)$
	load factors	1.520	1.178	0.120	0.102		
$\sigma_{22}$	results	-0.11	0.12	-0.086	0.091	$-0.175~(Y_N^c)$	$0.064 \; (Y_N^t)$
	load factors	0.629	1.875	0.491	1.422		
$ au_{12}$	results		0.14		0.05		$0.076~(S_{12,N})$
	load factors		1.842		0.658		
$ au_{13},  au_{23}$	results		0.16		0.063		$0.095~(S_{IL,N})$
	load factors		1.684		0.663		

Figure 7.8 corresponds to the result presented in Table 7.6 and shows the critical stress type for a bending load applied to the transverse member.

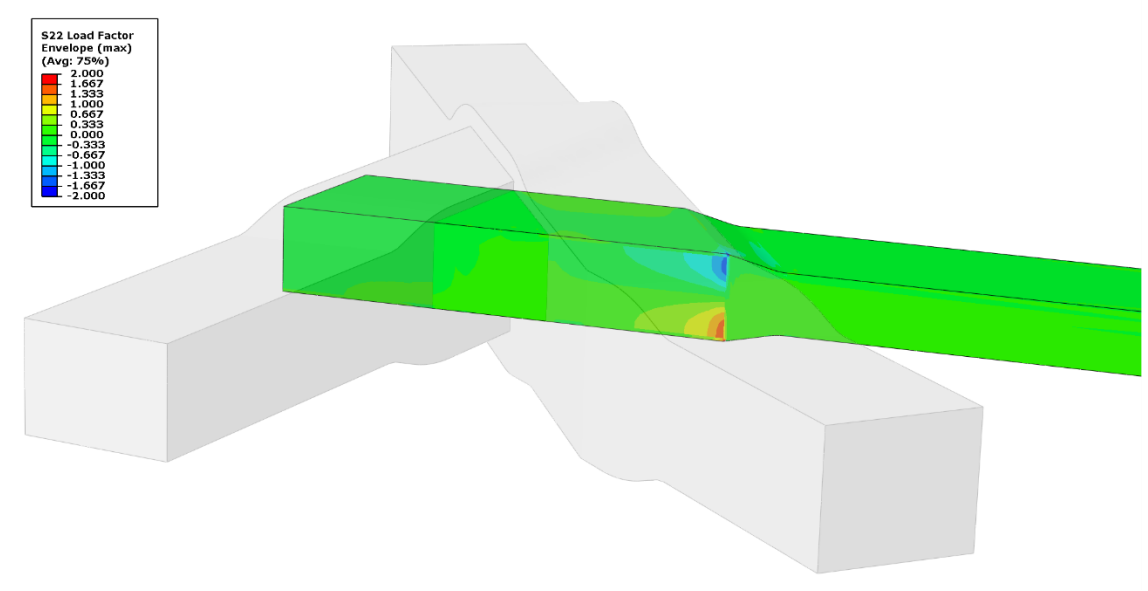


Figure 7.8 Load Factor plotted for  $\sigma_{22}$  in the transverse member, for load case 5 (bending load on member 2)

#### 7.2.2 Stiffness Analysis

As a first stiffness analysis, the fiber direction stiffness of individual members and joints is considered. Similar models are compared that were presented in Section 7.1, but with longer member sections. A different load case is used. The 1D beam model is pinned at its center node, representing the joint, while the two main members are both loaded at their ends with a compressive force of 10kN. The change in distance between the two end points is measured as 0.2566mm.

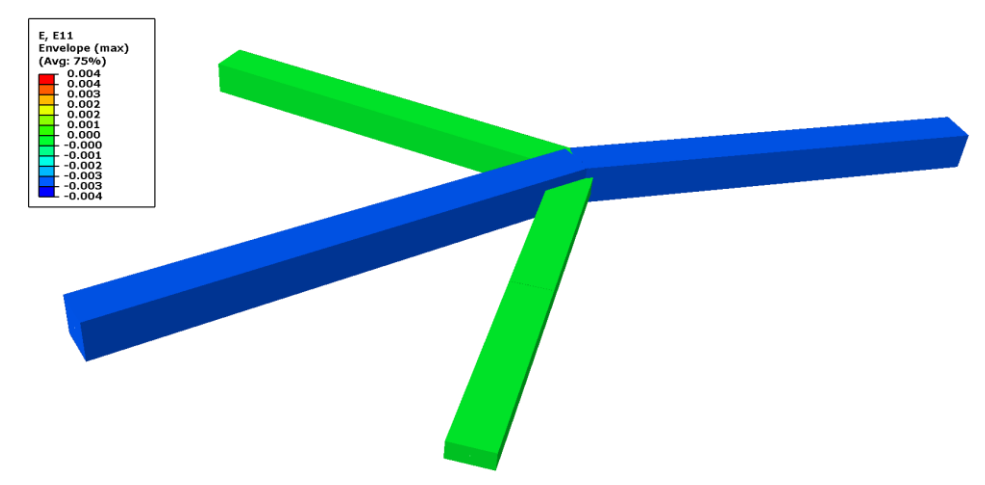


Figure 7.9  $\epsilon_{11}$  in beam model with both main members under compressive load of 10kN.

A similar load case is set up for the solid model by fixing the plane that is highlighted in red in Figure 7.10, and subjecting the joint to the same load. In this simulation, the change in distance between both end points is 0.2528mm. Figure 7.10 compares the strain along the fibers (and thus along the members) to the strain in the simpler model, depicted in Figure 7.9.

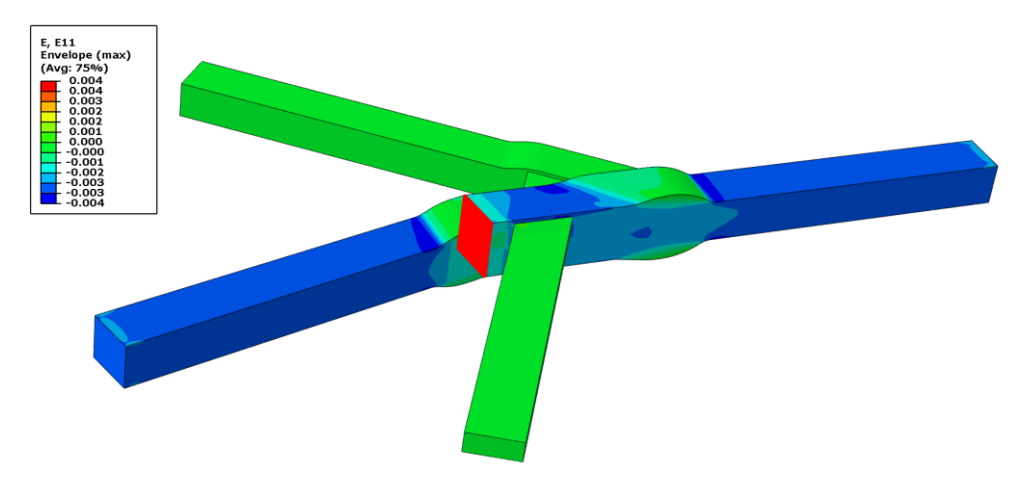


Figure 7.10  $\epsilon_{11}$  in solid model with both main members under compressive load of 10kN. Fixed plane indicated in red.

FEA Results 87

It can be seen that the joint itself is thicker than individual members, due to the increased amount of material at the sections where multiple members overlap. These sections exhibit lower strain. The greater cross section, and resulting lower strains, are not taken into account within the beam model. This explains the lower relative displacement of the member ends, although the difference is relatively low at 1.5%. As can be seen, this difference is mostly due to the stiffer joint. Strains within members themselves match more closely between the two models. Therefore, including longer member sections would lower the error in this comparison. In other words, the exact figure of 1.5% is the result of the choice of member length in this particular model. Shorter members would result in a higher discrepancy, but in a typical structure, members are on average likely to be longer relative to the overlap regions. It should be noted that either way, the estimates for fiber direction joint stiffness in the Optimization Framework are conservative.

While the above analysis gives insight into fiber direction stiffness in individual members and overlap regions, the boundary conditions used are not representative of how this type of joint is loaded in reality. Figure 7.11 shows how the entire joint rotates when loading both main members in compression, as in the previous load case shown in Figure 7.10, while constraining the ends of the other two members. It can be seen how the loads in the three most heavily loaded members contribute to a net moment around the joint.

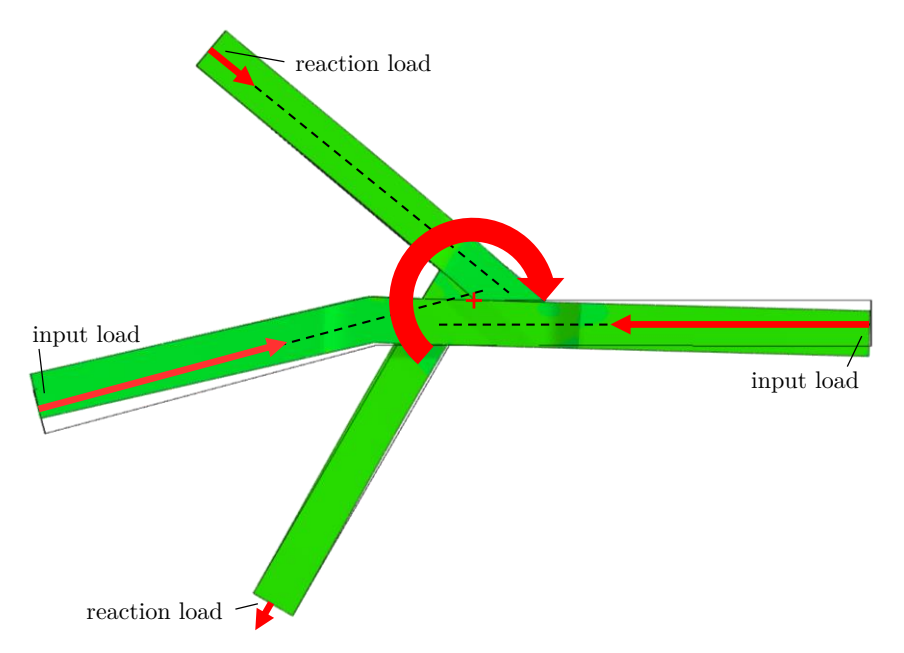


Figure 7.11 Local rotation of the joint due to moment imbalance, undeformed shape displayed as outline.

Direction and approximate magnitude of input loads and reaction loads at member ends indicated.

This behavior is a result of the fact that this particular joint has been developed primarily as a manufacturing prototype, without taking this effect into account. Section 7.3 details how net moments can be prevented, which this result indicates is critical in order to achieve predictable behavior.

#### 7.3 Moment balance and joint redesign

This section showcases how moment balance can be achieved in a typical joint. This is desirable for reasons of both strength as well as stiffness:

#### 1. Stiffness:

A moment-neutral joint exhibits no or very little local rotation of the type that was shown in Section 7.2.2 (see Figure 7.11). This leads to a structure that is stiffer in the direct sense of exhibiting lower displacement for a certain load, but also in the sense that no additional buckling sensitivity is introduced by preventing bending loads in members, which is the direct result of moment-imbalance.

#### 2. Strength:

Moment imbalance leads to bending loads in all connecting members. The analyses presented in Section 7.2.1 often showed load factors between 2 and 3 over larger areas. However, the bending loads in the connections often lead to asymmetric loading, giving rise to much higher, very local peaks, resulting in the much higher load factors that were observed.

A brief overview of the moment-neutral joint design methodology is shown in this section by means of an example, as well as the strength results for the redesigned joint.

Figure 7.12 shows the members (numbered 1 through 4) of the same joint that has been considered in Section 5.4 and previously in this chapter, but with a different design. Shown here is a situation where members 1 and 3 are heavily loaded, loads shown in red. Reaction loads in this example are introduced at the ends of members 2 and 4 and are shown in orange. The cross sections of all members are sized accordingly.

This example problem is simplified by assuming the mutual angles of each of the members as being fixed, approximating the common situation of relatively long, slender beams where a small change in position will not significantly influence their orientation. For an actual design, orientation changes can easily be taken into account in CAD as the joint locations at the other end of each of the members are known. Since the reaction loads are known from the Optimization Framework result, these can be used as an input for a detailed 3D design in a CAD model. The goal is to achieve a low net moment around the center of the joint. How to define the center of the joint is somewhat arbitrary, but most sensible definitions give the desired result. For this example, the crossing point of members 1 and 3 (the two largest and most heavily loaded members) is used as the center of the joint. A rigorous analytical approach for exactly cancelling out the moment for a joint is not deemed required: A quick, sensible approach delivers results that are drastically better compared to a design where no attention is given to moment cancellation. Any available further improvements require more detailed types of analysis, without

delivering additional real life advantages in terms of magnitude: See the results of the joint redesign at the end of this section.

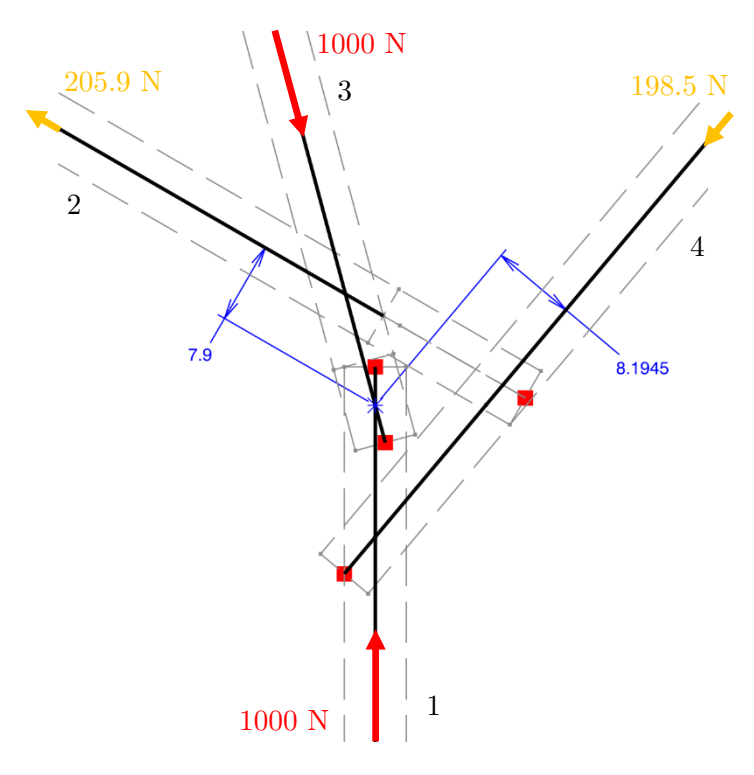


Figure 7.12 Schematic of moment-balanced joint, members numbered 1 and 3 are subjected to compression loads (red). Reaction loads on members 2 and 4 indicated in orange.

Adhering to the approach introduced in Section 5.3, first the two major members are connected using the reduced-buildup method shown in Section 5.3.2. To achieve moment balance around the center, members 2 and 4 need to be on different sides of this connection. Both possible layouts result in a joint that is about equally compact. Member 2 is chosen to connect above the member 1-3 connection. The more highly loaded member will need to connect closer to the center, so member 2 is place first, as close as possible to member 1. The position of member 4 now follows:  $7.9 \cdot \frac{205.9}{198.5} = 8.1945$ . Figure 7.13 compares the joint shown in Figure 7.11 to the redesigned joint in Figure 7.12, and plots the resultant moment around each point in the joint as a result of the four axial loads that are introduced. Members are overlaid as dashed lines, the joints as solid lines. It can be seen how each point in the first joint (a) contributes to a net negative moment. This necessarily results in reaction bending loads in each of the four connecting members. In the redesigned joint, there is a net positive moment in the top region of the joint, but it is counteracted in the bottom half. This leads to local bending in the center section of the joint. However, this middle section is not buckling sensitive, and the resulting displacements are negligible. The joint as a whole, therefore, is not exerted to a net moment, leading to almost purely axial loads for the connecting members, which was the goal of the redesign. This same approach can be applied to joints with more than four members, although more iteration may be required to come to the most compact solution, which is desirable for minimizing internal bending stresses in the joint.

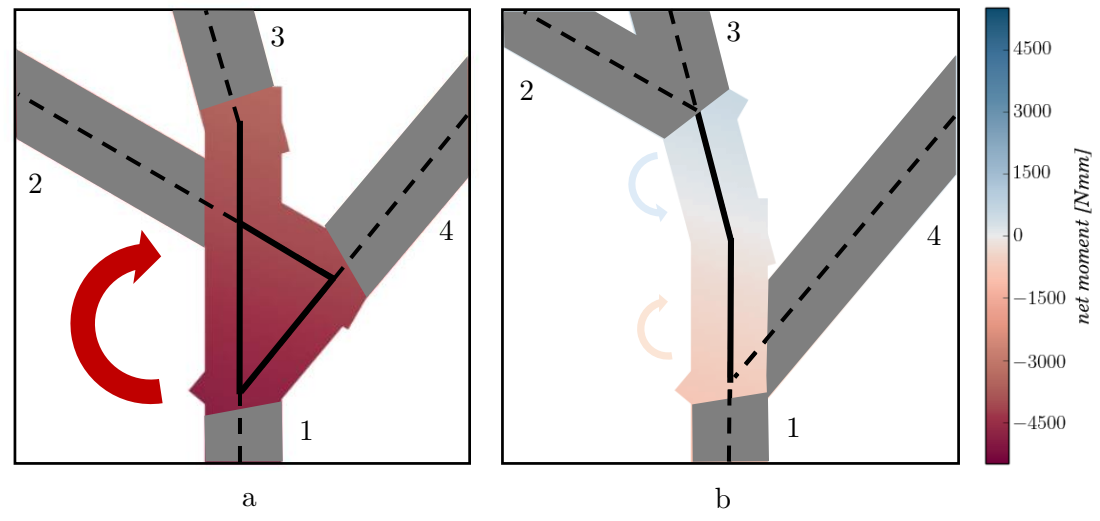


Figure 7.13 Resultant moment due to axial member loads for each point of the initial joint (a) and redesigned joint (b). Member numbers are indicated.

Figure 7.14 shows the FEA result for the new design with the same load case that is applied in Figure 7.5: compression of member 1, with the other 3 members pinned on their ends. Table 7.7 shows the corresponding load factors for different stress types. These results should be compared to those in Table 7.2.

Table 7.7 Load factors for load case 1: member 1 loaded in compression						
stress type		$\sigma_{min}$	$\sigma_{max}$ , $\tau_{max}$	failure stre	sses (norm)	
$\sigma_{11}$	results	-2.128	0.88	$-1 (X_N^c)$	$1.57 \; (X_N^t)$	
	load factors	2.128	0.561			
$\sigma_{22}$	results	-0.352	0.072	$-0.175 \ (Y_N^c)$	$0.064 \; (Y_N^t)$	
	load factors	2.011	1.122			
$ au_{12}$	result		0.180		$0.076~(S_{12,N})$	
	load factor		2.376			
$ au_{13}$ , $ au_{23}$	result		0.193		$0.095~(S_{IL,N})$	
	load factor		2.032			

Table 7.7 Load factors for load case 1: member 1 loaded in compression

It can be seen that all load factors are lower for each type of stress, especially tensile  $\sigma_{22}$ , which was critical earlier.  $\tau_{12}$  is now critical, although it should be noted that the observed shear peak stresses occur very locally near transitions, and their exact magnitude is highly dependent on the exact FEA model geometry. For other load cases, lower stresses are observed as well, indicating that careful joint design significantly reduces the safety factors that are required to prevent joint failure for strength critical designs. For stiffness critical designs, the advantages are significant as well. The previous design

Conclusions 91

showed significant rotation when subjected to the load case shown in Figure 7.11: close to 0.22 mm displacement of the tip of beam 1 for an axial load of 1000 N of beams 1 and 3. For the new design, this value is roughly 400 times smaller.

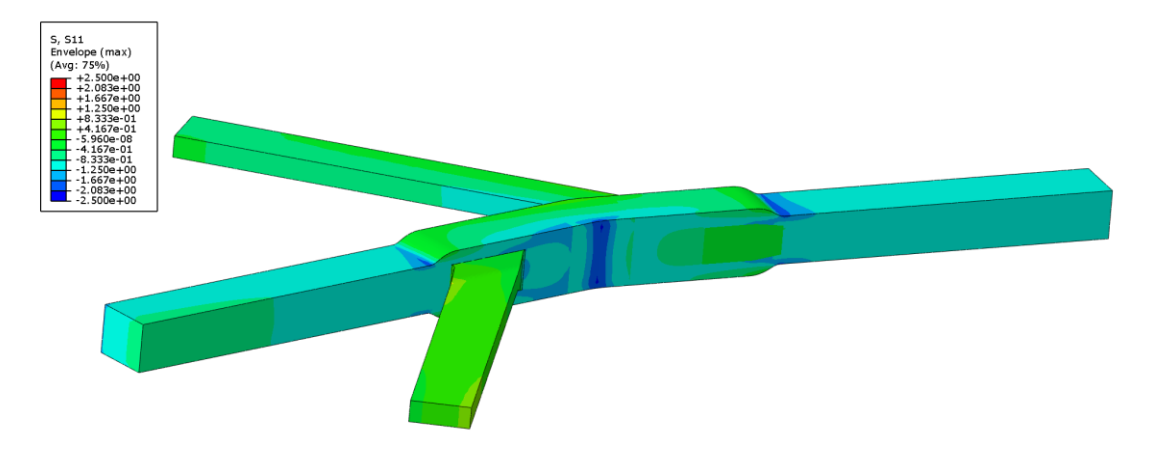


Figure 7.14 FEA result for redesigned joint, compression load of member 1 (right), compare to Figure 7.5

This factor of 400 reinforces a point that was made earlier on the relative unimportance of the exact location of the neutral point for balancing the net moment exerted on a joint: A relatively arbitrary point near the center of gravity was chosen in this example, yet the resulting moment balance is such an improvement that any remaining net moment is in the order of newton millimeters for most real life examples. Any further tuning will likely have less influence on the final product than for example manufacturing tolerances.

#### 7.4 Conclusions

High load factors are found in all load cases considered in Section 7.2.1. Compared to a bending load case, purely axial loading leads to higher average strain energy densities in a member, since all fibers in that member are loaded to their peak allowable stress, as opposed to only the most outward plies of the same member. These purely compressive and tensile load cases also lead to the highest load factors. There are several observations to be made:

- The results presented in Section 7.2.1 are for a joint design that had not yet been designed to reduce net moments around the joint center. Nevertheless, these results are useful for two main reasons:
  - 1. It serves as a case study of how to model and analyze these joints
  - 2. It shows the importance of proper joint design

- Many peak stresses are found at mesh singularities near sharp features which do
  not accurately represent the more gradual transitions found an actual manufactured product. This can be seen in Figure 7.5 and Figure 7.7. Stress peaks are
  generally less severe in joints that were designed with proper moment balancing.
- The load factors listed in Tables 4 through 8 relate to First Ply Failure (FPF). For some structures, depending on their requirements, ultimate failure of members may be a better measure of whether a structure can still fulfil its task. Physical testing would be required to determine:
  - 1. Whether the found load factors accurately predict FPF, considering the smoother transitions in the actual product.
  - 2. How much further the structure can be loaded beyond FPF until ultimate failure occurs.
- For all axial load cases, high values of  $\sigma_{22}$  are observed. Criticality of this failure mode is not unexpected, because of the magnitude of the ratios  $X^t/Y^t$  and  $X^c/Y^t$ , combined with the fact that primarily  $X^t$  and  $X^c$  are used to predict failure in the Optimization Framework.
- For strength critical structures, further development is required to determine the most feasible method of connecting individual members within a composite skeletal structure. Two possible approaches are:
  - 1. Increased joint cross sections which account for the observed load factors
  - 2. 3D printed metal joints which are bonded to individual members.
- As long as net moments are prevented when designing a joint in detail, as explained in Sections 5.3 and 7.3, no significant discrepancies are found in stiffness behavior between the 1D beam model and the 3D solid element model, indicating that the Optimization Framework can appropriately assess stiffness of structures that are evaluated, including the joints. The current joint design and manufacturing approach for joints is therefore suitable for structures that remain stiffness-critical, i.e. structures for which an optimized design which exactly meets stiffness requirements, results in strength safety factors that are sufficiently high. The analyses described in this section suggest that for individual joints, strength safety factors of at least 8 are required for all incoming members to not require further detailed analysis of the joint, although the results from the redesign that was presented in Section 7.3 suggest that this value may be lower for appropriately laid-out joints. Further research into a wider range of different joints and load conditions may lead to a better load factor prediction.

Next to the load cases presented in Section 7.2, four more load conditions were investigated, namely combined loading of members 1 and 2, both of them alternately loaded in

Conclusions 93

pure axial compression or tension. These results are not extensively presented here, but it was concluded that simultaneous loading of crossing members results in higher load factors in most cases. However, it can also result in lower effective load factors. Table 7.8 lists the load factors for a compression-compression load case, showing how this combined load case results in the tensile  $\sigma_{22}$  failure mode no longer being critical, while increasing the load factor for compressive  $\sigma_{11}$ , compared to cases 1 and 3.

Table 7.8 Load factors for load case 6: combined loading of members 1 (compression) and 2 (compression)

		me	mber	je	oint		
stress type	•	$\sigma_{min}$	$\sigma_{max}, \tau_{max}$	$\sigma_{min}$	$\sigma_{max}$ , $\tau_{max}$	failure stre	sses (norm)
$\sigma_{11}$	results	-5.32	3.52	-3.00	2.29	$-1 (X_N^c)$	$1.57 \; (X_N^t)$
	load factors	5.320	2.242	3.000	1.459		
$\sigma_{22}$	results	-0.657	0.308	-0.372	0.091	$-0.175~(Y_N^c)$	$0.064~(Y_N^t)$
	load factors	3.754	4.813	2.123	1.422		
$ au_{12}$	results		0.367		0.303		$0.076~(S_{12,N})$
	load factors		4.829		3.987		
$ au_{13},  au_{23}$	results		0.343		0.360		$0.095~(S_{IL,N})$
	load factors		3.611		3.789		

One failure mode which cannot be assessed with this model is delamination due to propagation of inherent flaws. Physical tests are proposed as the most appropriate method to determine joint strength with respect to this failure mode.

The specific joint presented here is designed to carry loads in one plane. Its design was driven primarily by requirements that followed from goals of the manufacturing test described in Section 5.4. In this context, mold manufacturability (i.e. simplicity) was prioritized over the added lessons that could be learned by including out-of-plane members. This means that no conclusions can be drawn from simulations using this model on the behavior of joints which deal with one or more out-of-plane loads that result from members that come in under an angle relative to the 'neutral plane'. Such a connection would introduce significant local bending stresses in that joint, near the member, as well as out-of-plane stresses within the joint, requiring additional reinforcement. However, for joints subjected to such loads, the general approach that is presented in this section (derivation of safety factors based on comparing different stress types to their maximum allowed values) can also be adopted when designing joints which are subjected to out-of-plane loads.

Based on the results in this chapter, it should be expected that significantly different load factors will be found for different relative angles between members and different member thickness ratios. This means that for strength critical structures, each joint must be analyzed individually, using the approach described in this section. Furthermore, the

importance of proper joint design is clear from the results presented in Section 7.3. Physical testing is proposed as a method to correlate observed load factors, which often follow from localized stress peaks, to actual failure of joints.

# Chapter 8

## **Conclusions and Recommendations**

This chapter presents conclusions that can be drawn based on the development and analysis that has been presented in previous chapters.

Furthermore, it was acknowledged at the onset of this research that full development into an industry-ready technology was too large a scope for a single thesis. It follows that much remains to be investigated. Some recommendations with regard to this are made in Section 8.2.

#### 8.1 Conclusions

- A conventional 3D topology optimization approach for isotropic materials is not equipped to design structures that make use of highly anisotropic materials, such as Carbon Fiber Reinforced Polymers. Additional design variables would be required to locally describe the direction of the material throughout the design domain, which cannot be a priori determined. Rather, the directions of load carrying members, to the extent that those can be individually identified as such, only become clear after load paths have been established, towards the final result of the optimization.
- Rather than using isotropic 3D FEA elements in a design optimization, using 1D beam elements provides a method to fill a design domain with a highly anisotropic material that is initially present in all directions at all locations, which can allow an optimizer to take into account and exploit the fact that a fiber reinforced material is most efficiently loaded along the fiber direction.

- Section 2.2 introduces the Ground Structure approach combined with 1D elements. Chapter 6 explains how this basic principle has been implemented for use within an automated Optimization Framework, showing that this is a feasible way to model, manipulate and optimize composite 3D skeletal structures.
- This setup provides a balance between on the one hand the complexity and width of applicability of structures that can be developed and on the other hand the complexity of the optimization process: 3D skeletal structures can be applied to a broad range of design problems, yet can also be relatively simply parametrized such that they can be subjected to a design optimizer in an automated procedure.
- When using 1D elements, separate topology, shape and sizing operations must be implemented to obtain a similar degree of design freedom that a 3D isotropic topology optimizer exhibits. Three separate sub-processes were realized within a larger Optimization Framework in Python, as a single process that incorporates all three types of functionality concurrently is not robustly realizable for any but the most basic design problems. This can at least be stated for the built-in Nastran optimizers. The complexity of the design space likely plays a role in this.
- The order in which these three operations are carried out influences the final result. Purely sequentially carried out topology → shape → size optimizations are commonly employed, but are unlikely to lead to a global optimum as the final result: A change in member size in the final step is likely to retroactively influence the optimality of the previously determined shape of the structure.
- To solve this, a nested setup is proposed, where a sizing optimization is always carried out before assessing the fitness increase that a proposed topology optimization step or shape change step provides. This method provides two main advantages:
  - 1. Only solutions that actually fulfill all requirements with respect to strength and stiffness and manufacturing constraints are compared.
  - 2. More robustness is provided in the sense that the optimization algorithm is less likely to prefer solutions earlier in the optimization process that at a later optimization stage turn out to be less optimal than others.
- Various manufacturing constraints can be incorporated within this optimization scheme. Most manufacturing constraints have bearing on either the shape of the structure (node locations) or the size of individual load carrying members, and are implemented within the corresponding optimization sub-processes. This reaffirms the need for a nested setup for the optimization sub-processes: A manufacturing constraint that has bearing on member sizing is not taken into account

Recommendations 97

during an isolated shape optimization step, so the merit of any proposed shape step can only be appropriately assessed after a subsequent sizing optimization.

- The resulting skeletal structures consist of straight, solid beams with rectangular cross sections with high Fiber Volume Fractions. A method has been proposed to manufacture these structures monolithically, or in monolithic segments for larger or more complex structures, using an out-of-autoclave process which ensures compression of the beams from all sides, while providing the design freedom required for an open, 3D skeletal frame.
- The beams are monolithically connected in joints for which a design methodology has been proposed, which needs to be carried out as a *translation step* with the result from the Optimization Framework as a starting point.
- Especially for strength-critical structures, these joints need to be analyzed in more detailed FEA. Typically significant stress peaks are observed near edges and transitions between fiber directions. The resulting load factors need to be taken into account by locally increasing joint cross sections.
- Appropriately designed stiffness-critical joints will typically not require the same level of detailed analysis and safety factor application.

#### 8.2 Recommendations

- A more sophisticated shape optimization algorithm can be developed. Within this thesis, the decision was made to prioritize simplicity and robustness, but in terms of efficiency there are significant gains to be found, as explained in Section 6.2.3.
- Further manufacturing testing should be done, involving more complex geometries compared to the tests described in Section 5.4.
- Additional FEA for fully modelled nodes, as described in Chapter 7, can give further insight into the range of load factors that can be expected for typical load cases. This is specifically the case for out-of-plane loading (i.e. loads with a z-component relative to the locally flat plane of the joint).
- Based on the previous point, a simple prediction model could be implemented
  which already within the Optimization Framework takes into account an estimate
  of the required additional mass for strengthening joints to account for local internal stress peaks.
- Further investigation into joint interior design may lead to methods to shape transitions between fiber direction bundles in ways that give rise to lower stress peaks.

- Physical testing should be carried out to correlate the results presented in Chapter 7 with the actual stiffness and failure behavior of the joints.
- Implementation can be explored of additional manufacturability constraints which relate to mold simplicity, compact joint design and other aspects. As an example, an individual node can be made more compact if the overlap principles presented in Section 5.3.2 can be applied, reducing joint thickness build-up significantly. This requires mutual angles of major members below a value of about 15°. Thus, incorporating into the objective function within the shape optimizer a preference for lower angles between nearly collinear members in major load paths may lead to flatter, more compact joints which are loaded more efficiently. Another example is the addition of the ability to define planes of symmetry within structures.

- Adeli, H., & Balasubramanyam, K. V. (1987). Interactive Layout Optimization of Trusses. *Journal of Computing in Civil Engineering*, 1(3), 183.
- Bakhvalov, Y. O., Petrokovskii, S. A., Polynovskiy, V. P., & Razin, A. F. (2009). Composite irregular lattice shells designing for space applications. *ICCM-17 International Committee on Composite Materials*, 1–10.
- Balling, R. J., Briggs, R. R., & Gillman, K. (2006). Multiple Optimum Size/Shape/Topology Designs for Skeletal Structures Using a Genetic Algorithm. Journal of Structural Engineering, 132(7), 1158–1165.
- Bendsøe, M. P. (1995). Optimization of Structural Topology, Shape, and Material.

  Antimicrobial Agents and Chemotherapy (Vol. 58).
- Bendsøe, M. P., & Kikuchi, N. (1988). Generating optimal topologies in structural design using a homogenization method. *Computer Methods in Applied Mechanics and Engineering*, 71(2), 197–224. https://doi.org/10.1016/0045-7825(88)90086-2
- Bendsøe, M. P., & Sigmund, O. (2003). Topology optimization: theory, methods, and applications. Engineering (Vol. 2nd Editio).
- Blom, a. W. (2010). Structural performance of fiber-placed, variable-stiffness composite conical and cylindrical shells.
- Camp, C., Pezeshk, S., & Cao, G. (1998). Optimized Design of Two-Dimensional Structures Using a Genetic Algorithm. *Journal of Structural Engineering*, 124(May), 551–559.
- Christensen, P. W., & Klabring, A. (2009). An introduction to structural optimization. https://doi.org/10.1007/978-1-4020-8666-3
- Cowper, G. R. (1966). The shear coefficient in Timoshenko's beam. *Trans. ASME: J. Appl. Mech.*, 33(4), 335–340. https://doi.org/10.1115/1.3625046
- Creemers, R. J. C. (2009). Interlaminar shear strength criteria for composites. National Aerospace Laboratory NLR. Retrieved from http://reports.nlr.nl/xmlui/handle/10921/232

Habibi, A. (2011). A New Approximation Method for Structural Optimization. *Journal* of Computing in Civil Engineering, 1(1), 92. https://doi.org/10.1061/(ASCE)CP.1943-5487.0000133

- Huybrechts, S. M., Meink, T. E., Wegner, P. M., & Ganley, J. M. (2002). Manufacturing theory for advanced grid stiffened structures. *Composites Part A: Applied Science and Manufacturing*, 33(2), 155–161.
- Ijsselmuiden, S. T. (2011). Optimal Design of Variable Stiffness Composite Structures Using Lamination Parameters.
- Kaveh, a., & Shojaee, S. (2006). Optimal design of skeletal structures using ant colony optimization. *International Journal for Numerical Methods in Engineering*, (October 2006), 1885–1891. https://doi.org/10.1002/nme
- Kirsch, U., & Topping, B. H. V. (1992). Minimum Weight Design of Structural Topologies. *Journal of Structural Engineering*, 118(7), 1770.
- Labanda, R. (2015). Mathematical programming methods for large-scale topology optimization problems PhD Thesis.
- Li, Y., & Chen, Y. (2010). Beam Structure Optimization for Additive Manufacturing Based on Principal Stress Lines. 21st Annual International Solid Freeform Fabrication Symposium, 666–678.
- Maes, V. K. (2015). Design, Analysis, Optimization and Testing of Grid-Stiffened Composite Structures. TU Delft.
- MSC Software Corporation. (2011). MSC Nastran 2012 Design Sensitivity and Optimization User's Guide.
- MSC Software Corporation. (2011). MSC Nastran 2012 Linear Static Analysis User's Guide.
- MSC Software Corporation. (2011). MSC Nastran 2012 Quick Reference Guide.
- Nomura, T., Dede, E. M., Lee, J., Yamasaki, S., Matsumori, T., Kawamoto, A., & Kikuchi, N. (2014). General topology optimization method with continuous and discrete orientation design using isoparametric projection. *International Journal for Numerical Methods in Engineering*, 101(8), 571–605.
- Rajan, S. D. (1995). Sizing, Shape and Topology Optimization of Trusses using Genetic Algorithm. *Journal of Structural Engineering*, (1), 1480–1487.
- Shrestha, S. M., & Ghaboussi, J. (1998). Evolution of Optimum Structural Shapes Using Genetic Algorithm. *Journal of Structural Engineering*, 124(11), 1331–1338. https://doi.org/10.1061/(ASCE)0733-9445(1998)124:11(1331)
- Sigmund, O., & Maute, K. (2013). Topology optimization approaches: A comparative review. Structural and Multidisciplinary Optimization, 48(6), 1031–1055.

Smeets, B. J. R. (2016). Development of an in-panel attachment method for fiber-placed composite lattice and grid-stiffened structures. TU Delft.

- Soh, C. K., & Yang, J. (1996). Fuzzy Controlled Genetic Algorithm Search for Shape Optimization. *Journal of Computing in Civil Engineering*, 10(2), 143–150.
- Sokolowski, J., & Zochowski, A. (1999). On the Topological Derivative in Shape Optimization. SIAM Journal on Control and Optimization, 37(4), 1251–1272. https://doi.org/10.1137/S0363012997323230
- te Kloeze, I. (2015). Design, Analysis, Manufacturing and Testing of Load Introductions in Grid-Stiffened Composite Structures. TU Delft.
- Totaro, G., & De Nicola, F. (2012). Recent advance on design and manufacturing of composite anisogrid structures for space launchers. Acta Astronautica, 81(2), 570– 577.
- Van Campen, J. M. J. F. (2011). Optimum lay-up design of variable stiffness composite structures.
- Vanderplaats, G. N. (1985). A Fortran program for automated design synthesis. Hampton Virginia.
- Vasiliev, V. V., Barynin, V. A., & Rasin, A. F. (2001). Anisogrid lattice structures survey of development and application. *Composite Structures*, 54(2–3), 361–370.
- Vasiliev, V. V., Razin, A. F., Barynin, V. A., & Razin, A. F. (2006). Anisogrid composite lattice structures for spacecraft and aircraft applications. *Composite Structures*, 76(3), 1117–1127.
- Vasiliev, V. V, Razin, A. F., Totaro, G., & Nicola, F. De. (2005). Anisogrid Conical Adapters for Commercial Space Application. *AIAA/CIRA 13th International Space Planes and Hypersonics Systems and Technologies*, 1–9.
- Wächter, A., & Biegler, L. T. (2006). On the implementation of an interior-point filter line-search algorithm for large-scale nonlinear programming. *Mathematical Programming*, 106(1), 25–57. https://doi.org/10.1007/s10107-004-0559-y
- Wang, M. Y., Wang, X., & Guo, D. (2003). A level set method for structural topology optimization. Computer Methods in Applied Mechanics and Engineering, 192(1-2), 227-246. https://doi.org/10.1016/S0045-7825(02)00559-5
- Wei, P., Ma, H., & Wang, M. Y. (2014). The stiffness spreading method for layout optimization of truss structures. *Structural and Multidisciplinary Optimization*, 49(4), 667–682.
- Xiao, A., Wang, B., Sun, C., Zhang, S., & Yang, Z. (2014). Estimation Based Particle Swarm Optimization Algorithm for Layout Design of Truss Structures. Mathematical Problems in Engineering, 2014.

Xie, Y. M., & Steven, G. P. (1993). A simple evolutionary procedure for structural optimization. Computers and Structures, 49(5), 885-896. https://doi.org/10.1016/0045-7949(93)90035-C

Ye, H. L., Chen, Y. M. L. N., & Sui, Y. K. (2010). Topology Optimization of Anisotropic Materials under Harmonic Response Based on ICM Method, (2000), 1–8.

# Appendix A

Joint manufacturing campaign layup

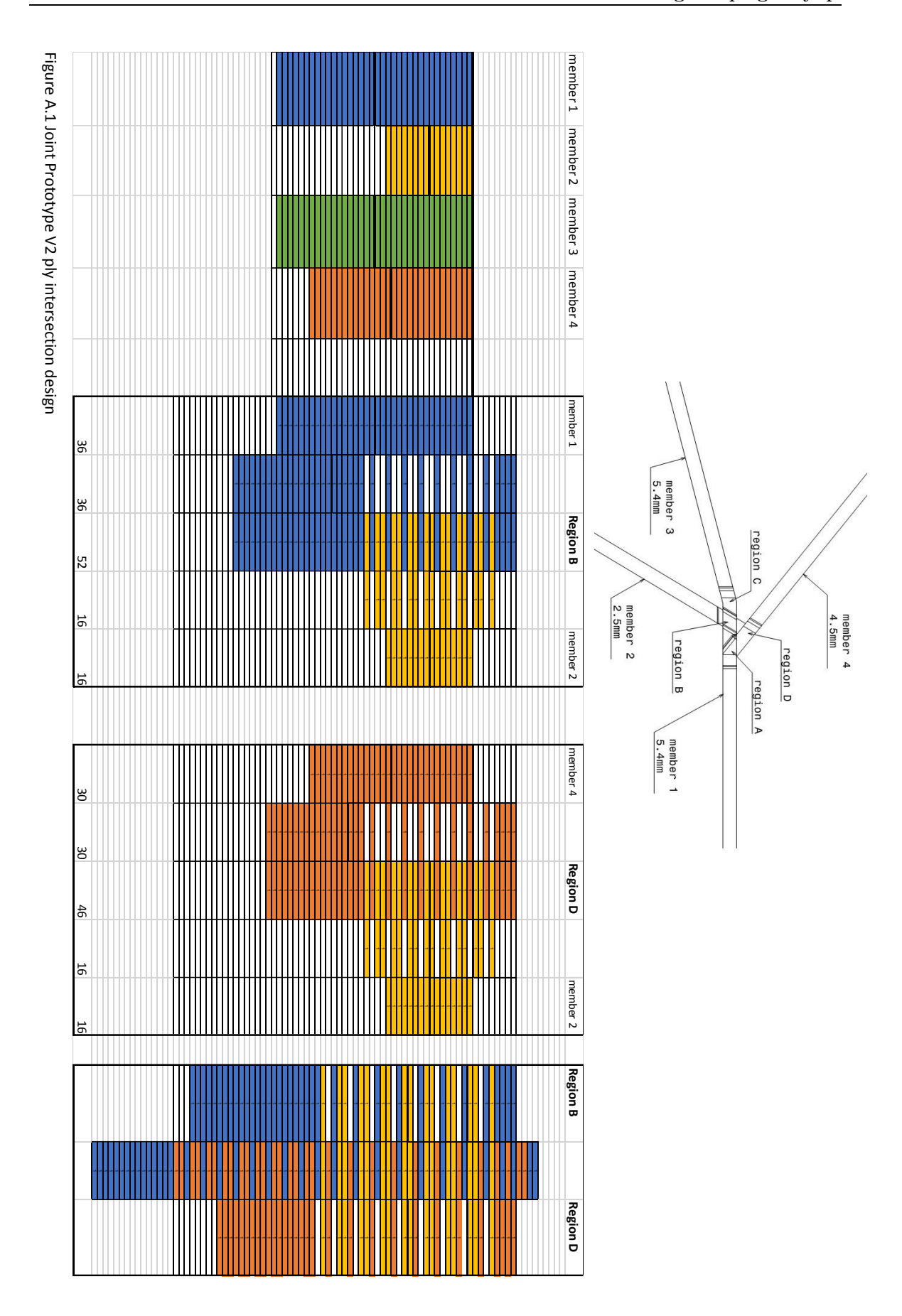
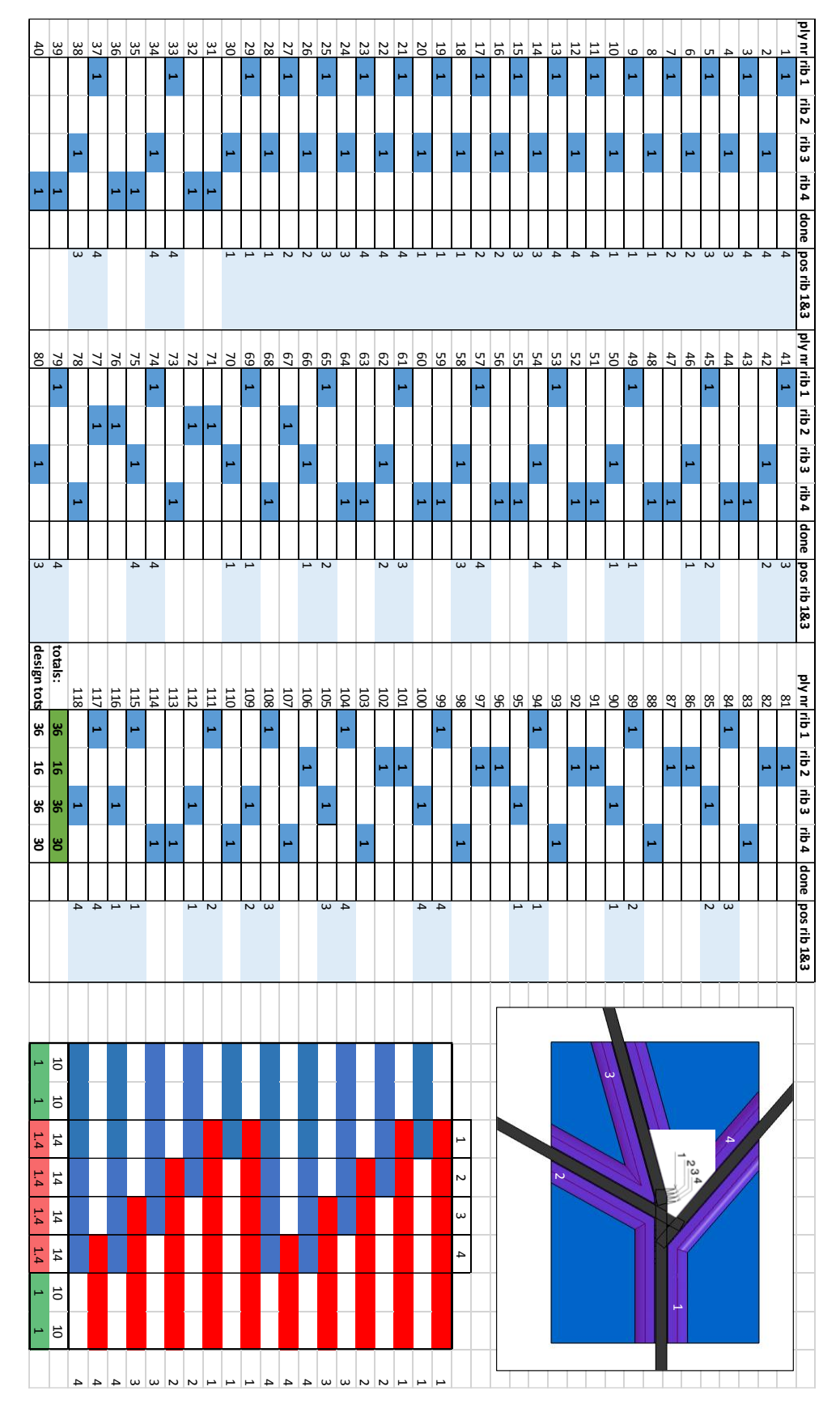


Figure A.2 Joint prototype V2 layup sheet



## Appendix B

## FEA Element type considerations

A good combination of element, element property type and material needs to be chosen for modeling the 1-D members in the Nastran topology and sizing analyses. There are several options:

#### • Rod elements (CROD + PROD + MAT1)

This is a simple element with 6 DOFs.

 $\circ$  Advantages:

Needs little input to be properly defined, and speeds up calculations. Successfully used in early iterations of optimization analyses

o Disadvantages:

Does not model bending and twisting behavior, and can therefore not accurately analyze structures were axial elements see loads that are not purely axial, as will be the case for most real-world structures. Can only be used with an isotropic material, and can therefore not model much behavioral aspects of a composite beam. This is true for modeling stiffness, but crucially also for determining failure loads even semi-accurately, since few failure mechanisms can be modelled, other than failure due to a purely axial tensile load.

#### • Bar elements (CBAR + PBAR/PBARL + MAT1)

A simple beam elements with 12 DOFs

o Advantages:

Fully models bending and twisting behavior. Still very computationally efficient compared to most alternatives.

Provides Shear Correction factor input possibility (only PBAR, not PBARL)

#### $\circ$ Disadvantages:

Like Rod elements, this combination can only use isotropic materials.

#### • Beam elements

A beam element with 12 or 18 DOFs and additional functionality over Bar elements

#### • CBEAM + PBEAM/PBEAML + MAT1: (12 DOFs)

#### $\blacksquare$ Advantages:

Provides extra functionality compared to bar elements, such as tapered beams and more realistic handling of non-symmetric sections

→ not within the scope of this research

Provides Shear Correction factor input possibility (only PBEAM,

Disadvantages:

not PBEAML)

requires control over more input parameters during optimization without

#### • CBEAM3 + PBMSECT + PCOMP + MAT8: (18 DOFs)

#### $\blacksquare$ Advantages:

Implements the Variational Asymptotic Beam method. Although the inputs into Nastran take the form of a beam elements, this is actually a far more complex way of modeling beams. It uses a stack of shell elements.

#### lacktriangleright Disadvantages:

Apart from the fact that this method is much more computationally expensive, making beam thicknesses dependent on a design variable needs a workaround that lacks in robustness. The amount of plies cannot be made dependent on a design variable. However, the thickness of individual plies can be, so use can be made of either a few very thick plies with variable thickness, or a stack of many thin plies, some of which may be assigned a thickness of 0.

There are however many known errors within Nastran associated with VAB, which can often be easily circumvented on a case-by-case basis, but that is not a suitable approach for an automated optimization sequence.

The decision is made to go for CBAR + PBAR + MAT1, with shear correction factors to closely approximate the stiffness behavior of unidirectional fiber beams. This offers a good trade-off between simplicity and the ability to model relevant characteristics.

## Appendix C

## Beam modeling property derivation

This section presents how a shear correction factor can be derived to appropriately model bending behavior in a composite beam, modelled using a Nastran CBAR element combined with a MAT1 material.

Proposed method: Derive analytical solution for bending load on a ply stack.

The shear correction factor is defined such that  $\int_A \tau dA = \kappa AG\varphi$ 

For an isotropic material and a solid rectangular cross section, Cowper (1966) has shown that  $\kappa$  can be approximated as:

$$\kappa = \frac{10(1+\nu)}{12+11\nu} \approx 0.85 \tag{C.1}$$

For a composite material with highly anisotropic properties however, this is not correct. A correction must be made to account for the significant difference between the actual measured shear modulus  $G_{comp}$  of the composite material, and the shear modulus, which for isotropic materials is normally derived from the E-modulus and Poisson's ratio:

$$G_{iso} = \frac{E}{2(1+\nu)} \tag{C.2}$$

A more accurate shear correction factor is acquired using:

$$\kappa = \frac{G_{comp}(2(1 + \nu_{iso}))}{E_{iso}}$$
 (C.3)

For the UD material for which stiffness properties are listed in Table C.1, this results in:

$$\kappa = \frac{5.2(2(1+0.32))}{143} = 0.096 \tag{C.4}$$

Values for A, I<sub>1</sub>, I<sub>2</sub>, J for each beam depend on a fixed width and a variable height, which is coupled to a design variable.

Table C.1 Stiffness properties for Hexcel 8552 IM7

Variable	Value
E <sub>11</sub>	143 GPa
$E_{22}$	11.4 GPa
$G_{12}$	5.2  GPa
$ u_{12}$	0.32

Using DVPREL2 and DEQATN, these can be coupled, using the following formulas, with b and h the base and height:

$$A = bh$$

$$I_1 = \frac{bh^3}{12}$$

$$I_2 = \frac{b^3h}{12}$$
(C.5)

J can be approximated to within 4% using the following formula, as long as h is the short side of the beam:

$$J = bh^3 \left( \frac{1}{3} - 0.21 \frac{h}{b} \left( 1 - \frac{h^4}{12b^4} \right) \right)$$
 (C.6)

To ensure this works for all cases, the above equation is generalized in the program as:

$$J = \max(b, h) \cdot \min(b, h)^{3} \left( \frac{1}{3} - 0.21 \frac{\min(b, h)}{\max(b, h)} \left( 1 - \frac{\min(b, h)^{4}}{12 \max(b, h)^{4}} \right) \right)$$
(C.7)

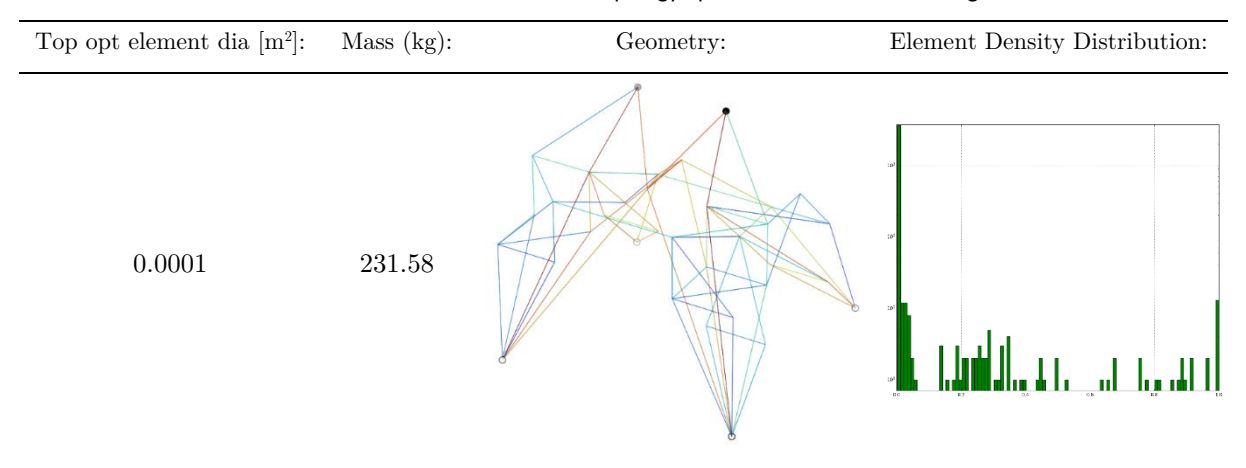
# Appendix D

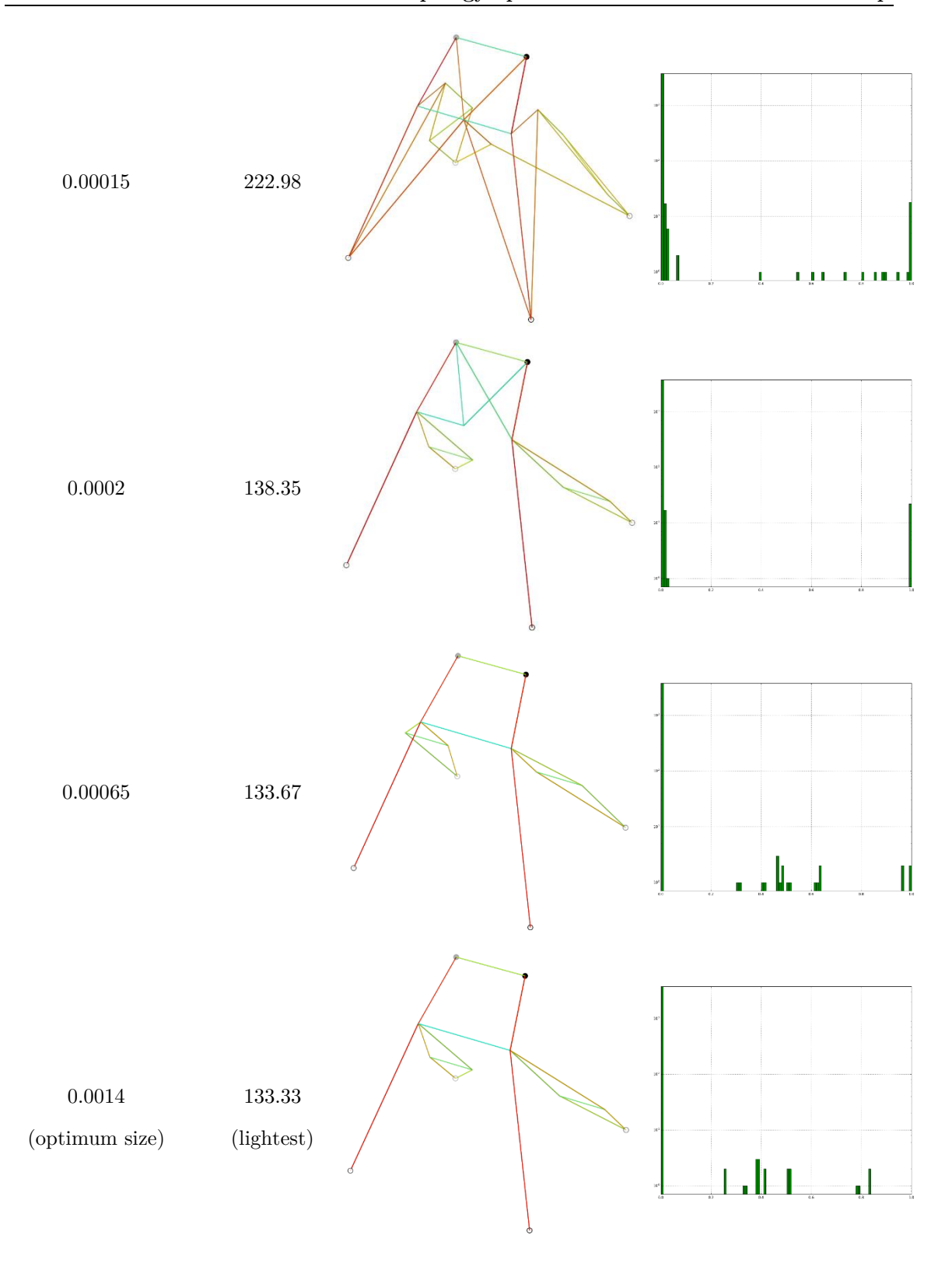
# Topology optimization initial element size sweep

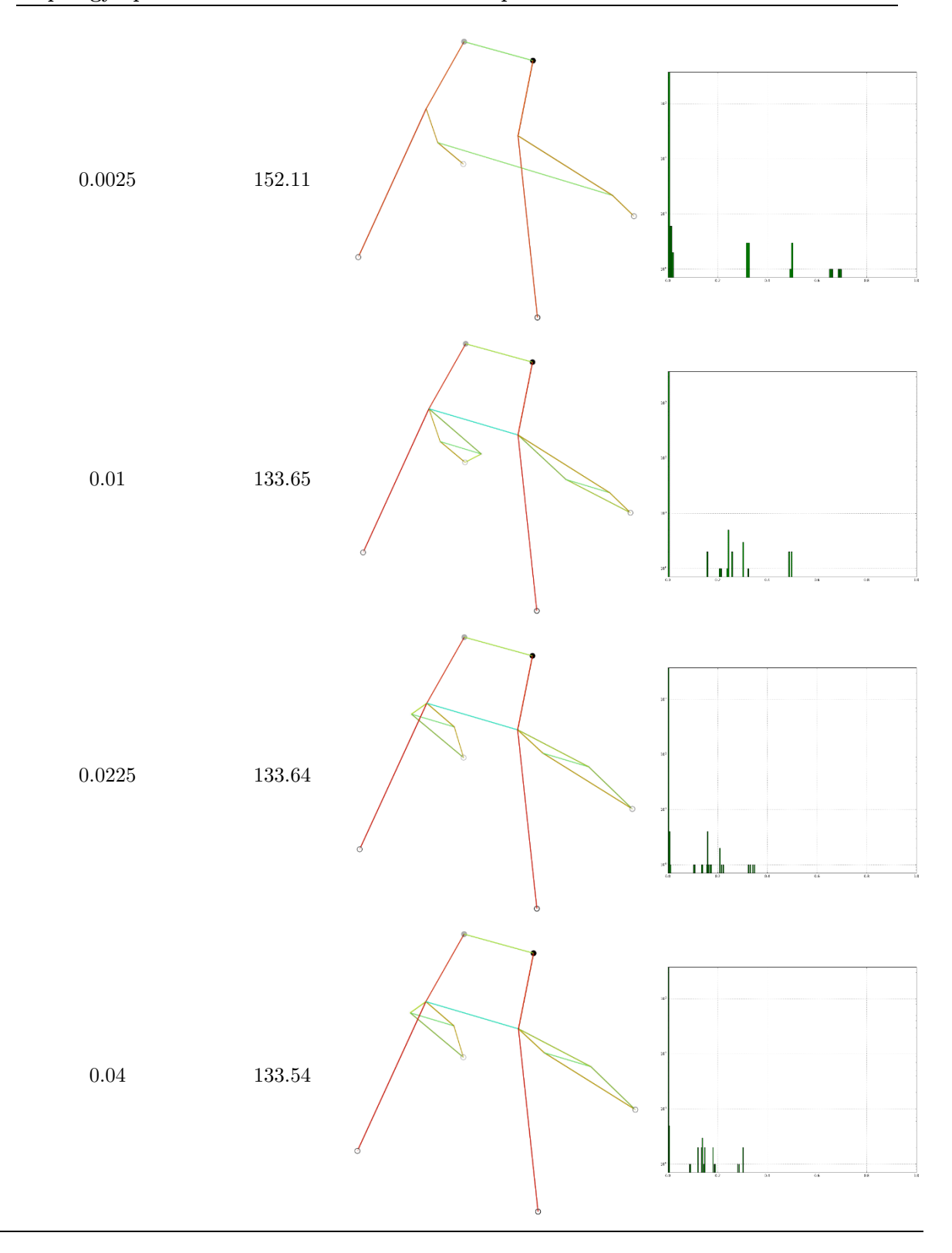
Table D.1 shows the geometry and corresponding EDDs of topology optimization results for a range of initial element sizes.

The principles behind this are explained in Section 6.5. The starting point for each of these results is the ground structure seen in Figure 6.5. The shown figures are similar to Figure 6.9 and Figure 6.10

Table D.1 Topology optimization results for a range of initial element sizes







Note 1: All results have been topology optimized, and subsequently size optimized, according to the Phase 1 procedure explained in Chapter 6. During this size optimization, minimum size constraints are enforced, which explains the high weight of the first few structures.

Note 2: In all of the lightest solutions (there are several with a mass of around 133 grams), the largest members after sizing optimization have a cross section of  $0.0014 \mathrm{m}^2$ . That means that in hindsight, this would have been the 'correct' size for the topology optimization. However, there is no way to predict this reliably, hence the need for the initial member size sweep that is demonstrated above.

# Appendix E

## Fluttering in Sizing Optimization

This section presents a closer inspection of fluttering behavior between two close-tooptimal solutions in Nastran that prevents convergence.

A four bar stool with a single load is considered, as seen in Figure E.1. The goal for this design problem is weight minimization.

Comparison: a buckling optimized structure would weigh 33.38kg. When a modal analysis is performed (and a certain minimum Eigen frequency required), the structure becomes critical in local modes of the individual beams. The algorithm should converge at 179.5kg, but instead bounces between two solutions, with two sets of design variables (widths beams 1 and 3 versus beams 2 and 4) both alternating between two values. The algorithm becomes stuck, and continues until the maximum allowed number of cycles, after which the solution is declared a best compromise infeasible design.

This happens for this design problem when frequency is made to be the only critical design constraint.

None of the internal optimization algorithms within Nas-

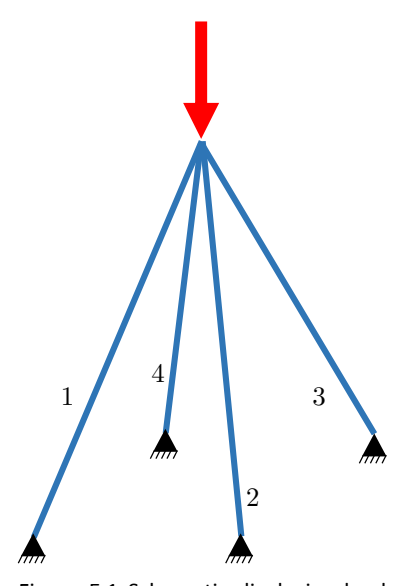


Figure E.1 Schematic displaying load case and member number-ing of sizing test problem

tran take into account the design history which would allow it to recognize this pattern. Nor does it accept the result when the value of one or multiple design variable values have not stabilized **even if the overall solution shows a sufficient degree of convergence when considering the weight of successive cycle solutions.** This means that simply relaxing the overall convergence criterion is not a suitable workaround, even it were otherwise acceptable. Figure E.2 plots the weight of the structure (the objective function for this problem). It can be seen that this value has effectively converged to within roughly 0.1%. Even though the convergence criterion was 1% for this particular

run, this fact did not prompt the optimizer to terminate the run, since the individual design variables still saw changes between iterations in the order of 10% of their current value.

Section 6.6.3 explains how this issue has been solved.

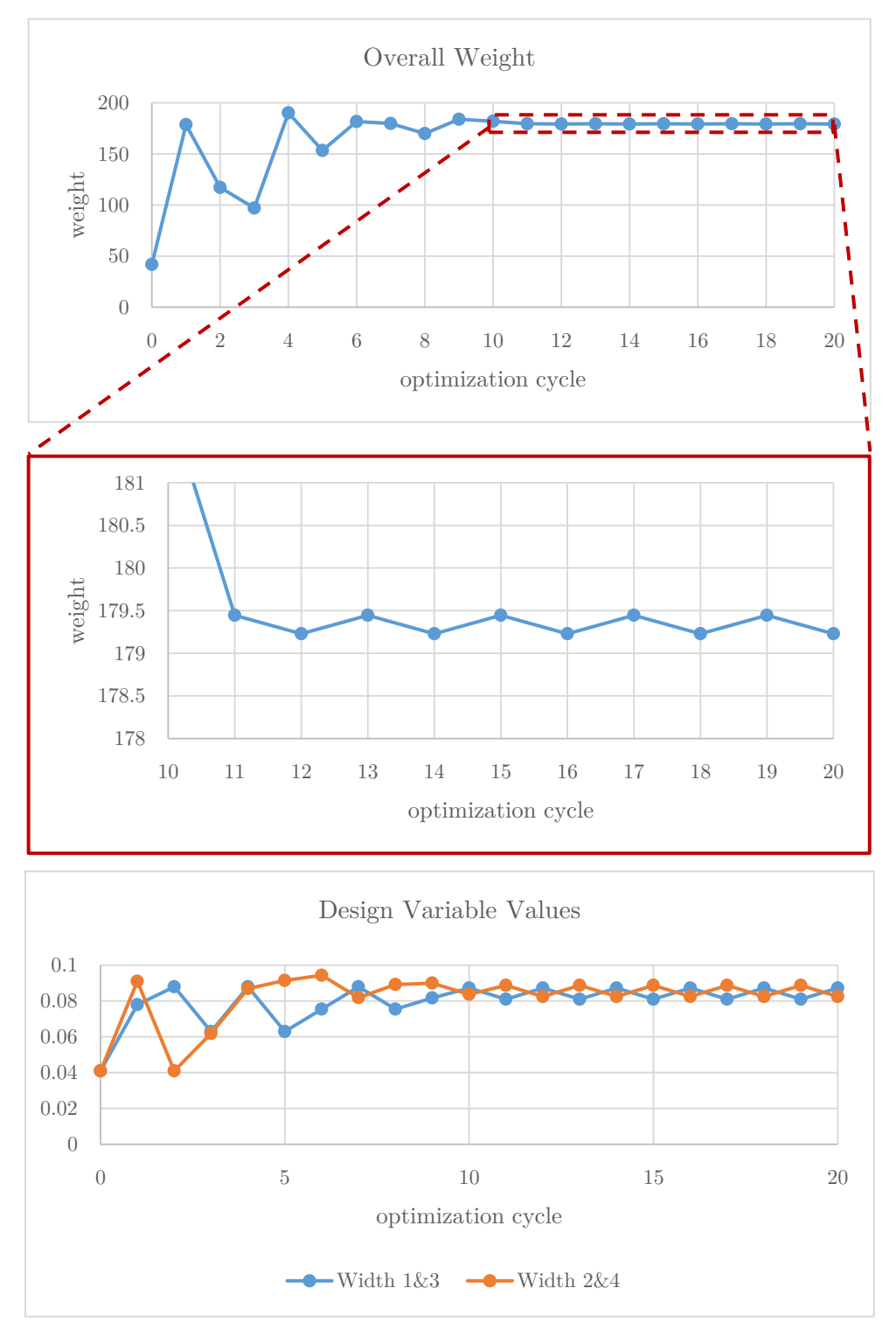


Figure E.2 Non-convergence due to design variable fluttering